Characterization of protein interactions of a novel Ciliopathy-associated EML3 protein

by

Raieda Z. Sadeq

A thesis submitted in conformity with the requirements for the degree of Master of Science

Graduate Department of Biochemistry

McGill University

Characterization of protein interactions of a novel ciliopathy-associated EML3 protein

Master of Science 2016

Raieda Z. Sadeq

Department of Biochemistry

McGill University

Abstract

The Echinoderm Microtubule Associated Protein (EMAP) was first discovered in sea urchins where it co-purified with microtubules. In mammals, the homologs of the EMAP protein constitute the EML (EMAP-like) protein family. Six EML proteins (EML1-6) have been identified. EML proteins share very little sequence homology with other microtubule-associated proteins and their functions are yet to be fully elucidated. Our initial studies have revealed that EML3, a member of the EML protein family, is required for mouse development and post-natal viability.

To fully understand the molecular functions of EML3, it is important to identify its interaction network. For this reason, the aim of this study was to identify interacting protein partners of EML3. A thorough screening of previously published literature and publicly available high-throughput protein interaction data was performed to create a list of the potential interacting partners of EML3. This study provides supporting evidence, as well as the potential functional implications, for the candidate interactors. EML3 contains a DYNLL-binding motif which is unique to EML3 within the EML family. We therefore undertook co-immunoprecipitation studies in a mammalian co-transfection cultured cell system and found that EML3 associates with Dynein Light Chain (DYNLL), a component of the cytoplasmic dynein motor complex which

takes part in anterograde transport across microtubules. In addition, to investigate the ability of EML3 to form hetero-oligomers with other members of the EML protein family, we tested for the interaction of EML3 with the paralogs EML1, 2 and 4. We found that EML3 interacts with EML1 and EML2 but not EML4 in this system.

Co-localization analysis using both direct and indirect immunofluorescence was performed to examine the spatial association of EML3 and DYNLL to determine whether EML3 and DYNLL co-localize *in vivo*. Immunofluorescence analysis was performed using adult mouse retinal sections, where the EML3 protein is highly expressed. Confocal microscopy following staining with antibodies directed against the two interacting proteins demonstrated that EML3 with DYNLL co-localize to the in the inner segment of the photoreceptors of the retina. These findings suggest a functional interaction between EML3 and DYNLL proteins in the adult mouse retina.

My findings open new perspectives in the study of the molecular functions of EML3 by analyzing its novel interactions in mammalian cells and mouse retinal sections. Specifically, our work provides a framework for investigating the functional relevance of the interaction between EML3 and DYNLL in adult mouse retina, as well as the ability of EML3 to interact with a subset of the EML protein family. It is the first step towards elucidating the essential role played by EML3 in mouse development and post-natal viability.

Caractérisation des intéractions protéiques d'une nouvelle protéine associée aux ciliopathies : EML3

Résumé

La protéine EMAP (Echinoderm microtubule-associated protein) a été découverte chez les oursins où elle a été co-purifiée avec les microtubules. Chez les mammifères, les homologues de la protéine EMAP constituent la famille des protéines EML (EMAP-like). Six protéines de type EML (EML1-6) ont été identifiées. Les protéines EML partagent très peu d'homologie de séquence avec les autres protéines associées aux microtubules et leurs fonctions ne sont pas encore complètement élucidées. Nos études préliminaires ont révélées que EML3, un membre de la famille des protéines de type EML, est nécessaire pour le développement des souris et pour la viabilité post-natale.

Pour bien comprendre les fonctions moléculaires d'EML3, il est important d'identifier ses principaux partenaires d'interaction. Pour cette raison, l'objectif de cette étude était d'identifier les protéines qui interagissent avec EML3. Une recherche détaillée de la littérature scientifique et des bases de données à haut débit d'interaction des protéines a été effectuée pour créer une liste des partenaires potentiels d'interaction d'EML3. Cette étude fournit des éléments de preuve à l'appui, ainsi que les implications fonctionnelles potentielles, pour les molécules candidates d'interaction avec EML3. EML3 contient un site de liaison à DYNLL qui est unique à EML3 parmi les protéines EML. Nous avons donc entrepris desétudes de co-immunoprécipitation dans un système de cellules mammifères cultivées et co-transfectées pour démontrer qu'EML3 s'associe avec DYNLL (Dynein Light

Chain), une composante du complexe moteur dynéine cytoplasmique qui participe dans le transport antérograde le long des microtubules. De plus, pour enquêter sur la capacité d'EML3 de former des hétéro-oligomères avec d'autres membres de la famille des protéines detype EML, nous avons testé l'interaction d'EML3 avec les paralogues EML1, 2 et 4. Nous avons constaté qu'EML3 interagit avec EML1 et EML2 mais non avec EML4 dans ce système.

Une analyse de co-localisation par immunofluorescence directe et indirecte a été réalisée pour examiner l'association spatiale d'EML3 et de DYNLL *in vivo.* L'analyse par immunofluorescence a été effectuée en utilisant des sections de la rétine d'une souris adulte, où la protéine *EML3* est fortement exprimée. La visualisation par microscopie confocale de la coloration avec des anticorps dirigés contre les deux protéines a démontré que DYNLL co-localise avec EML3 dans les segments intérieurs des photorécepteurs de la rétine. Ces résultats suggèrent une interaction fonctionnelle entre les protéines EML3 et DYNLL dans la rétine de souris adultes.

En analysant les nouvelles interactions dans les cellules mammifères et les sections de la rétine de souris, nos résultats ouvrent de nouvelles perspectives dans l'étude des fonctions moléculaires d'EML3. Plus précisément, mon travail fournit un cadre pour étudier la pertinence fonctionnelle de l'interaction entre EML3 et DYNLL dans la rétine de souris adultes, ainsi que la capacité d'EML3 d'interagir avec un sous-ensemble de la famille des protéines de type EML. Cette étude est la première étape vers l'élucidation du rôle essentiel joué par EML3 dans le développement des souris et dans la viabilité post-natale.

Acknowledgements

Many people have made my graduate career at McGill University an enriching experience. To begin with, I wish to thank my supervisor Dr. Roderick R. McInnes for giving me the wonderful opportunity to work in his lab. Being an international student in Canada for the first time, I received a welcoming, supportive attitude from him and the rest of the lab which made my student life in Canada even more wonderful. I learnt immensely about science and my abilities, and I hope that our friendship will continue well into the future.

I would like to thank my research advisory committee members, Dr. Philippe Gros, Dr. Michel Cayouette, and Dr. Albert Berghuis for their guidance and for believing in me.

The members of the McInnes lab provided a wonderful environment in which to work and learn. I have been lucky to work with my lab members: Eduardo Diez, Isabelle Carrier, Rina Lall and Jessica Digiovanni. I am extremely grateful to both Eduardo and Isabelle for their continuous support, guidance and for always taking the time to provide assistance in the lab. I would not have been able to complete my graduate degree without their support. Thank you for making my graduate experience especially wonderful.

My family and friends have always been supportive of my work. I give special thanks to my parents, Ammu, Abbu and my sister, Ina, for always supporting me and believing in my capabilities. Lastly, I would like to thank my husband, Ahmed Adnan for his continuous encouragement, unconditional love and always pushing me to go that extra mile.

Table of Contents

List of Figures and Tables

Chapter 1

Chapter 2

Chapter 3

Chapter 4

Chapter 1: Introduction

1.1 The mouse retina

Complex organs like the brain consist of billions of cells assembling and communicating to ensure that the body is fully functional. Over the years, researchers have found simpler model systems to study the complexity of the brain. One such model is the mammalian retina.

1.1.1 The anatomy and physiology of the retina

The retina constitutes the interior surface of the eye. Santiago Ramon Cajal first began characterizing the variety of neurons that compose the retina. This work was continued by many other scientists and is nearing completion- the first time this has been accomplished for any significantly complex structure of the mammalian CNS. The mammalian retina contains 55 different cell types each with a different structure and function [1]. The retina comprises five classes of neurons: photoreceptor cells, bipolar cells, ganglion cells, horizontal cells and amacrine cells. The neurons are arranged in a manner that has been less difficult to unravel than the circuits in the brain (Figure 1.1). Light rays must pass through the non-light-sensitive layers of the retina to reach the outer segment of photoreceptors where photons are absorbed. The outer most layer of the retina is the retinal pigmented epithelium (RPE). It is a monolayer of cells which is critical for the survival and function of retinal photoreceptors [2]. There are two types of photoreceptors in the retina- rod cells and cone cells. Rod photoreceptor cells govern vision in dim light. They are more numerous and sensitive than the cone photoreceptor cells which collect photons in day light. Cone cells mediate color vision and provide high visual acuity. Each rod and cone photoreceptor cell consists of an outer segment (OS), a connecting

cilium (CC) that links the outer segment with the inner segment (IS), a cell body and a synaptic terminal. The OS of rod and cone photoreceptor cells are composed of stacks of discs containing the photo pigments required for photon absorption. The apical membrane of the RPE lies adjacent to the OS of the photoreceptor cells. The IS of each photoreceptor cell contains organelles such as mitochondria and Golgi bodies which perform the metabolic functions of the cell [3]. The outer nuclear layer (ONL) is composed of the cell bodies of rod and cone photoreceptor cells. The layer adjacent to the ONL is the outer plexiform layer (OPL) where the axons of rod and cone photoreceptor cells form synapses with the dendrites of bipolar and horizontal cells. The inner nuclear layer (INL) contains the nuclei and cell bodies of bipolar, horizontal and amacrine cells, as well as Müller glial cells. The inner plexiform layer (IPL) is the site of synapse formation between the axons of the bipolar cells and dendrites of amacrine and ganglion cells. The ganglion cell layer (GCL) contains nuclei of the ganglion cells and displaced amacrine cells (Figure 1.1) [4].

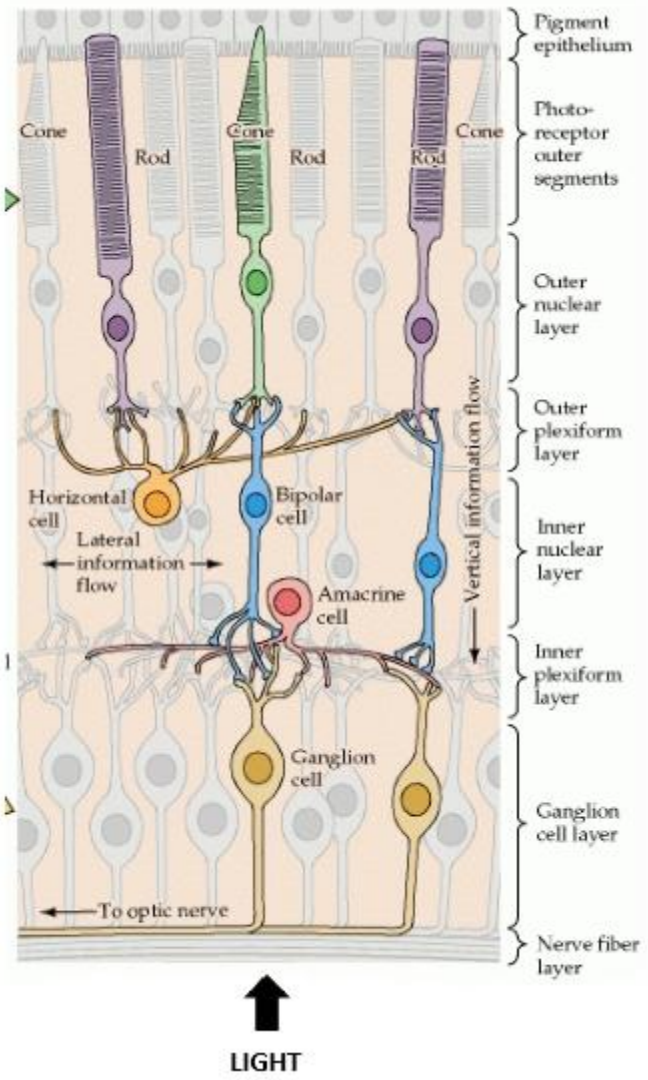

Figure 1.1: Cross section of the retina showing overall arrangement of the retinal layers [4].

The photoreceptors convert light signals into chemical and electrical signals by communicating with the downstream circuit of neurons which in turn pass signals to the brain to eventually generate vision [1]. The diversity of horizontal, amacrine and ganglion cells in the retina is the basis for pathways that convey a variety of visual information in the form of electric signals to central targets in a parallel manner. Adapted from [4-6].

1.1.2 The mouse retina as a model for neuronal development and maintenance

The retina is a simple model of the brain that is used to study how a network of neurons processes information. Retinal neurons communicate by forming synapses with other retinal neurons and by expressing neurotransmitters. The advantages of using the retina as a model system include its simple structure and its physical accessibility [7, 8]. As a result, most aspects of cell division and differentiation, from lineage tracing of progenitors to the morphological aspect of division to the molecular mechanisms involved have been studied in the retina [9]. Mice display high levels of similarity to human physiology and anatomy making them suitable models for studying the genetics of retinal development and disease. A major advantage of using mice is the availability of well-developed tools for manipulating the mouse genome to produce specific mutations. Mouse mutations can be maintained on controlled genetic backgrounds making it possible to analyze the effects of a mutation in same sex and same age littermates that differ only by whether they carry a specific mutation. The mouse retina provides the platform for generating better controls to study the genetics of retina development and disease [10].

1.1.3 Development of the mouse eye:

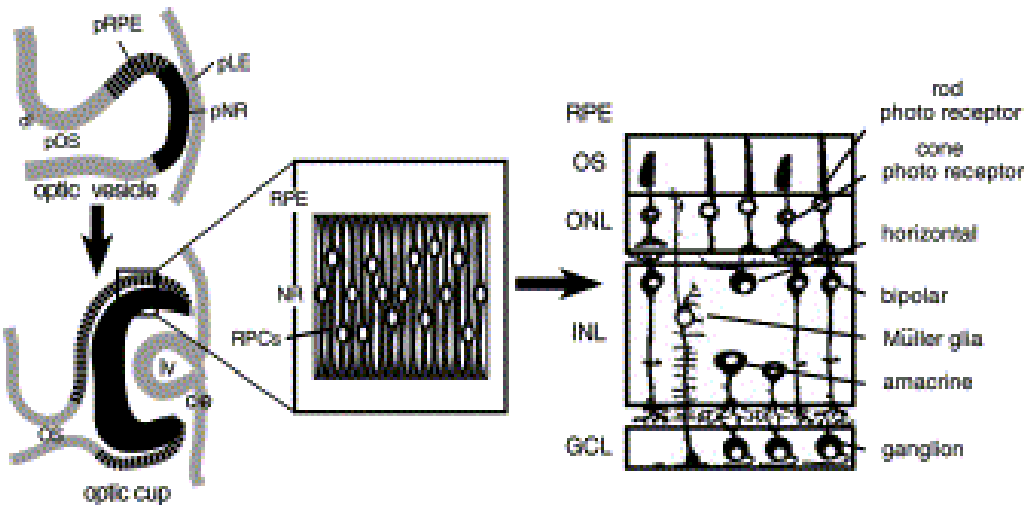

Figure 1.2: Development and origin of the neural retina. The distal neuro-epithelium of the optic vesicle represents the presumptive neural retina and will eventually invaginate to form the inner layer of the optic cup (neural retina), while the outer layer will give rise to the retinal pigment epithelium (RPE) [11].

The retina develops from dividing cells in the anterior neural plate in mammals [12]. The mammalian retina originates from a protrusion of the diencephalon called the optic vesicle which begins forming at around embryonic day 8 in mouse [13]. The optic vesicle then invaginates to form the cup structure of the retina with an outer epithelial layer of cells eventually forming the retinal pigmented epithelium (RPE) and an inner neuro-epithelium that becomes the retina (Figure 1.2) [9]. During embryonic development the retinal neurons are derived from a population of multipotent retinal progenitor cells (RPCs) residing in the inner neuro-epithelium of the optic cup (Figure 1.2). Early progenitor cells divide to expand the tissue. The progenitor cells then exit the cell cycle and differentiate [9]. The onset of retinal cell differentiation occurs in the center of the optic cup, close to the optic nerve head, and

progresses towards the periphery in a wave-like fashion until the region of the presumptive iris is reached [14]. The retina is ultimately transformed into a three layer structure containing five major types of differentiated neurons and one major type of glial cell [15]. Retinal ganglion cells are generated first, followed in overlapping phases by horizontal cells, cone photoreceptor cells, amacrine cells, rod photoreceptor cells, bipolar cells and finally Müller glial cells (Figure 1.3) [16]. The process of cell diversification in the developing nervous system is affected by cell intrinsic mechanisms and extracellular signals. Studies of postnatal cell differentiation in the retina reveals that the majority of cells (73%) produced postnatally differentiate as rods. This also represents their population in the mature retina. In contrast, 20% of cells formed by mitosis in the postnatal period differentiate as bipolar cells and 6% of cells are converted to Müller cells. Predecessors of bipolar and Müller cells stop dividing primarily after birth. All the cone cells and about half the rod cells arise from precursors that stop dividing prenatally [17].

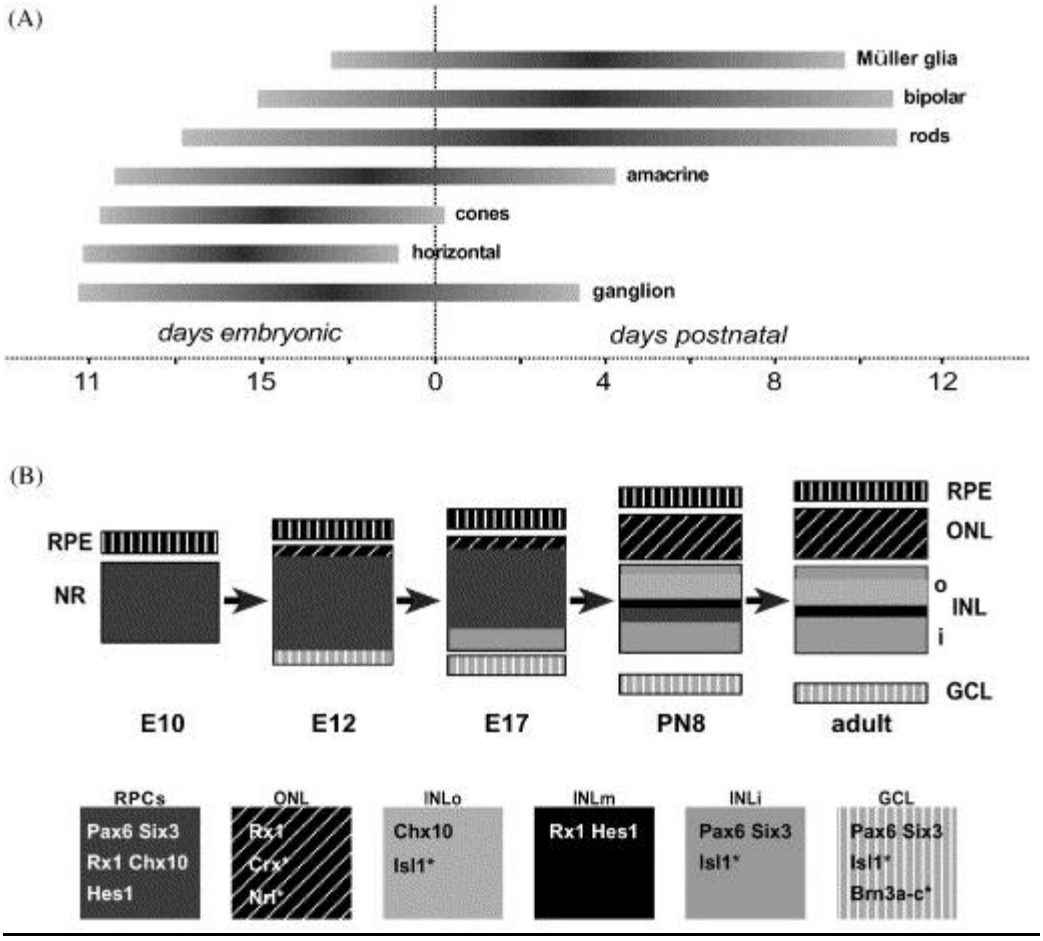

Figure 1.3: Retinal neurogenesis proceeds in a fixed histogenetic order. Ganglion cells and horizontal cells are born first, followed by cone photoreceptors, amacrine cells, rod photoreceptors, amacrine cells and Müller glia cells (Panel A). The prenatal (E) and postnatal days (PN) refer to the respective stages of mouse development. A set of transcription factors is initially co-expressed in mitotic retinal progenitor cells (RPCs). However with advancing retinogenesis, their expression domains start to segregate so that finally each retinal layer expresses a unique combination of these factors (Panel B) [11, 17].

1.1.4 Photoreceptor structure, modified cilium and transport

Vertebrate rod and cone photoreceptors are sensory neurons whose functions depend on the formation of a complex modified sensory cilium. Cilia are slender, microscopic, hair-like organelles that project from the surfaces of nearly all mammalian cells and are involved in coordinating signaling pathways during development and tissue homeostasis. Cilia are broadly

divided into two categories: - motile cilia, which possess a wave-like motion, and non-motile or primary cilia, which act as a sensory organelle for the cell. The backbone of a cilium is comprised of microtubules (MTs) which form the ciliary axoneme that is surrounded by the plasma membrane. Primary cilia have a “9+0” arrangement where the central pair of MTs are lacking (Figure 1.4, panel A). Motile cilia typically possess the “9+2” architecture where the MTs are arranged in the form of nine doublet MTs surrounding a pair of MTs at the center (Figure 1.4, panel B) [18]. The axonemal MTs emanate from a structure called the basal body.

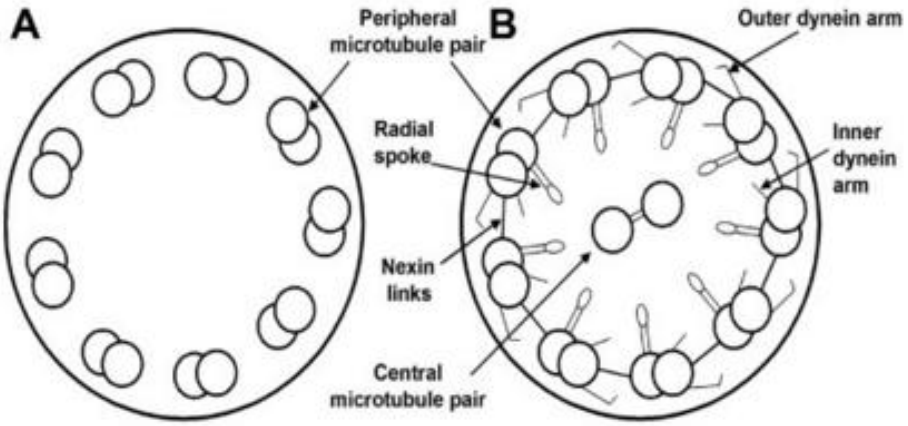

Figure 1.4: Schematic cross section diagrams of a typical primary (non-motile) cilium (panel A) and a motile cilium (panel B) [19].

Primary cilia play critical roles in many aspects of mammalian development and physiology such as detection of chemical or mechano-sensory signals [20] and coordination of a plethora of cellular signaling pathways [21]. The outer segments of rod and cone photoreceptor cells are referred to as photoreceptor sensory cilia (PSC) [22, 23]. (Figure 1.5) and contains an axoneme which begins at the basal body and passes through a ”transition zone” called the connecting

cilium (Figure 1.5) [24]. As for most primary cilia, the core of the PR axoneme consists of nine "-MT doublets-" (9+0) [25].

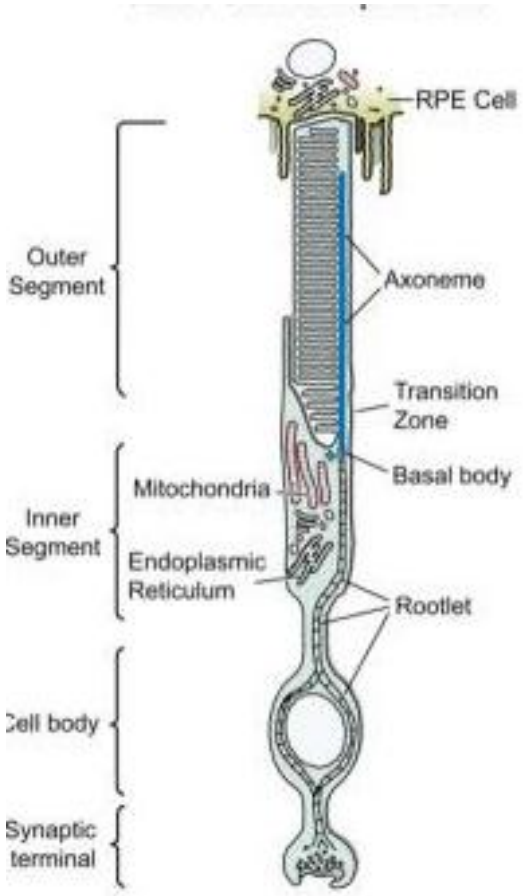

Figure 1.5: Schematic of a rod photoreceptor cell. A transition zone called the connecting cilium connects the inner and outer segments [24].

The outer segment (OS) of a rod photoreceptor cell is composed of individualized disks stacked tightly along the axoneme and surrounded by plasma membrane (Figure 1.5) [24]. The OS of cone photoreceptors is much shorter than that of rods. The cone OSs arise initially as evaginations with subsequent formation of a series of disks (or invaginations) which are continuously connected to the plasma membrane of the OS. The cone disks retain connection to the cilium that extends the entire length of the OS [26]. In mature rod cells, the axoneme

extends more than half the length of the OS [27-29]. Evidence of axonemes that extend the entire length of the cone OS and which turn over during the process of disk shedding of the distal OS tip can be found in the literature [30, 31]. The dendritic region between the nucleus and OS is called the inner segment (IS) [31]. The ciliary rootlet is a prominent cytoskeleton that originates from the proximal end of basal bodies and extends proximally towards the cell nuclei [32]. In a photoreceptor, the rootlet appears as a very thick striated filament that traverses the entire cell body all the way to the synaptic terminal [33, 34]. The ciliary rootlet is a polymer of rootletin. The rootlet serves to anchor the cilium to the cell and functions as a channel for proteins destined for the OS [23, 35].

The process of intra-flagellar transport (IFT) is responsible for the assembly and maintenance of cilia. IFT is a MT-based conveying system in which motor protein complexes such as Dynein and Kinesin transport cargo across the MTs in opposing direction [36-38]. Anterograde IFT (towards the plus end of MTs) is essential for photoreceptor OS formation and maintenance, as well as for opsin trafficking [39]. Retrograde IFT (towards the minus end of MTs) plays a role in recycling IFT proteins and other ciliary components by returning them to the basal body from the tip of the cilium [40, 41]. The Kinesin motor protein complex transports cargo away from the basal body by the process of anterograde transport. The Dynein motor protein complex transports cargo towards the basal body by retrograde transport [42].

1.2 The *Rom1/Eml3* project

1.2.1 The ROM1 protein and its discovery

Formerly, the McInnes lab hypothesized that evolutionarily conserved genes that are predominantly and abundantly expressed in the retina are likely to be important for its structure, function and development. These evolutionarily conserved genes should also constitute candidate genes for retinopathies. Thus, to identify such genes, the process of differential hybridization was used to select conserved, abundant retina-specific cDNA clones [43]. As a result of the differential hybridization process, 10 retinal cDNA clones were identified amongst which 2 were novel. One of the discovered clones encoded the 205 amino acid ROM1 protein. Northern blot analysis revealed that the *Rom1* transcript was detected specifically in the retina (Figure 1.6) [43].

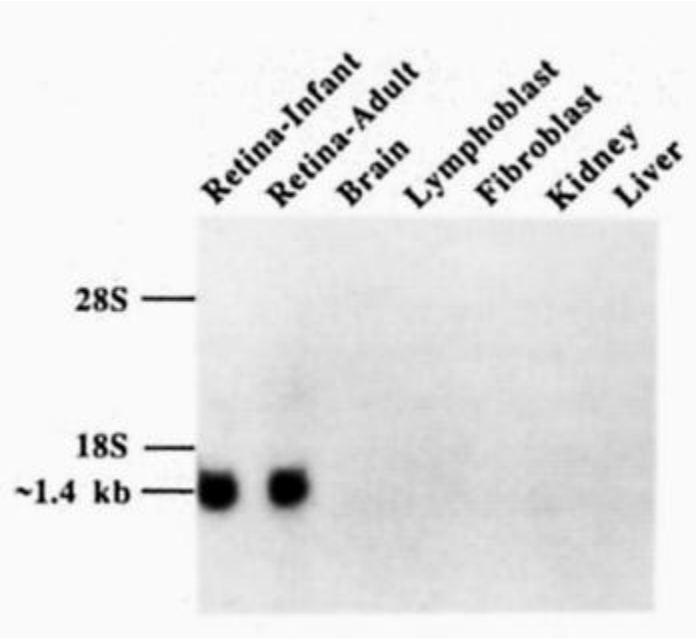

Figure 1.6: Northern blot of human tissues. The 1.4kb *Rom1* transcript was detected specifically in the retina [43].

Peripherin/*rds* is an integral membrane glycoprotein found in the rim regions of vertebrate photoreceptor cell disks [44]. Human ROM1 and Peripherin 2 (PRPH2) share 55% nucleotide sequence identity and 35% amino acid sequence identity. The abundance, retinal specificity and evolutionary conservation of the *Rom1* transcript, together with the resemblance of the ROM1 polypeptide to PRPH2 encoded by the gene affected in the murine degenerative retinopathy *retinal degeneration slow (rds)*, indicated that ROM1 plays an important role in the outer segment of rod photoreceptors. Immunostaining showed that ROM1 protein localizes to the disk rim of rod photoreceptor cells (Figure 1.7) where ROM1 plays a critical role in disk rim morphogenesis [43, 45]. Cases of digenic Retinitis Pigmentosa (RP) have been observed following the simultaneous presence of mutations in *Prph2 (RDS)* and *Rom1* genes [46, 47].

The fact that the homozygous *rds* mutant mice suffer from the absence of disk morphogenesis and improper outer segment formation further supports the suggestion that both ROM1 and PRPH2 play a role in the biogenesis of the disks in rod photoreceptors and in maintaining the structure of the rod photoreceptor outer segments. ROM1 and PRPH2 dimers associate non-covalently in disk membranes [43]. It should be noted that PRPH2 is expressed in both rod and cone photoreceptor cells and that ROM1 is majorly expressed in rod cells. ROM1 may be expressed at very low levels or not at all in cones [43].

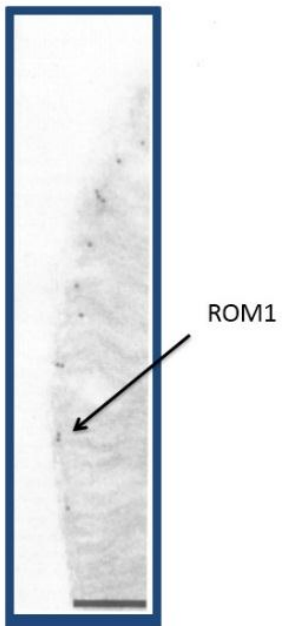

Figure 1.7: Transmission electron micrograph of human rod outer segment immuno-labeled with affinity purified antibodies to ROM1 showing that it is localized to the disk rim of rod photoreceptors. Adapted from [43].

1.2.2 Generation of Rom1 knockout mice

The strategy adopted to characterize the biological function of the ROM1 protein was to generate a *Rom1* null allele in mice. A (4.5) kb fragment of the Balb/c inbred strain genome containing part of the *Rom1* gene was used to screen a phage library of the mouse strain 129sV genomic DNA to get an 18.9 kb clone that spans the entire *Rom1* genomic locus. To generate the *Rom1* null allele, a targeting vector was designed in which the bacterial neomycin resistance gene replaced the first exon of *Rom1*, which encodes 56% of the ROM1 protein, and approximately 500 bp of upstream sequences containing the transcriptional start site (Figure 1.8). Thus, approximately 1500 bp from the 5' genomic region of the *Rom1* gene was deleted. Chimaeras were generated by using two targeted cell lines (A81 and P70) for morula aggregation with CD1 embryos. Chimaeras from the A81 cell line exhibited germline

transmission but chimaeras from the P70 cell line did not. Thus, *Rom1*$^{+/-}$ mice were generated by crossing chimaeric A81 males with CD1 females. Crosses of outbred heterozygous mice produced wild-type, heterozygous *Rom1*$^{+/-}$ and homozygous *Rom1*$^{-/-}$ animals.

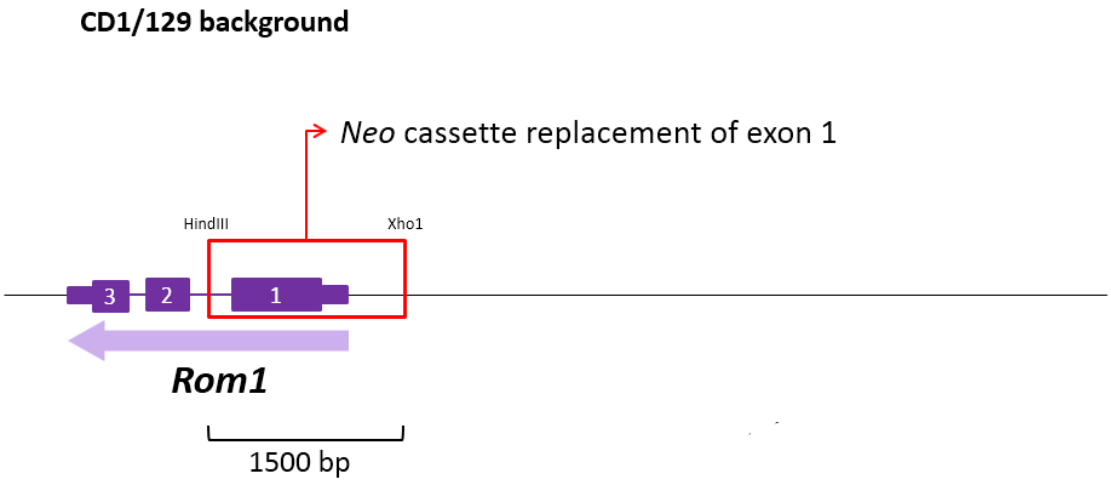

Figure 1.8: Map of the *Rom-1* targeted allele. Adapted from [45].

Immunoblotting was carried out to examine the expression of the ROM1 protein in mouse retinal lysates. The *Rom1*$^{+/-}$ mouse retinal lysates contained levels of the ROM1 protein similar to that of wild type mouse retinal lysates. However, there was an absence of expression of the ROM1 protein in the *Rom1*$^{-/-}$ mouse retinal lysates, thus validating the generation of the null allele (Figure 1.9).

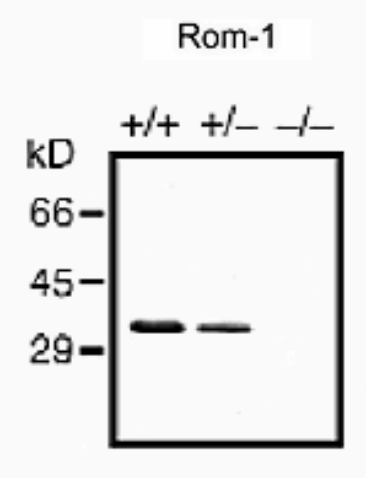

Figure 1.9: Western blot analysis of retinal protein extracts from 8 week-old mice probed with an antibody to ROM1 [45].

1.2.3 Retinal phenotype observed in the Rom1 knock out mice (CD1/129 genetic background)

Loss of ROM1 expression caused photoreceptor death [45]. Measurement of the ONL thickness on thin sections of wild type, heterozygous and homozygous mutant retinas revealed a progressive reduction in the ONL thickness of the *Rom1*$^{-/-}$mice compared to that of the *Rom1*$^{+/+}$ and *Rom1*$^{+/-}$mice beginning at two months of age (Figure 1.10). Whereas the number of rod PRs had decreased, there was no difference in the number of cone photoreceptor cells between wild type and *Rom1*$^{-/-}$mice at 18 months of age. This data confirmed that ROM1 is required for the maintenance of rod photoreceptors and not for the maintenance of cone photoreceptors.

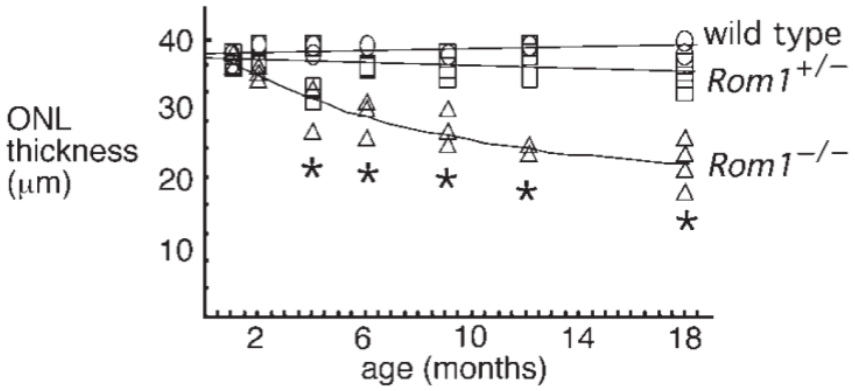

Figure 1.10: Graphical representation of the ONL thickness of the *Rom1* wild type (circle), *Rom1*$^{+/-}$ (square) and the *Rom1*$^{-/-}$ mice (triangle) with progression of age. Each symbol represents results from an individual mouse. ONL thickness in *Rom1*$^{-/-}$ mice is significantly less than that of wild type retinas by approximately 4 months. Adapted from [45].

Upon analysis of *Rom1*$^{+/+}$ and *Rom*1$^{-/-}$ retinal sections by electron microscopy, it was demonstrated that the rod outer segments of *Rom1*$^{-/-}$ mice contained elongated disks suggesting that the loss of ROM1 protein caused disruptions in the regulation of disk size. The disk diameters of the surviving rod photoreceptor cells were measured in 2 and 18 month old mice. While the mean disk diameters of wild type and heterozygous mice remained similar at the two ages examined, there was a 39% (P<0.001) increase in the mean disk diameters of *Rom1*$^{-/-}$ mice at both ages. In addition, whereas the rod OS disks of a 2 month old wild type mice were flat and well organized, the rod OSs of *Rom1*$^{-/-}$ mice had large inter disk gaps and were highly disordered. As the mice aged, the disorganization became less evident. In the *Rom1*$^{-/-}$ mice the cone OS ultrastructure was normal, suggesting that ROM1 is not required for the development or maintenance of cone OSs [45].

The phenotypes observed suggested that the early disorganization of the outer segment in the *Rom1*$^{-/-}$ mice was due to an increased disk diameter. With progression of age in the

homozygous mutant mice, the rod photoreceptors slowly died by apoptosis. This lead to a reduction in the lateral pressure exerted by the adjacent outer segments allowing the enlarged disks to fit better into the outer segments. This is the reason behind the temporary disorganization of the OS of rod photoreceptor cells in the *Rom1*$^{-/-}$ mice.

1.2.4 Perinatal lethality observed in Rom1-KO mice (B6-congenic background)

The *Rom1*-KO mutation was transferred from the CD1/129 mixed genetic background to the B6 congenic background. Successive back crossing for a total of ten generations yielded C57BL/6J congenic mice. When the B6-congenic *Rom1* heterozygous mice were inter-crossed, there were no surviving knock out (KO) offspring. The genotypic ratios (25% WT, 25% KO, and 50% heterozygotes) at embryonic day 18.5 were determined to be normal. The homozygous deletion of *Rom1* on a C57BL/6J inbred genetic background resulted in perinatal lethality. Most of the KO mice die within the first few hours after birth. Occasionally B6-congenic knockout mice survive beyond the weaning age - to date we have had 5 live congenic KOs out of 247 weaned progeny from the heterozygote intercrosses. Since 25% of the mice were expected to be KO (62 mice) we have 8% survival of KO mice at weaning age. A chi-square test defines the genotypic ratios as significantly different from expected with $p<0.0001$.

1.2.5 The discovery of the Rom1/Eml3 double knockout

The fact that perinatal lethality was obtained by deleting a rod photoreceptor-specific gene was surprising. Two hypotheses were then formulated: perhaps a *de novo* mutation was acquired during back-crossing into the B6 genome, alternatively, perhaps a neighboring gene had been disrupted. The first hypothesis was dismissed by restarting the backcrossing from surviving

outbred KO mice: the perinatal mortality phenotype was obtained again within the first three generations. To test the second hypothesis, the newly available mouse genome sequence was revisited. Analyses of the sequence annotations revealed the presence of a contiguous gene called the Echinoderm Microtubule-Associated Protein-Like 3 *(Eml3)*, present in a head-to-head fashion with *Rom1* separated by only 300 bps of DNA (Figure 1.11, panel A). The 1500 bp deletion in the *Rom1* genomic region removed more than two-thirds of the 5' untranslated region (UTR) of *Eml3* as well. The deletion of the 5' UTR region of *Eml3* did not affect the coding sequence of the gene. However, it was determined that although the entire *Eml3* coding DNA sequence is transcribed but is not translated (Figure 1.11, panel B). EML3 codes for an 897 amino acid protein and is therefore predicted to have an apparent molecular weight of approx. 90kDa in immunoblots. Immunoblotting performed using adult retinal lysates from wild type and KO mice show absence of expression of both ROM1 at 37 kDa and EML3 at 90kDa in the KO retinal lysates. The absence of EML3 protein expression is observed when anti-EML3 antibodies against both the N- and C-terminal of EML3 are used (Figure 1.11, panel B). The immunoblot results thus determined that the mice are *Rom1/Eml3* double knock-outs (DKO).

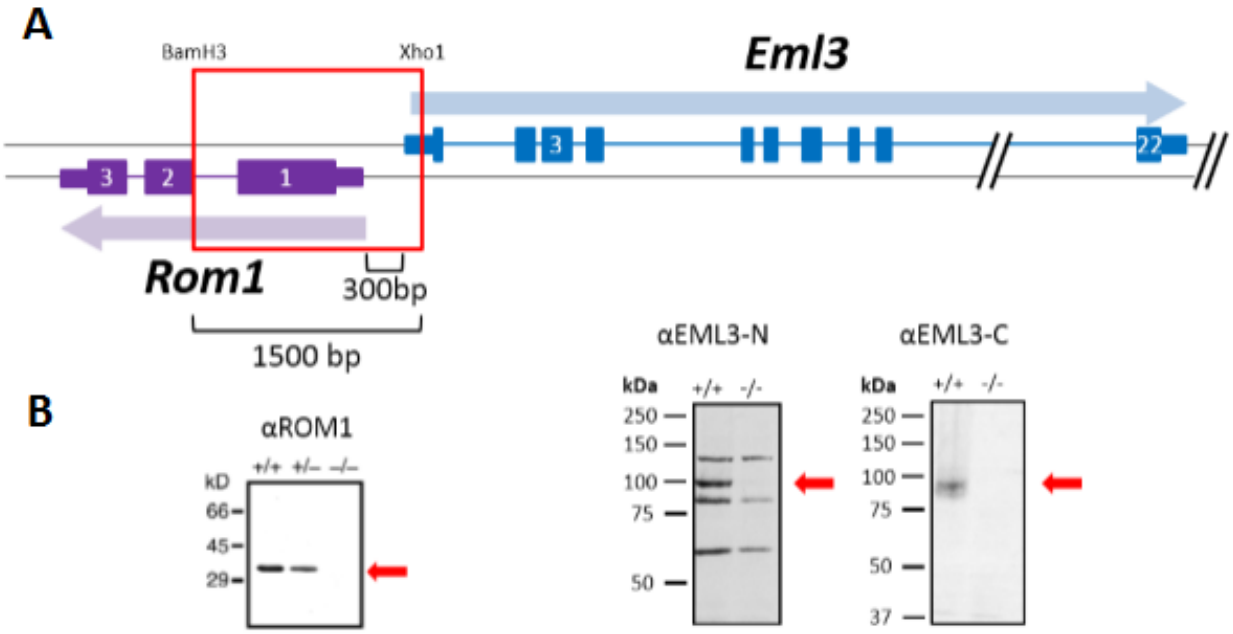

Figure 1.11: Map showing position of *Rom1* and *Eml3* in the mouse genome (Panel A). Immunoblot analysis reveals absence of expression of both ROM1 and EML3 protein in the *Rom1/Eml3* double knockout (Panel B). McInnes lab, unpublished.

Revisiting the *Rom1/Eml3* genomic sequence of the mutant mice, we realized that the neomycin resistance gene is oriented with its 3' end pointing towards the *Eml3* gene. The neomycin cassette with its strong promoter, splice donor and stop codons thus effectively silences the *Eml3* gene. Transcription starts at the strong Phospho glycerate kinase promoter included in the Neo-cassette. After transcription of the Neo coding sequence, the messenger RNA is spliced into *Eml3* exon 2, thus skipping transcription of exon 1 which contains the translation start site. For this reason, the *Neo-Eml3* mRNA is transcribed; however, the end

product of translation is the neomycin resistance gene product and not EML3 (Figure 1.12).

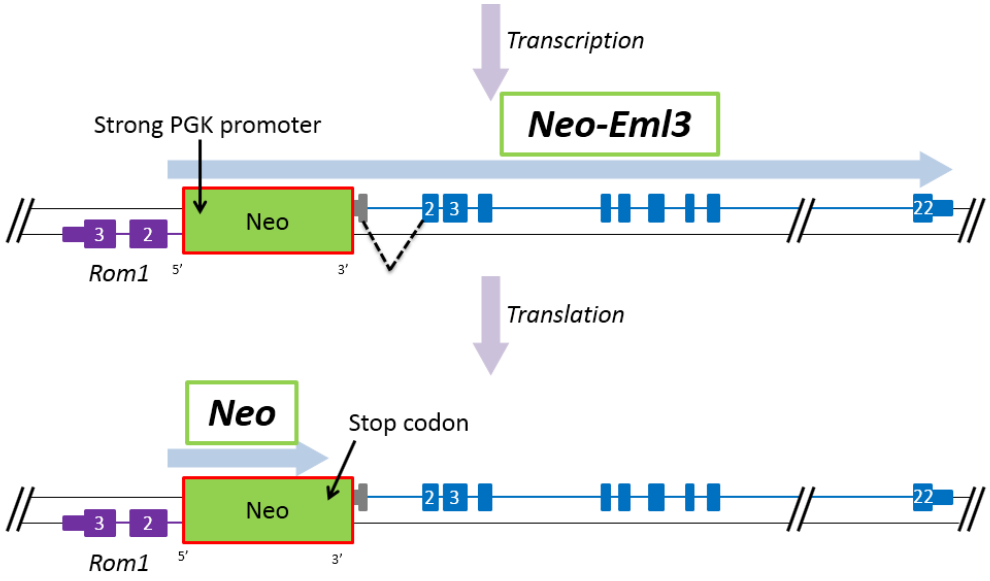

Figure 1.12: Representation of the position of the Neomycin resistance gene in the knockout construct. McInnes lab, unpublished.

1.2.6 Distinguishing the two genetic defects present in the DKO mice

There were two major phenotypes observed for the DKO mice depending on their genetic background: photoreceptor degeneration in the CD1/129 mixed genetic background and perinatal lethality in the C57BL/6J in-bred genetic background. The DKO mice in a CD1/129 mixed genetic background do not exhibit the perinatal lethality phenotype. They have normal lifespans, appear healthy and are fertile. When the mutation is transferred from the CD1/129 genetic background to the B6-congenic background, the *Rom1/Eml3* DKO mice show perinatal lethality. One hypothesis is that each of the two genetic defects present in the DKO mice is responsible for only one of the two phenotypes observed. That hypothesis can be extended to predict that the modifier alleles present in the CD1 outbred genetic background neutralize the

genetic defect responsible for perinatal lethality but not the one responsible for the rod photoreceptor degeneration phenotype.

To find out which gene is responsible for each of the two genetic defects observed, we delved into the literature and found a study that showed that the presence of a dominant-negative single base pair N-ethyl-N-nitrosurea-(ENU) induced mutation in *Rom1* in DBA X B6 inbred mice recapitulates the photoreceptor death phenotype without the perinatal lethality phenotype [48]. We therefore speculate that *Eml3* is a strong candidate for the perinatal lethality phenotype observed in the DKO mice on the B6 congenic background.

Currently, our lab is generating an *Eml3*-specific knockout as well as a rod photoreceptor-specific *Eml3* knockout using the European Conditional Mouse Mutagenesis Program (EUCOMM) (Figure 1.13). Briefly, the targeting cassette contains a trapping element with an *En2* splice acceptor, and SV40 polyadenylation sequences; signals that have proven highly effective in creating null alleles in mice [49, 50]. The targeted ES cells obtained from EUCOMM contain a gene-trap reporter allele (called tm1a allele) that contains a trapping cassette with an IRES*: LacZ* reporter and a fixed promoter-driven neo cassette, all inserted into the intron located between exon 10 and 11 of *Eml3,* to disrupt gene function. The neo promoter allows selection of targeted cells for genes that are not expressed in ES cells (Figure 1.13, panel A). The tm1a allele can be modified in ES cells or in crosses to transgenic *FLP* and *Cre* mice. The Tm1b allele is generated when Cre deletes the promoter-driven selection cassette and floxed exons (exons 11-16) of the tm1a allele (Figure 1.13, panel B). Thus, the tm1b allele can be generated to ensure disruption of the target gene should the gene-trap fail to do so. The conditional allele tm1c is generated by removal of the gene trap cassette *(Lac Z)* by FLP recombinase, thus

restoring gene activity and leaving *loxP* sites on either side of the second set of exons (exons 11-16) (Figure 1.13, panel C). Deletion of the floxed exons of tm1c allele by Cre generates the tm1d allele which is the organ- or cell-type specific null allele (Figure 1.13, panel D) [51].

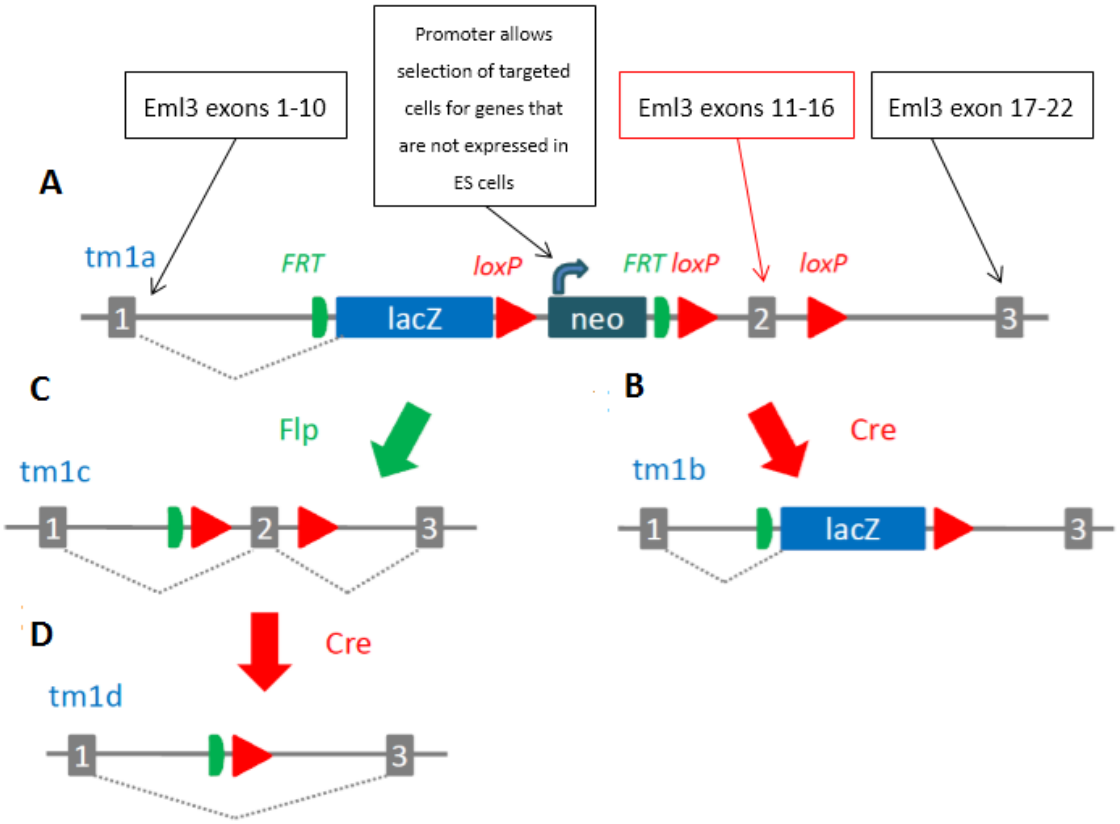

Figure 1.13: Schematic of the Eml3 alleles that can be generated. Panel A: Tm1a represents the targeted trap allele that was generated in the ES cells and founder mice. Panel B: Tm1b represents the "lacZ tagged null allele". Panel C: Tm1c is the "conditional allele", which is essentially a WT allele that enables the production of tm1d allele. Panel D: Tm1d is the "organ or cell-type specific null allele". Adapted from [51].

We have already generated tm1a (gene-trap) homozygous mice and we have determined that some of the phenotypes observed in the *Rom1/Eml3* DKO mice are recapitulated in the *Eml3* gene-trap mice - including perinatal lethality, small size of the mutant embryos (compared to

the WT and heterozygous littermates) and Focal Neuronal Ectopias (FNEs) in the brain. Our laboratory is currently characterizing further these *Eml3*-specific gene-trap mice and we have begun to generate the rod photoreceptor-specific KO allele.

In conclusion, from the phenotypes observed in the ENU mutagenesis-induced *Rom1* mutant mice and the phenotypes observed in our *Eml3*-specific gene-trap mice, we can hypothesize that deletion of *Rom1* causes the photoreceptor degeneration phenotype while the perinatal lethality phenotype is caused by the deletion of *Eml3*.

1.3 The Echinoderm Microtubule-Associated Protein-Like 3 (EML3)

1.3.1 The EML protein family

The formation and function of microtubules is regulated by proteins called microtubule associated proteins (MAP) that have an effect on the structure, assembly, disassembly and interaction of microtubules with other proteins. The dynamic process of microtubule formation is essential for cell polarity, migration, division and mechano-transduction. Despite the essential role performed by microtubules in eukaryotic cells, little is known about the precise function of many MAPs [52]. Structural and biochemical studies initially revealed a role of MAPs in neurons [53, 54]. *In vivo* experiments suggested that MAPs stabilize microtubules in the brain [55, 56] and MAPs have the capacity to alter the morphogenesis of neuronal cells [57, 58]. The echinoderm microtubule associated protein (EMAP) was first discovered in sea urchins where it co-purifies with microtubules [52]. In sea urchins, EMAP is abundant in embryonic and differentiated cells. EMAP localizes to the mitotic apparatus and the cytoplasmic microtubules in interphase cells [52, 59]. In mammals, the homologs of the EMAP protein constitute the EML

(EMAP-like) protein family. Six EML proteins (EML1-6) have been identified. All the EML proteins in mammals have a HELP (Hydrophobic EMAP-like protein) domain which is unique to the family and WD40 repeats (Figure 1.14) [60-64]. The isoforms of EML1, EML2 (isoform2), EML3 and EML4 used to perform co-immunoprecipitation experiments in this study are presented in figure 1.14.

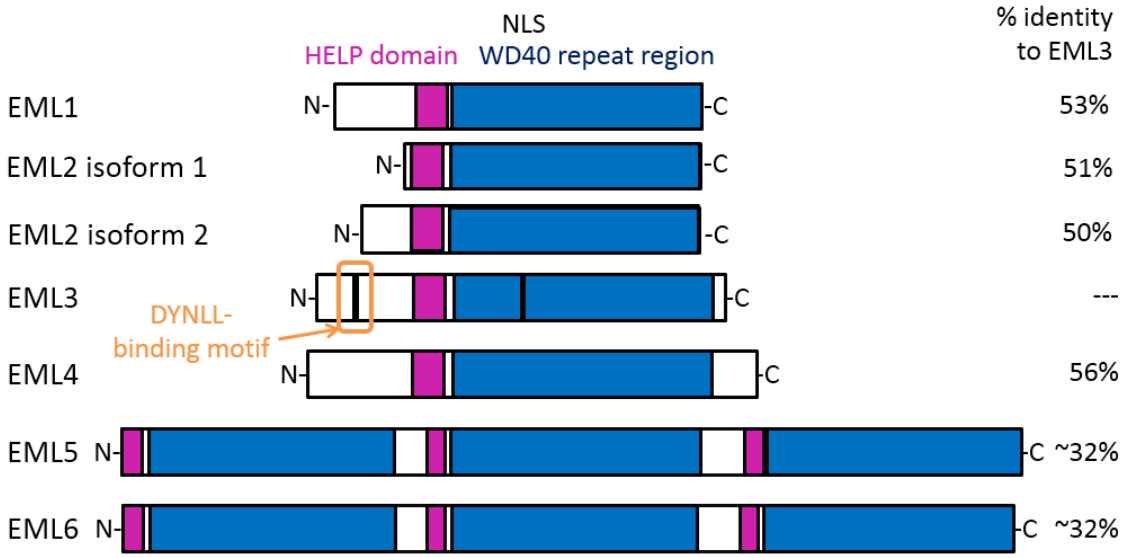

Figure 1.14: Similarities and differences between members of the EML family of proteins. McInnes lab, unpublished.

The WD40 repeat is a 40 amino acid motif often terminating in Tryptophan (W)-Aspartic acid (D) dipeptide. WD40 repeats are found in all eukaryotes and form a β-propeller structure that serves as an interacting domain [63, 65, 66]. In EML 1-4, the variable number of WD40 repeats fall within a core region of approximately 70kDa in size that includes the 60 amino acid conserved HELP motif (figure 1-16, Panel A). The paralogs EML5 and EML6 consist of three tandem repeats of the core 70kDa region [61]. EML1-4 have a coiled-coil (CC) region in their *N*-termini that allows oligomerization [67]. EML3 is particular amongst all the other paralogs since

it contains a DYNLL (Dynein light chain) binding motif and a nuclear localization signal (NLS). Although the EML proteins share high sequence similarity amongst each other, they have very little sequence homology with other microtubule-associated proteins and their functions are yet to be fully elucidated [60].

While one of the EMLs, EML2 is a microtubule destabilizing protein [60], some studies have reported the role for the other EMLs in spindle function during mitosis [52, 68]. Immunofluorescence analysis has shown that EML3 localizes both to the nucleus and to cytoplasmic microtubules during interphase. During mitosis, when the nuclear membrane has broken down, EML3 localizes to the mitotic spindle. Depletion of EML3 in HeLa cells using siRNA induces misalignment of chromosomes during metaphase and delays anaphase initiation [63]. Studies conducted on the other paralogs also suggest that the EML proteins play important roles during mitosis [62, 63]. Studies on EML4 revealed that it is required for organization of the mitotic spindle, attachment of mitotic spindle to kinetochores and recruitment of NUDC (a critical factor for mitotic progression) to the mitotic spindle. According to the literature, EML4 localizes to the mitotic spindle and its depletion prevents cellular proliferation [62, 69]. Despite the literature, a thorough understanding of the molecular function of the EML proteins during mitosis is lacking.

1.3.2 The EML protein domain architecture

A study on the crystal structure of the C-terminal 70kDa core of EML1 revealed a closely associated pair of β-propellers known as the TAPE (tandem atypical propellers in EML) domain (Figure 1.15, Panel B) [67]. The N and C-terminal β-propellers are each composed of seven blades. Each blade is a twisted, four stranded, anti-parallel β-sheet that radiates from the

center of the domain and is encoded by a separate WD40 repeat. The C-terminal β-propeller is unique, as one of the blades of the propeller is formed from a discontinuous subdomain which is unrelated to the WD40 motif. That study also revealed that the HELP motif is not an independent motif but is the hydrophobic core that joins the N and C terminal β-propellers. Deletion of the HELP motif causes disrupted folding of the TAPE domain [67]. The TAPE domain binds soluble α/β tubulin dimers through the conserved concave surface [67, 70]. Another more recent study on the crystal structure of the N-terminal region of EML1 revealed a trimeric oligomerization state adopted by the EML proteins. The N-terminal region of the EML protein family is poorly conserved compared to the TAPE domain. The trimerization domain (TD) is an island of conserved primary sequence within the N-terminal region that is consistent with a coiled-coil. That study showed that the trimerization domain (TD) is necessary and sufficient for self-association of the EML proteins. Cell-based and *in vitro* MT binding assays were used to demonstrate that MT binding of EML1 does not require the TAPE domain. The N-terminal region of EML1 confers MT binding and the TD is critical for MT binding. However, the TD is not sufficient for MT association which requires the 90-residue region between the TD and the TAPE domain [71].

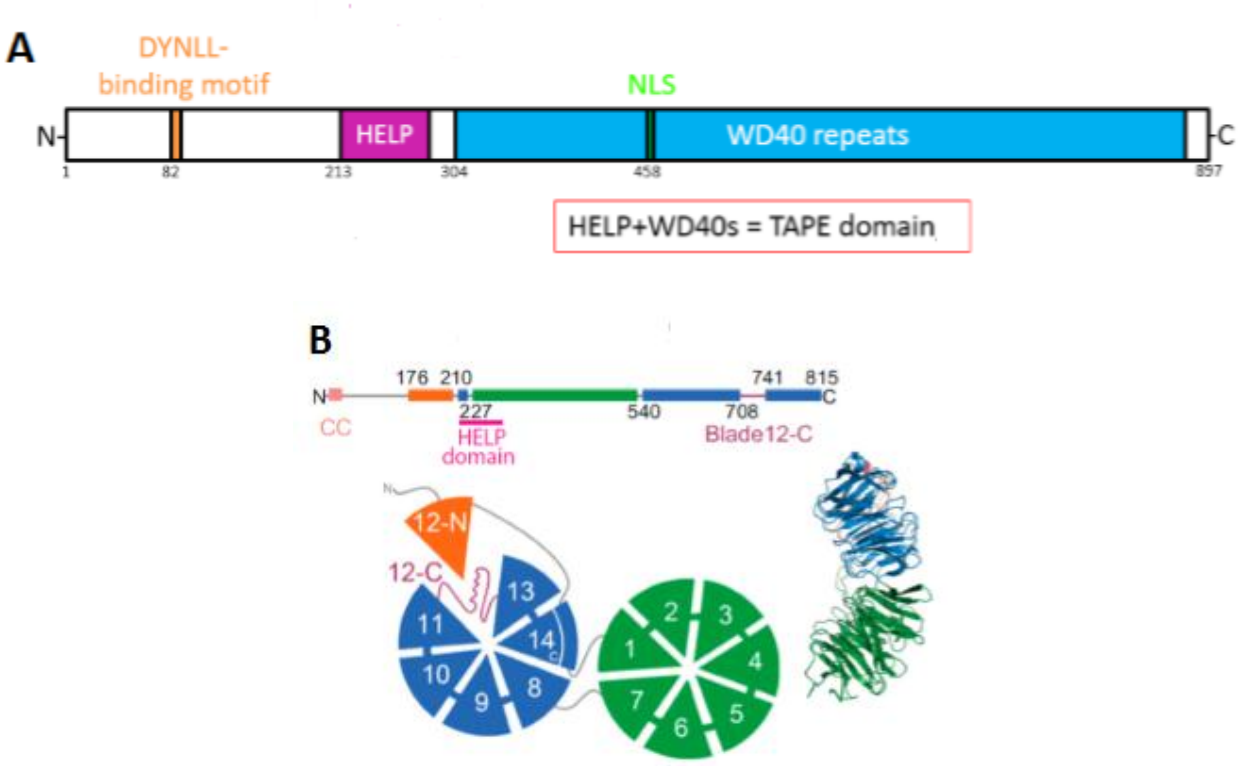

Figure 1.15: Panel A shows the protein interaction domains of the EML family of proteins. Panel B shows the structure of the EML TAPE domain. Adapted from [67].

1.3.3 Functions of EML3 in the cell

The function of EML3 in the cell has been studied by the group of O.J. Gruss. The localization of EML3 in HeLa cells was analyzed using indirect-immunofluorescence and siRNA-mediated knockdown revealed a role played by EML3 in the correct alignment of chromosomes in metaphase [63].

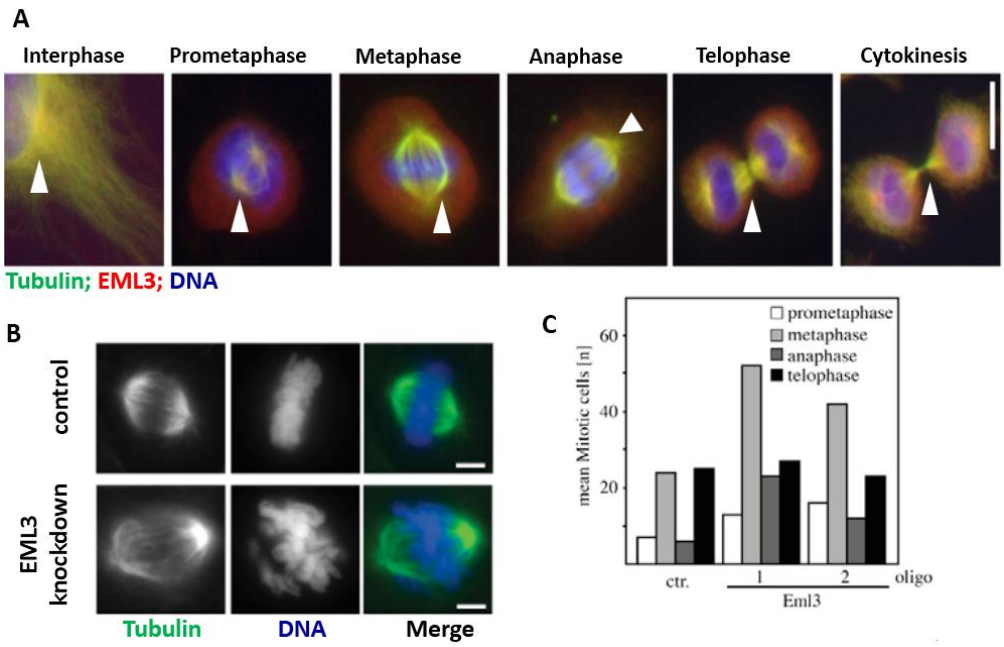

Figure 1.16: EML3 is a microtubule binding protein required for spindle function and chromosome capture. Panel A shows the characterization of EML3 localization by indirect immunofluorescence in different mitotic phases and interphase of HeLa cells. EML3 is stained in red, α-tubulin in green; DNA is stained in blue with DAPI. Panel B shows representative immunofluorescence images of aberrant metaphase like structures with unaligned chromosomes in cells where *Eml3* was silenced. Panel C shows the mean number of mitotic cells after EML3 knock down in HeLa cells [63].

To examine the localization of EML3, antibodies were raised against the human protein. Indirect immunofluorescence on fixed HeLa cells showed that EML3 localized to microtubules throughout the different stages of mitosis as well as in interphase (Figure 1.16, Panel A). To determine the role of EML3 in mitosis, *Eml3* was knocked down in HeLa cells using two different siRNA oligonucleotides. Cells with siRNA-mediated knock down of *Eml3* failed to align chromosomes properly to the mitotic spindle during metaphase (Figure 1.16, Panel B). Thus, siRNA mediated depletion of EML3 increased the mitotic index of cells. Specifically, there was an increase in the mean number of cells in the metaphase stage of mitosis (Figure 1.16, Panel C). In summary, a combination of localization analysis and an assay for cell division and

proliferation was used in that study to suggest that EML3 plays an important role in the 'search and capture' of chromosomes during mitosis. Loss of EML3 function in cells delays the bivalent attachment of chromosomes to microtubules and activation of the spindle assembly checkpoint during mitosis [63].

1.3.4 EML3 and ROM1 spatio-temporal expression

ROM1 and EML3 have similar expression patterns in the wild type adult mouse. Quantitative PCR analysis revealed predominant expression of both ROM1 and EML3 in the retina compared to other organs in wild type adult mice (Figure 1.17).

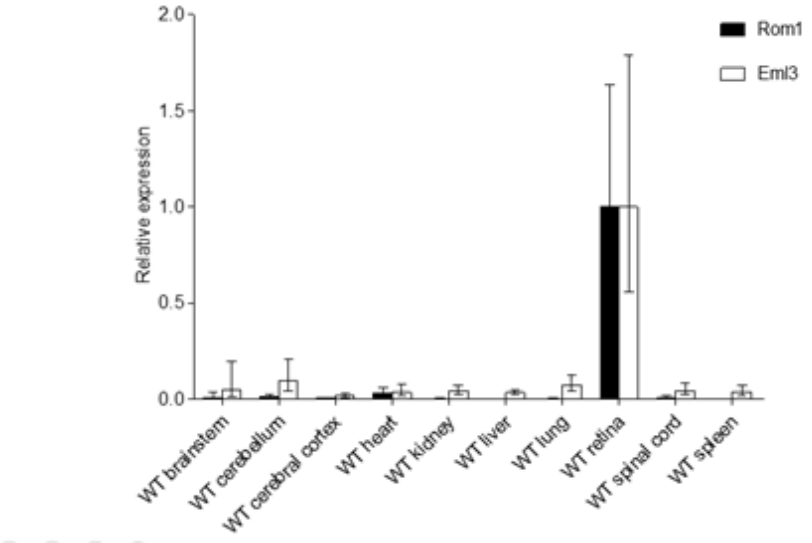

Figure 1.17 Graphical representation of the relative mRNA expression of *Rom1* and *Eml3* in different organs in mice relative to the retina as determined by quantitative RT-PCR. McInnes lab, unpublished.

EML3 is expressed at varying levels during mouse embryogenesis. Immunoblotting performed on whole-mouse embryonic lysates at different ages revealed varying levels of EML3 during mouse embryogenesis with highest relative expression of EML3 at around embryonic days 14.5 and 15.5 (Figure 1.18). Noteworthy, relative expression of EML3 in the E15.5 embryo is higher

than the relative expression of EML3 in the adult (PN50) retina. The protein expression data was normalized to the protein content of the tissue lysates and house-keeping protein GAPDH is shown in parallel for reference.

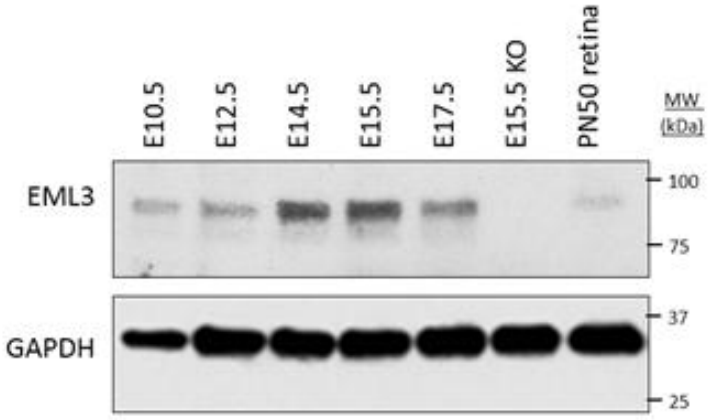

Figure 1.18: EML3 protein expression time course during mouse embryogenesis. WT mouse embryo (E10.5-E17.5), KO mouse (E15.5) and adult mouse (PN50) retina were homogenized and lysates were generated under co-IP conditions. A total of 12uL of sample consisting of lysate, co-IP buffer and 4X SLB were loaded on to the SDS gradient gel. Each lane was loaded with 10ug of protein. Immunoblot analysis were performed with rabbit anti-EML3C884A antibody, at a concentration of 1:2000 and rabbit anti-GAPDH antibody, at a concentration of 1:1000. McInnes lab, unpublished.

1.3.5 Phenotypes observed in the Eml3-knockout embryos

All *Eml3* knock out embryos from E9.5 to E18.5 are smaller than their littermate controls by an average of 38% as measured by weight (or volume in E9.5 embryos). The brains of E18.5-KO embryos display certain anatomical abnormalities such as focal neuronal ectopias (FNEs) in the dorsal telencephalon (Figure 1.19) and dilated lateral and third ventricles. About two-thirds of E18.5 embryos analyzed have FNEs and about half of E18.5 embryos analyzed have dilated ventricles. Some embryos present both phenotypes.

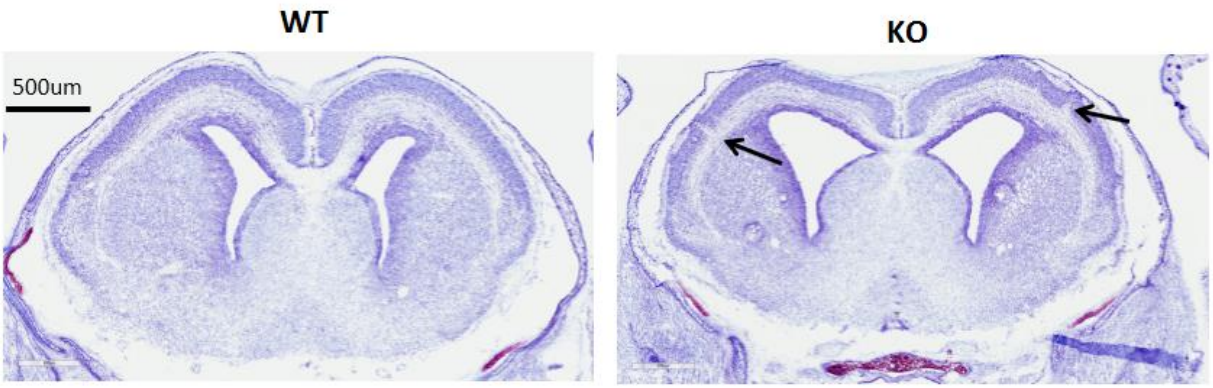

Figure 1.19: A representative view of a coronal section of the brain of an E18.5 *Eml3*-KO mouse with focal neuronal ectopias (arrows) compared to an equivalent of wild type section (left). McInnes lab, unpublished.

'Neuronal ectopia' refers to the defective positioning of neurons it is typically caused by neuronal migration defects. Malformations can be classified as type I lissencephaly, which is a consequence of an under-migration of neurons and type II lissencephaly (also known as cobblestone lissencephaly) which results from an over-migration of neurons [72, 73]. The focal neuronal ectopias observed in the *Eml3*-KO mice constitute a cortical dysplasia that resembles type II lissencephaly. Disorders such as lissencephaly and cortical band heterotopia have been associated with epilepsy and intellectual disability in humans. The HeCo mutant mouse model displays subcortical band heterotopia. *Eml1* is the mutant gene that was identified in the HeCo mice [74]. The mutant mouse develops a heterotopic cortex (HeCo) lying in the dorsolateral hemispheric region [75]. In early corticogenesis, the developing cortices of the HeCo mice exhibit a proportion of abnormally distributed cells in the intermediate zone (IZ) and cortical plate (CP) [74]. The *Eml1* mutant HeCo mice exhibit heterotopia in the brain due to misplaced apical progenitors. In the mutant mice, dividing progenitors were abnormally distributed throughout the cortical wall from embryonic day 13. Re-expression of *Eml1* rescued the

phenotype. The band heterotopia in the *Eml1* HeCo mutant mice is due to an under-migration of neurons [74]. Currently, our lab is investigating the abnormal neuronal migration observed in the cortices of the *Eml3*-KO mice. In contrast to the under-migration of neurons in the *Eml1* mutant HeCo mice, there is an over-migration of neurons in the cortex of the *Eml3*-KO mice. Neuronal migration is a critical phase of nervous system development. The process of neuronal migration is divided into two phases, one being the extension of the leading process and movement of the cell body and the second phase being nucleokinesis. Both phases rely on cytoplasmic dynein, cell polarity proteins and microtubule-associated proteins that remodel microtubules. [72]. There is a possibility that EML3 and its association with microtubules could affect neuronal migration

1.3.6 EML3 - A ciliopathy-associated protein

Ciliopathies comprise a group of disorders which encompass a broad array of clinical features mentioned below. Ciliopathies are associated with genetic defects in the biogenesis and/or function of both motile and non-motile cilia [36]. Ciliary dysfunction results in a variety of phenotypes some of which are retinal degeneration, growth defects, renal disease (cysts) and cerebral abnormalities [76]. The literature describes the generation of mouse models of Primary Ciliary Dyskinesia (PCD). One such model is the mouse model of Kartagener's syndrome which contains the presence of an insertional mutation in the axonemal dynein heavy chain gene (*Dnah5; also called Mdnah5 and Dnahc5 in older literature)*. Mice homozygous for this mutation exhibit most of the classical features of PCD that results from dysfunction of the motile cilia [37]. Our rare *Rom1/Eml3*-DKOs that survive beyond the weaning age (~8% survival) display ciliopathy-related defects such as reduction in size, unilateral or bilateral otitis

media, testicular immaturity, bone anomalies – lateral nasal septum deviation, deformity and fusion of sternebrae and deformity of tail vertebrae, as well as hydrocephalus. Some of the phenotypes exhibited by the rare DKO survivors are reminiscent of the *Dnah5*-KO mice. Both the *Dnah5*-KO mice and the surviving *Rom1/Eml3*-DKO mice exhibit perinatal lethality, growth retardation, deviated nasal septum, hydrocephalus and uni/bi-lateral otitis media. However, whether the *Rom1/Eml3*-DKO mice display ciliary immobility, which is one of the hallmark phenotypes of a dyskinesia is subject to further investigation. A phenotype clearly absent in the DKO mice that exists in the *Dnah5*-KO mice is *situs inversus*.

1.3.7 The photoreceptor is a modified cilium

Disruption of ciliary proteins in the photoreceptor gives rise to phenotypes such as retinal degeneration. Retinitis pigmentosa and retinal degeneration are characteristic features of ciliopathies such as Bardet-Biedel Syndrome, Primary ciliary dyskinesia and Senior-Loken syndrome [76]. Assembly and maintenance of motile and sensory cilia requires the transport of proteins via intraflagellar transport (IFT) [77]. (IFT) has been closely examined in the connecting cilium of rod photoreceptor cells (Figure 1.20).

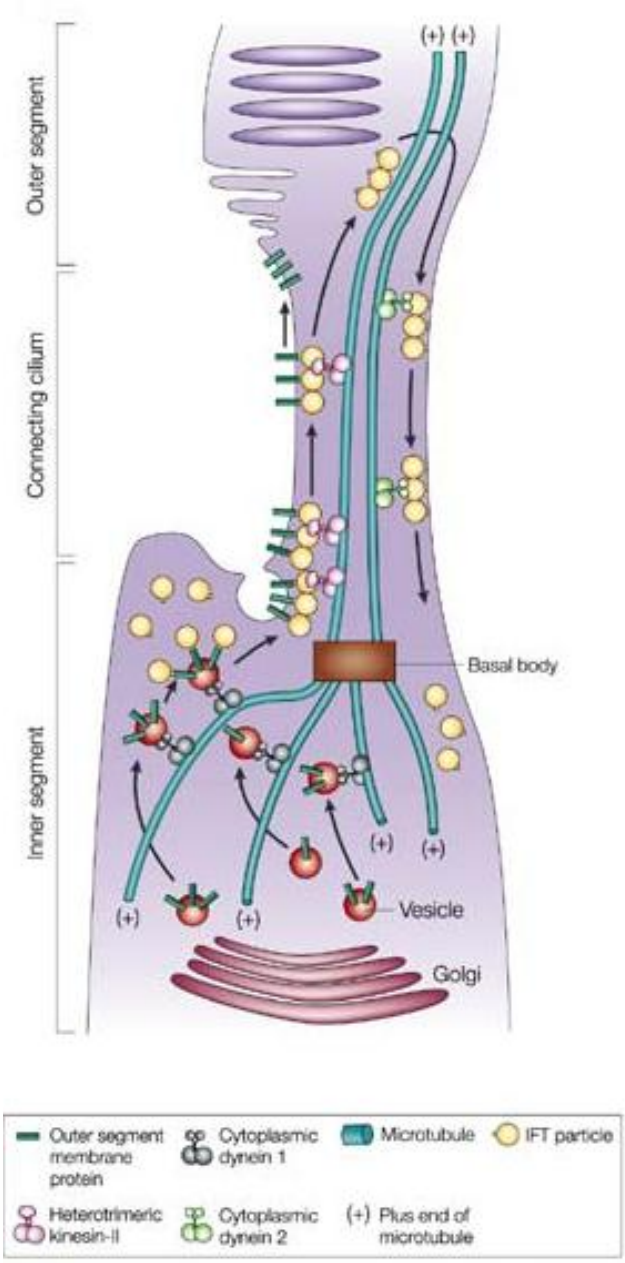

Figure 1.20: A model presenting intra-flagellar transport (IFT) in the connecting cilium (CC) of the vertebrate rod photoreceptor cell. Intracellular vesicles carrying membrane proteins destined for the OS are transported along microtubules by cytoplasmic Dynein motor complexes to the base of the CC, where they dock and fuse with the cell membrane at the peri-ciliary ridge. The membrane proteins destined for the OS become associated with IFT-particle proteins; they are then transported by Kinesin-II through the flagellar pore complex and distally along the microtubules of the CC. The IFT particles are then transported by cytoplasmic dynein 2 back down to the CC to the peri-basal body region [78].

In vertebrate rod and cone PR cells, the IFT motors and particle proteins travel to and from the basal bodies at the base of the connecting cilium [79]. IFT transports large protein complexes from the base of the cilium, through the CC, along the microtubule based axoneme, toward the distal tip in the OS by Kinesin motors (anterograde transport) and from the distal tip back to the cell body by Dynein-2 motors (retrograde transport) [80]. In the PR cell body, the motor protein complex known as cytoplasmic Dynein-1 carries intracellular vesicles containing proteins destined for the OS along microtubules by the process of retrograde transport towards the base of the connecting cilium (CC) [76]. IFT particle cargo complexes in the retina include opsin, phospholipids, proteins of the cytoskeleton, membranes and soluble proteins of the OS [77]. Immunofluorescence analyses performed by Isabelle Carrier, a research associate in our lab, on cryo-sections of adult mouse retina, revealed that EML3 localizes to the inner segment of the retina (Figure 1.21).

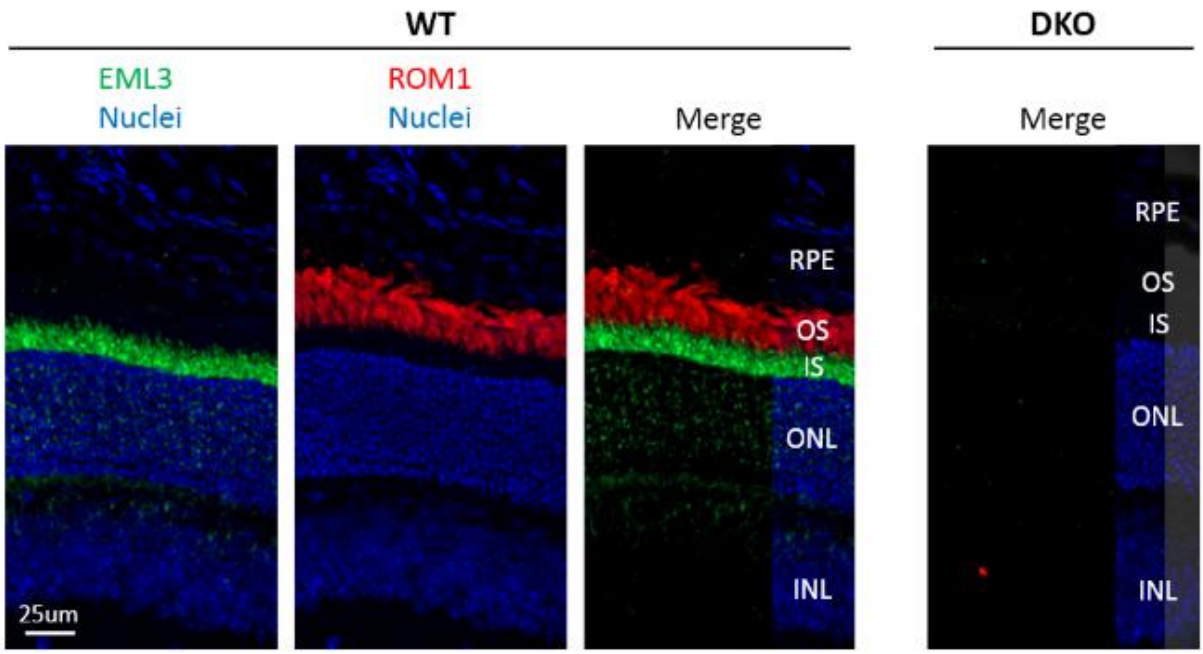

Figure 1.21: EML3 localizes to the inner segment of the retina. Indirect immunofluorescence was performed on TCA fixed adult (PN28) mouse retinas. The different layers of the retina in the WT and DKO retinal sections are labeled. EML3 (green), ROM1 (red) and the nuclei (blue) are shown. McInnes lab, unpublished.

Given the fact that, EML3 is a microtubule-associated protein and that it localizes to the IS of rod photoreceptors which is a modified cilium, as well as the fact that its deletion causes ciliopathy related phenotypes, defines EML3 as a ciliopathy-associated protein and suggests that it might be involved in the transport of IFT particles from the IS towards the basal body a the base of the connecting cilium.

1.4 Objectives

The overall objective of my thesis project was to identify the interacting partners of EML3. The specific aims of my project were, first, to identify the potential interacting partners of EML3 based on literature and available high-throughput protein interaction data. This work is

presented in section 3.1. The second specific aim was to test the candidate interactions by co-immunoprecipitation in a co-transfection system. The strategy was to over-express EML3 and the candidate interacting protein in HEK 293T cells. This was followed by preparation of cell lysates under mild co-immunoprecipitation conditions, followed by immunoprecipitation of EML3. Finally, immunoblot analysis was performed to check for interaction between EML3 and the candidate interacting partner. Converse experiments (immunoprecipitation of candidate interactor followed by detection of EML3) were carried out to confirm the results. That work is described in Section 3.2.

The third specific aim was to use immunofluorescence (when availability of antibodies made it possible) to show co-localization of EML3 with the confirmed candidate interacting partner(s). Confocal microscopy following staining with antibodies was used to show co-localization of EML3 and the interacting partner DYNLL. Immunofluorescence on retinal sections identified the particular cellular compartment where EML3 and its interacting partner DYNLL are expressed. This work is described in section 3.3.

Finally, this project will shed light on the molecular functions of *Eml3*, a gene which our initial studies have shown to be required for mouse development and post-natal viability.

Chapter 2: Materials and Methods

2.1 Mammalian expression constructs

Full-length mouse *Eml3* cDNA cloned into the pCMV6-Kan/Neo vector was purchased from Origene (catalog number MC201737). The mouse *Eml1-*$_{tGFP}$ construct cloned into the pCMV6-AC-GFP vector was purchased from Origene (catalog number MG217188). Mouse *Eml2-*$_{GFP}$ and mouse *Eml4-*$_{GFP}$ cDNA clones were made by Susanne Bechstedt, an active collaborator from the Brouhard lab at McGill University. Both the *Eml2-*$_{GFP}$ and *Eml4-*$_{GFP}$ constructs were cloned into a pCMV-EGFP vector by Susanne. Full-length mouse *Rom1* cDNA cloned into a pCMV6 Kan/Neo expression vector was ordered from Origene (catalog number MC205489). Full-length mouse *Neto2-*$_{HA}$ cDNA was cloned into a variant of pc-DNA-3.1 myc-His-A-(+) (Invitrogen) containing two copies of the influenza hemagglutinin (HA) epitope tag as described in Tang *et al*., Plos ONE 2012 [81]. Full-length mouse *Dynll1-*$_{MYC\text{-}DDK}$ cDNA and full-length mouse *Dynll2-*$_{MYC\text{-}DDK}$ cDNA expression vectors (pCMV6 entry vectors) were purchased from Origene (catalog numbers MR219424 and MR200217 respectively). All cDNA constructs used in this study were verified by Sanger sequencing at the McGill University and Génome Québec Innovation Centre. Protein sequences corresponding to the cDNAs used in this study are presented in Section 2.9.

2.2 Preparation of plasmid DNA for transfection

Mammalian expression construct DNAs were transformed into *E. coli* strain DH5α. A single colony was inoculated into 5 mL LB broth containing the appropriate antibiotic and grown with shaking at 250 rpm for 8 hours at 37°C. This inoculation was diluted 1:100 and 1:500 into 100 mL LB broth containing the same antibiotic and grown with shaking at 250 rpm overnight at

37°C. Cultures in late logarithmic growth phase were identified by optical density (OD) and chosen for the DNA preparations. Purification of plasmid DNA was completed using the Thermo Scientific GeneJET Plasmid Midiprep Kit (catalog number FERK0481) in accordance with the manufacturer's protocol.

2.3 Quantification of cDNA

The quantity and purity of the prepared plasmids were assessed by taking absorbance readings for dsDNA at 260 nm and 280 nm using the Eppendorf BioPhotometer plus. The reading at 260 nm allowed for calculation of the concentration of nucleic acid in the sample. The reading at 280 nm indicated the amount of protein in the sample. The ratio of nucleic acid to protein (OD260/OD280 ratio) was used as an indicator of the purity of DNA samples. The presence of the desired purified cDNA was verified by Sanger sequencing at the McGill University and Génome Québec Innovation Centre.

2.4 Cell culture and transfection

The HEK 293T/17 (ATCC CRL-11268) cells used for the co-immunoprecipitation experiments were generously provided by the lab of Dr. Gerasimos J. Zaharatos (Department of microbiology, McGill University). The cells were provided to us at a relatively early seventh passage after importation from the American Type Culture Collection (ATCC) and were never used in our experiments after a 20^{th} passage. Cells were passaged a minimum of two times before being used for experiments. When cell cultures had reached a confluence of 70%, the cells were collected and pooled. Three million HEK 293T cells were plated per 100 mm-diameter culture plate. After one overnight incubation, at approximately 70% confluence, HEK 293T cells

were transiently transfected with the optimum quantity of plasmid DNA using jetPRIME™ Polyplus transfection reagent (Polyplus-transfection SA) (Table 2.1). Typically, the total amount of cDNA transfected into each culture plate did not exceed 5 µg to obtain maximum transfection efficiency. The quantity of each cDNA transfected was optimized by observing the western blot results at the end of each co-immunoprecipitation experiment. The optimum quantity of each cDNA for transfection to obtain maximum protein yield and minimum loss in the flow-through is presented in Table 2.1. Cells co-transfected with the cDNA of EML3 and the cDNA of the candidate interacting protein were grown on 100 mm culture plates in the presence of Dulbecco's Modified Eagle's medium supplemented with glucose, L-glutamine and sodium pyruvate, 10% FBS, 100 lU/mL Penicillin, 100 µg/mL Streptomycin, and 10 mM HEPES at 37°C in a humidified 5% CO_2 incubator. 48h after transfection, cells were washed with ice-cold 1X Phosphate Buffered Saline (PBS) composed of (137mM NaCl, 2.7mM KCl, 10mM Na_2HPO_4, 1.8mM KH_2PO_4). The cells were lysed in ice cold lysis buffer (1 mL/ 100 mm culture plate) containing 50mM Tris-HCl, pH 7.4, 150mM NaCl, 1mM EDTA, 1% NP-40, supplemented with protease inhibitors- Aprotinin (800nM), Leupeptin (21uM), Pepstatin A (15uM) and Phenylmethylsulfonyl fluoride (PMSF) (1mM), and phosphatase inhibitors:- sodium vanadate (1mM), sodium fluoride (5mM), sodium pyrophosphate (1.35mM) and beta-glycerol phosphate (3mM). Lysed cells were incubated on ice for 30 minutes and centrifuged at 22,000*xg* for 15 minutes at 4 °C. The supernatants (cleared lysates) were transferred to new microtubes. The resulting clear lysates are mostly free of nuclei, large cell debris and insoluble components such as cytoskeleton. Microtubules are usually depolymerized down to tubulin dimers under these conditions.

Table 2.1 Quantities of cDNA used in this study

cDNA	**Quantity/(μg)**
Dynll1-DDK	1.25
Dynll2-DDK	1.25
Eml1-tGFP	1.25
Eml2-GFP	2.50
Eml3	1.25
Eml4-GFP	2.50
Neto2-HA	2.50
Rom1	2.50

2.5 Primary and secondary antibodies

The primary and secondary antibodies used for co-immunoprecipitations, immunoblotting and immunofluorescence experiments can be found in Table 2.2.

Table 2.2 Antibodies used in this study

Immunoprecipitations		
IP antibody	**Source**	**Working Dilution (v/v)**
Mouse α DDK; monoclonal	Origene (catalogue number TA50011-100)	1:200
Rabbit α EML3 C884A; polyclonal	In house (antibody raised against the C-terminal peptides C884-897 SRTPSLSPASSLDV)	1:200

Rabbit α GFP; polyclonal	Invitrogen (catalogue number A-11122)	1:400
Mouse α tGFP; monoclonal	Origene (catalogue number TA150041-100)	1:200
Western blot		
Primary antibody	**Source**	**Working Dilution (v/v)**
Mouse α DDK; monoclonal	Origene (catalogue number TA50011-100)	1:4000
Rabbit α EML3 C884A; polyclonal	In house (antibody raised against the C-terminal peptides C884-897 SRTPSLSPASSLDV)	1:4000
Rabbit α GFP; polyclonal	Invitrogen (catalogue number A-11122)	1:4000
Mouse α HA; monoclonal	Millipore (Cedarlane) (catalogue number 05-904)	1:500
Mouse α ROM1; monoclonal	Gift from Dr. Bob Molday (University of British Columbia, Vancouver)	1:40
Mouse α tGFP; monoclonal	Origene (catalogue number TA150041-100)	1:160000
Secondary antibody	**Source**	**Working Dilution (v/v)**
Sheep α mouse IgG HRP conjugated; polyclonal	VWR/GE (catalogue number CA95017-332L)	1:20000
Donkey α rabbit IgG HRP conjugated; polyclonal	VWR/GE (catalogue number CA95017-556L)	1:20000
Immunofluorescence		
Primary antibody	**Source**	**Working Dilution (v/v)**

Rabbit α DYNLL-AF647. The Anti-DYNLL antibody was conjugated to Alexa Fluor 647.	Origene (catalogue number TA303752); modified. Invitrogen (catalogue number A-10475	1:20
Rabbit α EML3- N1; polyclonal	In house (antibody raised against N terminal peptide amino acids GAAGPGEGPAHE)	1:1000
Mouse α ROM1; monoclonal	Gift from Dr. Bob Molday, University of British Columbia, Vancouver	1:20
Secondary antibody	**Source**	**Working Dilution (v/v)**
Donkey α mouse IgG-AF594; polyclonal	Invitrogen (catalogue number A-21203)	1:500
Donkey α rabbit IgG-AF488; polyclonal	Invitrogen (catalogue number A-21208)	1:500

2.6 Co-immunoprecipitations

1% of the total volume of cell lysates (12µL out of 1.25 mL) was stored at -80 °C to be used later as "INPUT" control samples. The remaining cell lysates (~1.5 mg protein) were incubated in the presence of antibodies (2.0 µg) overnight at 4 °C on a rotating platform. Lysates were subsequently incubated with 80 µL of Dynabeads® conjugated to either sheep anti-rabbit IgG antibodies or to sheep anti-mouse IgG antibodies (Thermofisher Scientific) for 3 hours at 4 °C on a rotating platform. The bead-bound proteins were separated from the rest of the cell lysate by placing the sample on a magnet. The beads were rinsed three times in wash buffer (1X PBS supplemented with 0.1% BSA and 2mM EDTA, pH 7.4). Bound proteins were eluted with SDS sample buffer (0.25 M Tris/HCl (pH 6.8), 10% 2-mercaptoethanol, 30% (v/v) glycerol, 8% SDS, 0.02% bromophenol blue, and 0.3 M DTT) followed by SDS-PAGE and immunoblotting.

2.7 Immunoblot analysis of co-IP samples

The protein samples were resolved on 15-well 4-15% gradient Mini PROTEAN TGX precast protein gels (Bio-Rad; catalog number 4561086). The protein samples were then electrophoretically transferred to a nitrocellulose membrane (GE NitroPure, supported, 0.22 micron, catalog number WP2HY00010) in a tank blotting apparatus at 100V, 300mA for 1 hour at 4°C. Membranes were Ponceau-stained and photographed followed by rinsing in 1XTBST (100mM Tris-HCl, pH 7.5, 150mM NaCl, 0.1% Tween (v/v)).

Membranes were blocked over-night at 4°C in 5% skim milk in 1X TBST (w/v), followed by incubation in primary antibody for 2 hours at room temperature. The antibodies used for immunoblotting are noted in Table 2.2. Membranes were washed in 1X TBST two times briefly and two times for a duration of 15 minutes each. Membranes were then incubated with 1:20,000 Horse radish peroxidase (HRP)-conjugated secondary antibody for 30 minutes at room temperature (Table 2.2) followed by washing in 1XTBST two times briefly and two times for a duration of 15 minutes each. Detection of target proteins was carried out by the use of Enhanced Chemi-Luminescent (ECL) Select detection reagents (Amersham; catalog number RPN2235) followed by exposure to Lumi-film Chemiluminescent Detection Film (Roche; catalog number 11666916001).

2.8 Immunofluorescence

2.8.1 Tissue preparation

Retinal tissue preparation was performed by Isabelle A. Carrier, a research associate in our lab. Mice aged post-natal day 24 were anesthetized by isoflurane inhalation, immediately followed

by euthanasia by cervical dislocation. The eyes were marked to keep track of orientation, enucleated, and placed in a petri dish containing ice-cold 1XPBS. The cornea and the lens were removed. The eye-cups were placed in 1XPBS until the fixation procedure. All eyes were fixed in ice-cold 10% TCA for 10 minutes. Following fixation, the tissues were rinsed three times in ice-cold 30mM glycine in 1XPBS for 10 minutes each followed by a brief final wash in ice-cold 1X PBS. Tissues were cryo-protected by incubation in 30% w/v sucrose in 1XPBS at 4°C until the eye settled to the bottom of the microtube.

After saturation in sucrose, the tissues were removed from the sucrose solution and swirled in an Optimal Cutting Temperature (O.C.T.) compound bath until thoroughly coated. The eye tissues were carefully placed in embedding blocks filled with fresh O.C.T. compound that were then frozen over a block of dry ice followed by storage at -80°C. The blocks were equilibrated to a temperature of -20°C 30 minutes prior to cryo-sectioning. 16 µm-thick sections were collected on SuperFrost Plus glass microscope slides (Fisherbrand) using a Leica CM3050S Cryostat set at -20°C. The slides were air-dried and then stored at -20°C until use.

2.8.2 Antibody conjugation

Both the anti-DYNLL and anti-EML3 antibodies used in this study were raised in rabbit. The use of labeled secondary antibodies directed against rabbit immunoglobulin will give rise to cross reactions, if both anti-EML3 and anti-DYNLL antibodies are incubated simultaneously on the tissue. For this reason, we decided to directly label the rabbit anti-DYNLL antibody with Alexa Fluor 647 (Invitrogen; catalogue # A-10475) and carry out sequential incubations. Direct

labeling of the anti-DYNLL antibody allowed simultaneous visualization of both rabbit anti-DYNLL and rabbit anti-EML3 antibodies in adult mouse retinal sections as outlined below.

2.8.3 Antibody staining

Slides were first thawed and air-dried for a minimum of 15 minutes. All incubations hereafter took place in a humid chamber. Sections were washed in HBS (50mM HEPES, 150mM NaCl, ddH_2O, pH 7.4) twice for 5 minutes. Sections were permeabilized by incubating in HBST (1XHBS, 0.1% Triton X-100) for 20 minutes, and then blocked in Mouse on Mouse (MoM; Vector laboratories) blocking solution for 1 hour at room temperature. After blocking, the sections were washed in HBST once for 10 minutes. Primary antibodies diluted in MoM antibody diluent were incubated with the WT and DKO retinal sections for 1 hour at room temperature. The order in which the primary and secondary antibodies were applied to the retinal sections is as follows. The rabbit anti-EML3-N1 antibody and mouse anti-ROM1 antibody (Table 2.2) were applied to the WT and DKO sections. Sections were washed twice briefly followed by three times 10 minutes in HBST. The secondary antibodies were diluted in MoM antibody diluent. Donkey anti-rabbit IgG AF488 and donkey anti-mouse IgG AF594 (Table 2.2) were added to the WT, DKO retinal sections as well as the WT and DKO sections used as secondary controls. The sections were incubated with appropriate secondary antibodies for 30 minutes at room temperature. Finally, the rabbit anti-DYNLL antibody conjugated to AF647 (Table 2.2) was added to the WT and DKO retinal sections for 1 hour at room temperature. Sections were then washed four times briefly followed by three times 10 minutes in HBST followed by once briefly and three times 5 minutes in HBS. The nuclei were counterstained with Hoechst 33258 dye (0.2ug/mL in 1X PBS) for 15 minutes. Finally, the sections were washed three times 5 minutes in

HBS. The sections were then cover-slipped using Fluormount-G aqueous mounting medium (Southern Biotech; catalog number 0100-01).

2.8.4 Confocal microscopy

TCA fixed mouse PN24 retinal sections were immuno-labeled with antibodies against EML3 (Alexa Fluor 488), ROM1 (Alexa Fluor 594), and DYNLL (Alexa Fluor 647). The nuclei were visualized by staining with Hoechst (Hoechst 33258). Fluorescence images were captured using the Quorum Wave FX Spinning Disc Confocal laser scanning microscope (Quorum Technologies). Images were captured using a Hamamatsu ImagEM CCD camera controlled with Volocity Acquisition software (PerkinElmer Inc.).

2.8.4.1 Image acquisition Parameters

Images were obtained using a 20X objective lens or a 63X Differential Interference Contrast (DIC) oil immersion objective lens. The acquisition settings applied (laser power, exposure time, intensity boost) are presented in Table 2.3. Excitation and emission filters used in this study were matched to the spectrum of the fluorescent probes that resulted in a better signal to noise ratio. Acquisition parameters used to image samples with the 20X objective lens are as follows. The 491nm laser was used to excite the AF488 fluorophore and a (525-50) nm filter was used for visualization. The 561nm laser was used to excite the AF594 fluorophore and a (620-60) nm filter was used for visualization. The 646nm laser was used to excite the AF647 fluorophore and a (690-50) nm filter was used for visualization. The 405nm laser was used to excite Hoechst and a (460-50) nm filter was used to visualize Hoechst emission.

When samples were imaged with the 63X oil immersion objective lens, the acquisition settings used were the same as for the 20X objective. A list of the fluorophores, ideal excitation wavelengths, wavelengths of the lasers used for excitation, range of filter wavelengths used for acquisition and exposure times used for each fluorophore are presented in Table 2.3.

Table 2.3 Image acquisition parameters for immunofluorescence analysis

Fluorophore				**Microscope**			
Name	**Maximum absorption wavelength (nm)**	**Maximum emission wavelength (nm)**	**Target**	**Excitation laser wavelength (nm)**	**Emission filter wavelength-bandwidth (nm)**	**Exposure time, 20X objective (ms)**	**Exposure time, 63X objective (ms)**
Hoechst	354	463	Nuclei	405	460-50	600	600
AF488	495	519	Rabbit anti-EML3-N1	491	525-50	600	600
AF594	590	617	Mouse anti-ROM1	561	620-60	400	168
AF647	650	665	Rabbit anti-DYNLL	646	690-50	1000	800

2.8.4.2 Normalization of images

For visualization of the immunostains, the AF488 signal (EML3) was displayed in green, the AF594 (ROM1) signal was displayed in white, and the AF647 (DYNLL) signal was displayed in red. Signals coming from areas labeled with both AF488 (EML3) and AF647 (DYNLL) appeared yellow.

The images were normalized using Volocity 6.3 (PerkinElmer Inc.). To perform normalization, the black point (BP) and white point (WP) values that were obtained for all the sections imaged during acquisition were noted. The average BP and WP values were calculated for Hoechst, AF488, AF594 and AF647. For Hoechst (which stains nuclei), equal labeling was expected in all

the sections imaged with the same settings. The BP value was set at 2200. The WP value was set to the average value of all WP values recorded for Hoechst.

Since we used retinal sections from an *Eml3/Rom1* DKO mouse, the labeling in the DKO sections represent the background coming from the anti-EML3, and anti-ROM1 primary, anti-rabbit IgG and/or anti-mouse IgG secondary antibodies (Table-2.2). The BP for AF488 (EML3) was set to the average value of WPs recorded in the DKO sections. The WP value of AF488 was set to the average value of the WPs recorded for the WT sections.

The BP for AF594 (ROM1) was set to the average value of WPs recorded in the DKO sections. The WP value of AF594 was set to the average value of the WPs recorded for the WT sections.

The BP for AF647 (DYNLL) was set to the average value of the WPs recorded for the secondary control sections. The WP was set to the average value of the WPs recorded for the WT and DKO sections.

Aberrantly high WP values due to the presence of speckles in the images of the WT and DKO sections were omitted while calculating the average values of BP and WP of each fluorophore.

The BP and WP values used to normalize the images captured using the 20X objective lens as well as the 63X objective lens are presented in Table 2.4.

Table 2.4 BP and WP values used in this study for normalization of images

20X objective		
Fluorophore	**BP**	**WP**
AF488 (EML3)	7800	34900
AF647 (DYNLL)	6000	28000
AF594 (ROM1)	16100	41100
Hoechst (nuclei)	2200	31000
63X oil immersion objective		
Fluorophore	**BP**	**WP**
AF488 (EML3)	4000	33000
AF647 (DYNLL)	5000	55000
AF594 (ROM1)	5500	27100
Hoechst (nuclei)	2000	6000

Once the images were normalized, they were exported as PICT files with the appropriate channels (Hoechst, AF488, AF594, or AF647) turned on. When two or more channels were displayed, they were merged using the “accumulate” function where the sum of the intensities of all the voxels at each location is taken to make up the merged channel.

2.9 Sequences of the relevant proteins used in this study

EML1 (*Mus Musculus*, full length EML1, source: Origene, length: 814 aa)

```
  1 medgfssyss lydtssllqf cnddsasaas smevsdrias leqrvqmqed diqllksala
 61 dvvrrlnite eqqavlnrkg ptkarplgqt lplrttvnng tvlpkkpsas lpapsgarke
121 vvvpvtksin rtssservsp ggrressgds kgsrnrtgst sssssgkkns eskpkepafs
181 peegyvkmfl rgrpvtmymp kdqvdsysle akaelptkrl klewvygyrg rdcrnnlyll
241 ptgetvyfia svvvlynvee qlqrhyaghn ddvkclavhp dritiatgqv agtskdgkql
301 pphvriwdsv tlntlhvigi gffdravtci afsksngggh lcavddsndh vlsvwdwqke
361 erladvkcsn eavfaadfhp tdtniivtcg kshlyfwtle gnslnkkqgl fekqekpkfv
421 lcvtfsengd titgdssgni lvwgkgtnri syavqgaheg gifalcmlrd gtlvsgggkd
481 rrliswngny qklhkaeipe qfgpirtvae gkgnviligt trnfvlqgtl sgdftpitqg
541 htdelwglai haskpqfltc ghdkhatlwd avghrpvwdk iiedpaqssg fhpsgsvvav
601 gtltgrwfvf dtetkdlvtv htdgneqlsv mryspdgnfl aigshdnciy iygvtdngrk
661 ytrvgkcsgh ssfithldws vnsqflvsns gdyeilywvp sackqvvsve ttrdiewaty
721 tctlgfhvfg vwpegsdgtd inavcraher kllctgddfg kvhlfsypcs qfrapshiys
781 ghsshvtnvd flcedshlis tggkdtsimq wrvi
```

EML2 (*Mus Musculus*, partial protein missing the N-terminal coiled coil region, source: Susanne Bechstedt, Dr Gary Brouhard's lab, Mcgill University, length: 649 aa)

```
  1 mssfgigktk evifsmeegs vkmflrgrpv pmlipdelap tysldtrsel pssrlkldwv
 61 ygyrgrdcra nlyllptgev vyfvasvavl ysveeqrqrh ylghnddikc lavhpdmvti
121 atgqvagttk egkplpphvr vwdsvslstl hvlglgvfdr avccvafsks nggnllcavd
181 esndhvlsvw dwakeskvvd skcsneavlv atfhptdpsl litcgkshiy fwsleggsls
241 krqglfekhe kpkyvlcvtf leggdvvtgd sggnlyvwgk ggnritqevq gahdggvfal
301 calrdgtlvs gggrdrrvvl wgsdyskvqe vevpedfgpv rtvaegrgdt lyvgttrnsi
361 llgsvhtgfs llvqghveel wglathpsra qfvtcgqdkl vhlwssethq pvwsrsiedp
421 arsagfhpsg svlavgtvtg rwllldteth dlvaihtdgn eqisvvsfsp dgaylavgsh
481 dnlvyvytvd qggrkvsrlg kcsghssfit hldwaqdstc fvtnsgdyei lywdpvtckq
541 itsadtvrnv ewatatcvlg fgvfgiwpeg adgtdinava rshdgkllvs addfgkvhlf
601 sypccqpral shkygghssh vtnvaflwdd smalttggkd tsvlqwrva
```

EML3 (*Mus Musculus*, full length, source: Origene, length: 897 aa)

```
  1 mdgaagpgeg pahetlqtls qrlrvqeeem elvkaalaea lrllrlhgst ttlqgsgisa
 61 ptrnssitvp pglpptcsps lvtrgtqtee eleivpssgp pglsngppal qqgseepsgt
121 qseggcssss gagspgppgi lrpvqplqrs dtprrnssss sspserprqk lsrkaassan
181 lllrsgstes rgnkdplssp ggpgsrrsny nlegisvkmf lrgrpitmyi psgirsleel
241 psgpppetls ldwvygyrgr dsrsnlfvlr sgevvyfiac vvvlyrpggg pggpgggggr
301 hyrghtdcvr clavhpdgvr vasgqtagvd kdgkplqpvv hiwdsetllk lqeiglgafe
361 rgvgalafsa adqgaflcvv ddsnehmlsv wdcsrgvkla eikstndsvl avgfsprdss
421 civtsgkshv hfwnwsggtg apgngllark qgvfgkykkp kfipcfvflp dgdiltgdse
481 gniltwgrsv sdsktpgrgg aketytivaq ahahegsifa lclrrdgtvl sgggrdrrlv
541 qwgpglvalq eaeipehfga vraiaeglgs ellvgttkna llrgdlaqgf spviqghtde
601 lwglcthpsq nrfltcghdr qlclwdgegh alawsmdlke tglcadfhps gavvvvglnt
661 grwlvldtet reivsdvtdg neqlsvvrys pdglylaigs hdnmiyiysv sscgtkssrf
721 grcmghssfi thldwskdgn fimsnsgdye ilywdvaggc kllrnryesr drewatytcv
781 lgfhvygvwp dgsdgtdins lcrshnervv avaddfckvh lfqypcarak apsrmysghg
841 shvtsvrfth ddsylvslgg kdasifqwrv lgagssgpap atpsrtpsls passldv
```

EML4 (*Mus Musculus*, full length, source: Susanne Bechstedt, Dr Gary Brouhard's lab, Mcgill University, length: 934 aa)

```
  1 mnrvssdpva ipddsisaas tsdvqdrlsa lesrvqqqed eitvlkaala dvlrrlaise
 61 dhvasvkksm pskgqpslre aismscitng sgisrkqnht ssvsiarket lssaaksikr
121 pptaekshns wensddsrnk lmktvstskl iskviknadk hkdvivnqak mstreknsqe
181 geyikmfmrg rpitmfipsd vdnyddirte lppeklklew vygyrgkdcr anvyllptge
241 ivyfiasvvv lfnyeertqr hylghtdcvr clavhpdkir iatgqiagvd kdgrplqphv
301 rvwdsvsltt lhviglgtfe rgvgcldfsk adsgvhlcvi ddsnehmltv wdwqkkskia
361 eikttnevvl avefhptdan tiitcgkshi ffwtwsgnsl trkqgifgky ekpkfvqcla
421 flgngdvltg dsggvmliws ktmvepppgk gpkgvyqinr qikahdgsvf tlcqmrngml
481 ltgggkdrki ilwdhdlnle reievpdqyg tiravaegra eqflvgtsrn filrgtfndg
541 fqievqghtd elwglathpf kdllltcaqd rqvcmwnsve hrlewtrlvd epghcadfhp
601 sgtvvaigth sgrwfvldae trdlvsihtd gneqlsvmry svdgtllavg shdnfiylyt
661 vlengrkysr ygkctghssy ithldwspdn khimsnsgdy eilywdieng cklirnrsdc
721 kdidwttytc vlgfqvfgvw pegsdgtdin alvrshnrrv iavaddfckv hlfqypcska
781 kapshkysah sshvtnvsft hndshlistg gkdmsiiqwk lveklpvpqn evitdasvtk
841 tpasssetar psnspplpps lpltgtaeee srmgssptlv ensleqiaep seeqsewgse
901 dlgvvideep aselsetqga telpeeergi tplc
```

ROM1 (*Mus Musculus*, Source: Cedarlane, length: 351 aa)

```
  1   mapvlpvvlp lqprirlaqg iwllswllal vggltllcsg hllvqlghlg tflapscsfp
 61   alpqtalaag tvalgtglgg agasraslda aqyppwrgvl tpllavgtaa gggllltlalg
121   lalalpvsln qgleegleaa lahykdtevp grcqakrlmd elqlryhccg rhgykdwfgv
201   qwvsnryldp sdqdvvdriq snveglylid gvpfsccnph sprpclqsql sdpyahplfd
241   prqpnlnlwa qgchevlleh lqglsgtlgs ilavtlllqi lvllglrylq taleglggvi
301   dgegeaqgyl fpgglkdilk tawlqgglah kpapeeappd eeppkevlae a
```

DYNLL1 (*Mus Musculus*, Source: Origene, length: 89 aa)

```
  1  mcdrkavikn admseemqqd svecatqale kyniekdiaa hikkefdkky nptwhcivgr
 61  nfgsyvthet khfiyfylgq vaillfksg
```

DYNLL2 (*Mus Musculus*, Source: Origene, length: 89 aa)

```
   1  msdrkavikn admsedmqqd avdcatqame kyniekdiaa yikkefdkky nptwhcivgr
  61  nfgsyvthet khfiyfylgq vaillfksg
```

NETO2 (*Mus Musculus*, Source: In house (McInnes Lab), length: 525 aa)

```
  1  maleqlcavl kvllitvlvv egiavaqktq dgqnigikhi patqcgiwvr tsngghfasp
 61  nypdsyppnk eciyileaap rqrieltfde ryyiepsfec rfdhleirdg pfgfsplidr
121  ycgmkspali rstgrfmwik fssdeelegl gfrakysfip dpdftylggi lnpipdcqfe
181  lsgadgivrs sqveqeektk pgqavdciwt ikatpkakiy lrfldyqmeh sneckrnfva
241  vydgssaien lkakfcstva ndvmlktgvg virmwadegs rlsrfrmlft sfveppctss
301  tffchsnmci nnslvcngvq ncaypwdenh ckekkkaglf eqitkthgti igitsgivlv
361  lliisilvqv kqprkkvmac ktafnktgfq evfdpphyel fslrekeisa dladlseeld
421  nyqklrrsst asrcihdhhc gsqassvkqs rtnlssmelp frndfaqpqp mktfnstfkk
481  ssytfkqahe cpeqaledrv meeipceiyv rgrddsaqas isidf
```

Chapter 3: Results

Since its initial identification, the biological function(s) of the Echinoderm microtubule associated protein (EMAP)-like EML family of proteins has been of great interest. Proteins belonging to the EML family contribute to formation, maintenance of the mitotic spindle and interphase microtubule (MT) network [67] and have been related to cell cycle regulation [62, 63, 69]. Amongst the mammalian paralogs of the EML proteins, EML3 is of interest to us because of the perinatal lethality phenotype observed in *Rom1/Eml3*-knockout mice. EML3 has been shown to co-localize with microtubules in interphase and during the different stages of mitosis where it associates with the spindle. During metaphase, EML3 appears to play a role in chromosome capture according to the phenotype of HeLa cells depleted of EML3 protein [63].

To fully understand the molecular functions of EML3 it is important to identify its interacting partners. While there are several studies that demonstrate the association of the EML proteins with microtubules, thorough studies on the interacting partners and molecular functions of EML3 are lacking.

Thus, the aim of this study was to identify the protein interaction network of EML3. The identification and verification of an interaction *in vitro* is the first step to understanding where, how and under what conditions EML3 interacts with a candidate protein *in vivo* and the functional implications of this interaction [82]. A combination of techniques is necessary to characterize and confirm protein interactions. Using co-immunoprecipitation in a cell culture system followed by co-localization analysis using both direct and indirect immunofluorescence, we attempted to detect the association of EML3 and its interacting partner(s) *in vitro* and *in*

vivo. Our findings open new perspectives in the study of the molecular functions of EML3 by identifying its novel interactions in mammalian cells and mouse retinal sections.

3.1 The candidate interacting partners of EML3

A thorough screening of previously published literature and high-throughput interactome datasets was performed to create a list of potential interacting partners of EML3.

The candidate interacting proteins identified are as follows: DYNLL1 (Dynein Light Chain 1), DYNLL2 (Dynein Light Chain 2), α/β-tubulin dimers or polymers (microtubules), ROM1 (Retinal outer segment membrane protein 1), EML1 (Echinoderm microtubule associated protein like 1), EML2 (Echinoderm microtubule associated protein like 2), EML4 (Echinoderm microtubule associated protein like 4), NPHP4 (Nephrocystin-4), NEK6 (Never in mitosis A related kinase 6), NEK7 (Never in mitosis A related kinase 7), 14-3-3 Gamma/YWHAG (Tyrosine-3-Monooxygenase/ Tryptophan-5-Monooxygenase activation protein gamma), and 14-3-3 Theta/YWHAQ (Tyrosine-3-Monooxygenase/Tryptophan-5-Monooxygenase activation protein theta). The isoforms of EML1, EML2, EML3 and EML4 used in this study are presented in figure 1.14. A thorough description of the supporting evidence as well as the potential functional implications for each candidate interactor are presented below.

3.1.1 The Dynein Light Chain (DYNLL1 & 2)

One of the putative interactors of EML3 is Dynein Light Chain (DYNLL)/Light Chain 8 (LC8), a component of the Dynein motor protein complex that functions in retrograde transport across microtubules. LC8 was first described as a subunit of *Chlamydomonas* axonemal dynein. The term LC8 derives from the observation that this component migrates at ~8kDa in SDS-PAGE gels

and it is also the smallest of the eight light chains then known within this *Chlamydomonas* axonemal dynein [83]. LC8 orthologs share more than 90% identity. The two mammalian paralogs of LC8 are DYNLL1 and DYNLL2. EML3 has a DYNLL binding motif. This motif is unique to EML3 within the EML family. (Figure 3.1).

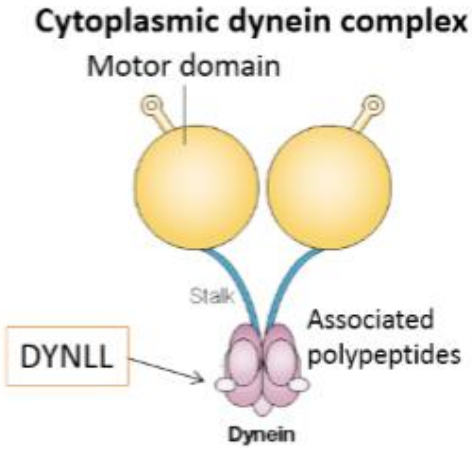

Figure 3.1: The cytoplasmic dynein complex consists of a dimer of two heavy chains whose catalytic domains are shown in yellow. The stalks which form extended coiled coils are shown in blue. Associated polypeptides such as the intermediate chains, light-intermediate chains and light chains are shown in purple. Adapted from [84].

The two mammalian paralogs, DYNLL1 and DYNLL2 share 93% sequence identity at the protein level [83, 85]. Previously, DYNLL/LC8 was described as a binding adaptor of both Dynein and Myosin 5a motor protein complexes and as an inhibitor of the neuronal enzyme NO-Synthase [86]. Subsequent studies revealed that DYNLL binds to dozens of proteins unrelated to cytoskeletal motors [87-91]. The fact that these proteins are involved in diverse cellular processes suggests a more general role of DYNLL as a eukaryotic hub protein that acts as a "molecular Velcro" [92]. Possible interaction modes of DYNLL/LC8 with its targets is presented in Figure 3.2. Interaction of DYNLL with a partner that contains a potential coiled-coil domain

near the DYNLL binding motif could lead to homo-dimerization or coiled-coil stabilization (Figure 1.23, Panel A) [85, 86, 93, 94].

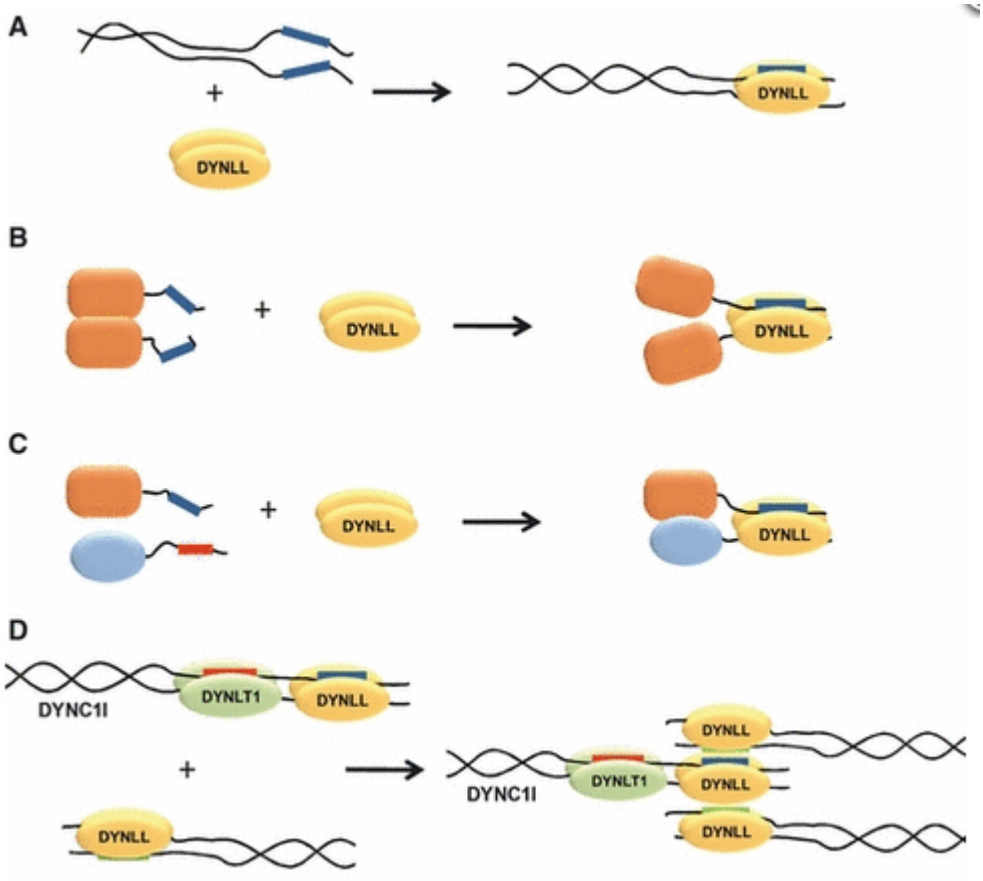

Figure 3.2: The possible modes of interaction of DYNLL with its binding partners. Panel A: the binding partner usually contains a coiled coil domain near the DYNLL binding motif that leads to homo-dimerization and stabilization of the DYNLL binding protein. Panel B: If the DYNLL binding motif is localized near interacting globular domains, DYNLL could pry apart the domains by steric constraints and might destroy further interaction sites. The same destabilizing effect may occur if the DYNLL binding site is located within a coiled-coil domain (not shown). Panel C: Hetero-dimerization of two targets could occur if two DYNLL binding motifs are located near two weakly interacting domains. Panel D: DYNLL could function as a direct cargo adapter on Dynein if one assumes that two homo-dimeric DYNLL-target complexes interact via their ligands [86].

The difference in cellular functions of the two mammalian paralogs DYNLL1 and DYNLL2 is not fully characterized. DYNLL 1 and 2 bind specifically *in vivo* to the dynein and myosin 5a complexes [95-97]. The two isoforms have identical *in vitro* binding characteristics to their interacting proteins, such as the pro-apoptotic protein Bmf (Bcl-2-modifying factor) [92, 95]. The versatility of the molecular recognition of DYNLL is due to the short linear motifs that DYNLL binds to- usually localizing in disordered segments of the DYNLL binding proteins, often in close proximity to potential dimerization domains such as the coiled-coil domain [94, 98, 99]. The group of Gabor Pal aimed to find novel DYNLL binding partners in the human proteome. They defined the naturally evolved binding motif of DYNLL by combining 41 identified canonical DYNLL binding motifs [100]. The literature shows affinities of the natural binding peptides are in the nano-molar range [95, 96, 101, 102]. A directed evolution approach was also applied by selecting DYNLL binders from a phage-displayed peptide library to define the *in vitro* evolved DYNLL binding motif. The amino acid preference of individual binding positions was illustrated in the form of a sequence logo using the WebLogo program available at http://weblogo.berkeley.edu/ [95] (Figure 3.3). WebLogo generates graphical representations of the patterns within a multiple sequence alignment. Each logo consists of stacks of letters, one stack for each position in the sequence [103]. The sequence logos of the naturally-evolved and *in vitro*-evolved DYNLL binding motifs are similar but the *in vitro* consensus sequence is extended by a Valine at position -5 which was shown to increase the affinity twenty-fold (Figure 3.3). The *in vitro* evolved binding pattern helps predict a large number of novel DYNLL binding partners in the human proteome [95].

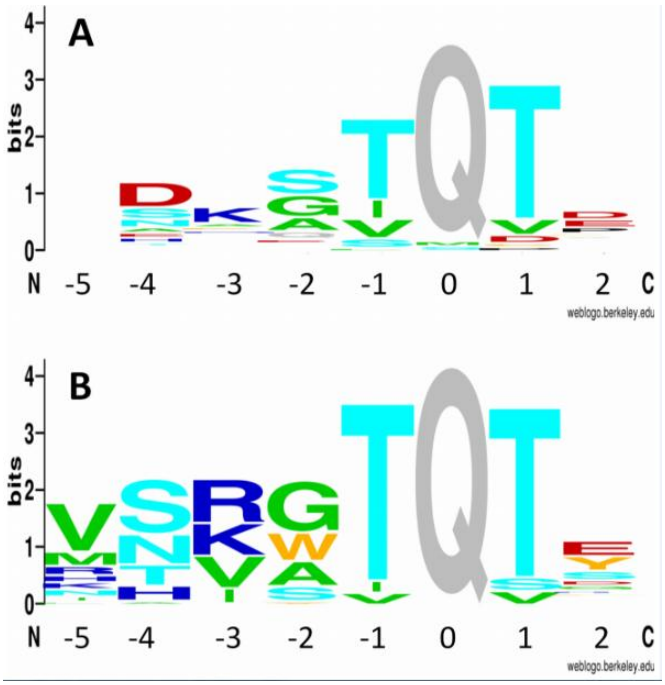

Figure 3.3: Sequence logos of the naturally evolved (Panel A) and the *in vitro* evolved (Panel B) binding motifs of DYNLL-binding proteins. The degree of sequence conservation is represented by the overall height of each stack of letters. Normalized amino acid proportions are represented by letter heights. Similar colors indicate similar chemical properties [95, 103].

A bioinformatics analysis was performed using the *in vitro* evolved sequence pattern to identify potential novel binding partners of DYNLL. Human EML3 protein contains the exact match of the phage selected consensus sequence motif, - "VSRGTQTE" required to bind DYNLL with nano-molar affinity [96]. For this reason, DYNLL1 and 2 have been chosen as potential interacting partners of EML3. In our study, we aimed to provide experimental verification of the binding capacity of EML3 to DYNLL. Thus, we tested the interaction of EML3 with DYNLL1 and DYNLL2 in a co-transfection system followed by co-localization of EML3 with DYNLL in adult mouse retinal sections.

3.2.2 Echinoderm Microtubule Associated Protein Like 1, 2 & 4 (EML 1, 2 & 4)

Recently literature has provided evidence of EML self-association by adopting a trimeric state of oligomerization [71]. In addition, the same group showed the association of EML3 with EML2, suggesting that EMLs may also hetero-oligomerize (ratios not studied) [71]. Richards and colleagues investigated in detail the oncogenic EML4-ALK fusion proteins. EML oncogenic fusion proteins such as EML4-ALK are naturally occurring and the fusions have constitutive ALK (Anaplastic lymphoma kinase) activity due to self-association through the coiled-coil region of EML4. Richards and colleagues studied the crystal structures of the coiled-coil domains of EML2 and EML4. The coiled-coil domains facilitate EML self-association and activation of the oncogenic fusion proteins [71]. The N-terminal region of the EML family of proteins is poorly conserved, often subject to splice variation and predicted to be mostly disordered. However, there is an island of conserved primary sequence within this region that is consistent with a coiled-coil. The conserved region in the EML N-terminus forms a trimerization domain (Figure 3.4, panel B) [71]. The coiled-coil or trimerization domain (TD) is necessary and sufficient for self-association. The TD which is located in the N-terminal of EML1-4 is composed of an amphipathic alpha helix with a series of nine conserved residues (Figure 3.4, panel A). The side chains of the hydrophobic residues form the core of the TD. Salt bridges between adjacent protomers are formed by conserved charged residues that are present in-between the hydrophobic residues.

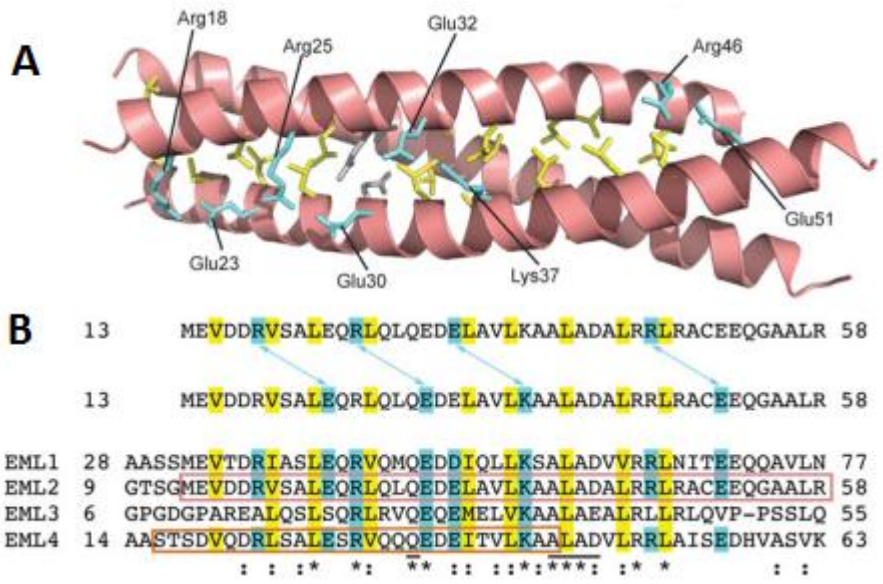

Figure 3.4: The N-terminus of EML proteins contain a (coiled-coil) trimerization domain. Panel A is a cartoon representation of the EML2 TD. Hydrophobic side chains are shown in yellow and charged residues forming salt bridges are shown in blue. Panel B represents an alignment of the EML TDs. Conservation is shown underneath. Identical residues and highly conserved residues are marked by an asterisk (*) and a colon (:), respectively [71].

A stretch of four amino acids with short side chains forms the ALAD motif (Ala-Leu-Ala-Asp) which is the most conserved sequence in the TD of EML 1-4. The ALAD motif constricts the shape of the coiled-coil. Immunoblotting was used to test the ability of various YFP-tagged EML1 constructs to co-immunoprecipitate with FLAG-tagged full-length EML1 from lysates of co-transfected HEK293 cells (Figure 3.5, Panel A). The constructs that showed association were full-length EML1, the isolated N –terminal region of the protein (residues 1 to 174) and residues (23-78) representing the TD. Moreover, it is the TD from EML2 and EML4 that was crystallized in a homo-trimeric structure. Thus, the TD is sufficient for EML self-association. Notably, deletion of the TD disrupted EML1 self-association and that is proof that the TD is necessary for self-association. Interestingly, mutation of the highly conserved “ALAD” motif within the TD did not disrupt self-association (Figure 3.5, Panel A). The isolated TAPE domain failed to co-

immunoprecipitate with full-length FLAG-tagged EML1. Thus, the TD is necessary for EML1 self-association.

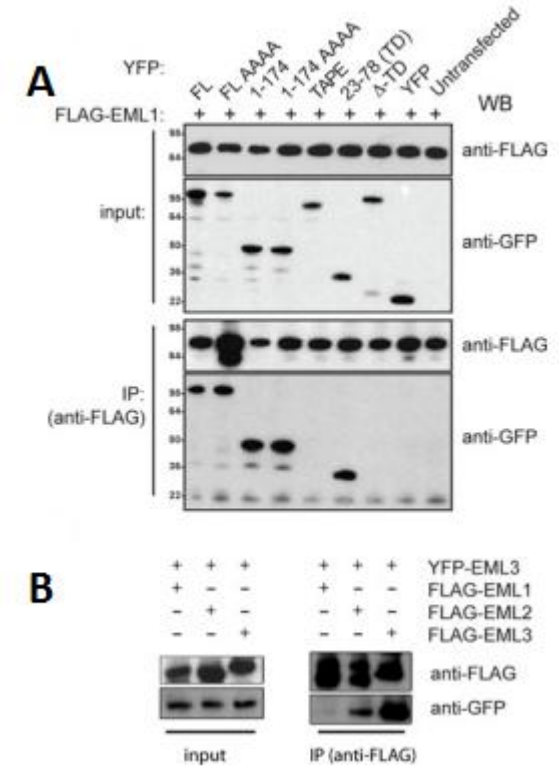

Figure 3.5: Oligomerization of EML1 depends on the TD. Panel A represents immunoblot analysis of EML1 self-association. HEK-293 cells were co-transfected with FLAG-*EML1* and various YFP-*EML1* constructs as indicated (top two panels). Proteins were immunoprecipitated using anti-FLAG M2 (Sigma) (lower two panels). Immunoblotting was performed using anti-FLAG M2 and anti-GFP antibodies. Panel B represents association of YFP-EML3 with FLAG-tagged EML1, 2 and 3. U2OS cells were co-transfected with YFP-*EML3* and FLAG-*EML1-3* as indicated. Immunoprecipitation and analyses was carried out as in (A) [71].

An alignment of the TDs of EML1-4 shows that the TDs are imperfectly conserved. EML3 has the most divergent TD amongst the four paralogs. To investigate the ability of EML3 to associate with itself and with other members of the EML family, co-immunoprecipitation analysis was carried out (Figure 3.5, Panel B). YFP-EML3 co-immunoprecipitated strongly with FLAG-EML3 and weakly with FLAG-EML2, but the authors claimed that it failed to co-immunoprecipitate FLAG-EML1 from lysates of co-transfected HEK293 cells [71]. The degree of interaction

appeared to correlate with the degree of conservation within the key residues involved in self-association of the EMLs. It is important to mention that there are two alternative splice isoforms of EML2. The brain/spinal cord variant isoform 2 used in that study contains the TD [104]. However, the more widely expressed isoform 1 lacks the TD and is hypothesized to be incapable of self-association due to the lack of a TD [71].

The paralogs EML 1, 2, 3 and 4 contain the coiled-coil region needed to form trimers but EML5 and EML6 do not possess coiled-coils. Hence, EML1, 2 and 4 are strong candidate interacting partners of EML3 as all three paralogs contain the TD required for self-association of the EMLs. I have presented some evidence in the literature for the ability of these paralogs to form trimers and/or dimers. Recent studies investigated the interactions of the EML proteins using human versions of the protein [67, 71]. Thus, we needed to test the interaction of the mouse proteins in our system. Moreover, the mouse *Eml2* and *Eml4* genes encode for a variety of isoforms and we are beginning to test the implications for protein interactions and function. [71]. The functional relevance of the homo- and hetero-oligomerization of the EML proteins remains to be elucidated. The potential of these interactions should be considered when trying to elucidate the mechanism of action of the EML proteins.

3.2.3 Retinal Outer Segment Membrane Protein 1 (ROM1)

The membrane protein ROM1 localizes to the disk rim of rod photoreceptor cells in the form of tetramers or large oligomers in association with the homologous membrane protein PRPH2. Disk rims are critical for the maintenance and function of rod photoreceptor cells. Important functions of the ROM1 protein in the OS of rod photoreceptor cells include regulation of disk morphogenesis and viability of rod photoreceptors [45]. Analysis of the mouse genome reveals

that *Rom-1* and *Eml3* are present in a head-to-head fashion separated by only 300 bps of DNA. Both genes share a common promoter region and exhibit similar expression patterns in adult tissues. While ROM1 protein is highly expressed in the OS of the retina, EML3 is predominantly expressed in the IS of the retina (Figure 1.21). ROM1 is made in the IS of rod photoreceptor cells where protein synthesis is carried out and needs to reach the OS to carry out its function. Our current hypothesis is that EML3 may be involved in the transport of ROM1 from the IS to the OS. The ROM1 and EML3 proteins are therefore likely to interact physically.

3.2.4 Tubulins/Microtubules

EML3 is a microtubule-associated protein. Literature aimed at finding novel proteins recruited by the spindle apparatus (microtubule-based structure with important roles during mitosis), identified EML3 as one such protein [63]. In that study, immunofluorescence analyses revealed co-localization of EML3 with microtubules throughout interphase and during mitosis in HeLa cells. The results from the study highlight the possibility of a direct interaction of EML3 with microtubules [63]. Furthermore, *in vitro* studies revealed co-purification of strep-tagged EML1 and EML2 TAPE domains with soluble α/β tubulin dimers from insect cell lysates [67]. Richards and colleagues set out to investigate the EML1-tubulin interaction by testing the ability of multiple YFP-EML1 constructs to co-purify tubulin from the lysate of HEK 293F cell lysates. The experiments were carried out under MT depolymerizing conditions and they observed co-purification of EML1 TAPE domains with soluble α/β tubulin dimers. By mapping the amino acid conservation of surface residues onto the EML1 structure, Richards and colleagues identified a conserved region on the concave surface of the TAPE domain that could mediate tubulin binding interaction. Site directed mutagenesis of seven residues within this region resulted in a

correctly folded EML1 mutant that was unable to bind soluble α/β tubulin dimers- confirming the importance of the concave surface region of the TAPE domain for soluble tubulin interactions [67, 105].

There is evidence in the literature of the ability of endogenous EML proteins to co-localize with the interphase MT network [60, 62, 63, 106]. Both the trimerization domain (TD), as well as the region between the TD and TAPE domains (Figure 3.6), are required for the co-localization of EML1 with polymerized microtubules.

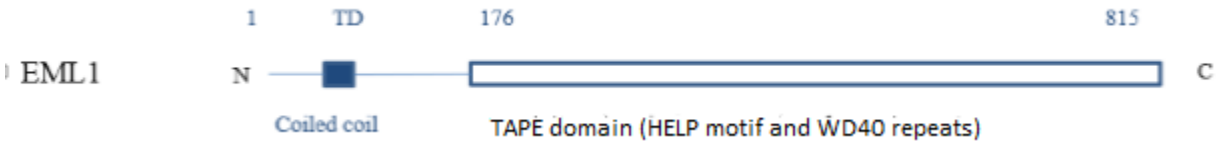

Figure 3.6: Schematic diagram of the domain organization in EML1. The TD is required for homotrimerization. The TD and the region upto the TAPE domain is required for binding to polymerized MTs. The TAPE domain is required for binding to soluble tubulins. The schematic diagram of the domain organization in EML1 is slightly different from the schematic diagrams of the EML protein family presented in Figure 1.15. Adapted from [91][67].

To investigate the MT-binding properties of the specific regions of the EML1 protein, immunofluorescence analyses were performed on interphasic HeLa cells transfected with various YFP-tagged constructs of EML1. The co-localization of YFP-EML1 proteins with microtubules was visualized (Figure 3.7, panel A) and quantified (Figure 3.7, panel B). The results confirmed the necessity of the TD as well as the N-terminal region between the TD and TAPE domain for co-localization of YFP-tagged EML1 with the interphase MT network. YFP-EML1 constructs lacking both the TD and the conserved N-terminal region failed to co-localize with interphase MTs. Noteworthy, the isolated TD or TAPE domain failed to co-localize with MTs [71].

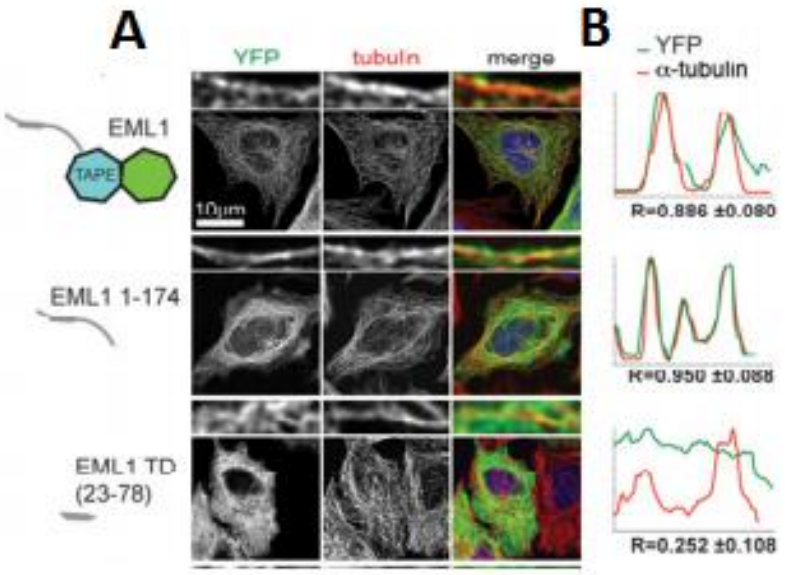

Figure 3.7: MT association of YFP-EML1. Panel A shows immunofluorescence microscopy images of interphasic HeLa cells transfected with YFP-tagged EML1 constructs. Panel B shows quantification of the immunofluorescence analysis. The lines represent intensity profiles showing co-localization of YFP-EML1 with MTs [71].

In conclusion, the TAPE domain binds soluble tubulins but binding of the EML protein to polymerized microtubules requires the TD and the N-terminal sequence between the TD and the TAPE domain [67, 71].

Additionally, studies on the EML4 paralog showed co-localization of GFP-tagged mouse EML4 with microtubules in COS7 and HeLa cells [106]. It has been shown previously that EML4 plays a role in microtubule organization [62] and that over-expression causes stabilization of interphase microtubules [106]. By contrast, published *in vitro* studies suggest that human EML2 is a microtubule destabilizing protein [60]. EML2 localizes to the mitotic spindle as well as interphase microtubules and it is a likely target for cell cycle activated kinase [107]. Although the precise mode of action of EML3 on microtubules is still unknown, the above stated studies

on EML3 as well as its paralogs indicate that EML3 interacts with microtubules/tubulins. Therefore, microtubules and tubulin dimers are potential interacting partners of EML3. Susanne Bechstedt, a member of the Brouhard lab at McGill, one of our collaborators, successfully showed through *in vitro* studies, the interaction of EML3 with polymerized microtubules in the absence of other proteins (data not shown). A question remains as to whether EML3 binds soluble tubulins.

3.2.5 Nephrocystin-4 (NPHP4)

Dysfunction of cilia results in a broad spectrum of disorders known as ciliopathies. Ciliopathy phenotypes include retinal degeneration, renal cysts, polydactyly, mental retardation and obesity [108, 109]. Nephronophthisis (NPHP), Joubert Syndrome (JBTS) and Meckel Gruber syndrome (MKS) are a group of linked autosomal recessive ciliopathies with over-lapping phenotypes such as renal cysts, retinal degenerations, *situs inversus,* and mental retardation [108, 110]. The proteins involved in NPHP, JBTS and MKS are found either within the primary cilium or at the basal body (Figure 3.8) [110, 111].

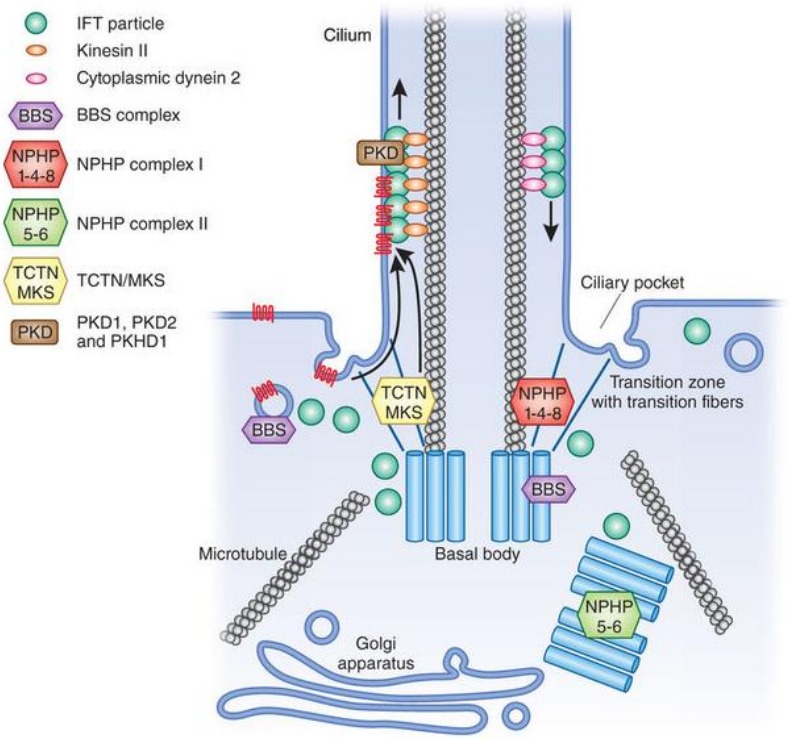

Figure 3.8: Schematic illustration of cilia based transport [111].

A 2011 study aimed at characterizing the molecular mechanisms of the NPHP-JBTS-MKS network, using a G-LAP tandem affinity method [112] identified interactors associated with nine disease proteins within the network [110]. The high throughput study identified EML3 as one of the prey proteins that was pulled by NPHP4, a member of the NPHP1-4-8 module that functions at the transition-zone of the cilium (Figure 3.8) [110]. The transition zone at the base of the cilium marks the boundary between the cilium and the rest of the cell. Vesicles carrying cargo proteins from inside the cell arrive at the transition zone and fusion of vesicles at the ciliary base allows binding of cargo proteins to transport complexes such as the NPHP1-4-8 complex. This complex then delivers the cargo to intra-flagellar transport particles (IFT) along the axoneme inside the cilium [111]. The results of the high throughput study [110] along with

the knowledge that EML3 is a ciliopathy-associated and microtubule-associated protein suggests that the NPHP4 protein may interact with EML3.

3.2.6 14-3-3 Proteins Gamma & Theta

14-3-3 proteins are expressed in all eukaryotic cells but have been found to be particularly abundant in brain extracts. The 14-3-3s are highly conserved acidic polypeptides, 28-33 kDa in size, that have a tendency to form dimers [113]. The name '14-3-3' was given based on the fraction number on DEAE-cellulose chromatography and the migration position on starch gel electrophoresis [114]. 14-3-3 proteins carry out a plethora of biological functions by binding to phosphoserine/ phosphothreonine- containing sequence motifs [115-117]. Some notable regulatory processes in which the 14-3-3 proteins participate include signal transduction, apoptosis, cell cycle progression and DNA replication. There are seven mammalian isoforms of 14-3-3 proteins (beta, gamma, epsilon, zeta, eta, theta and sigma) [118]. A published high-throughput study that used tandem proteomic and biochemical techniques to identify polypeptides associated with 14-3-3 proteins *in vivo* identified EML3 as a prey protein for the bait 14-3-3 gamma. In this study, they successfully isolated EML3 as a 14-3-3 interacting protein from extracts of proliferating HeLa cells. Many of the 14-3-3 affinity purified proteins were involved in processes that promote cell growth and proliferation. To investigate whether the phosphorylation of 14-3-3 binding sites on the interacting proteins was connected with the proliferation status of the cells, the HeLa cells used in the experiments were starved of serum. Although EML3 was present in 14-3-3 Sepharose precipitates from extracts of HeLa cells that were continuously grown in serum, it failed to bind to 14-3-3 in extracts of HeLa cells that were starved of serum to arrest cellular proliferation. This particular experiment highlighted the

ability of 14-3-3 proteins to bind serine- or threonine- phosphorylated EML3 during mitosis [119]. The group of Daniel Figeys performed a large-scale high throughput study of protein-protein interaction in human cells using the techniques of immunoprecipitation followed by mass spectrometry. False positives and redundant hits were filtered out and each interaction was given a confidence score. Two of the 14-3-3 isoforms, 14-3-3 gamma and 14-3-3 theta were used as bait proteins in this study. EML3 was identified as a prey protein for both the isoforms with moderate confidence score [120].

We performed a prediction of 14-3-3 binding sites within the primary sequence of the EML3 protein. Specifically, the online program Phosphomotif Finder (www.hprd.org/PhosphoMotiffinder) contains known kinase/phosphatase substrates as well as binding motifs that are curated from the literature. The software reports sites within the EML3 protein that could be bound by 14-3-3 proteins under the condition that a serine- or threonine-residue within the motif has been phosphorylated (Figure 3.9) [121]. We then performed an *in silico* prediction of phosphorylation sites in the primary sequence of EML3. The software NetPhos2.0 Server, a phosphorylation site prediction system (www.cbs.dtu.dk/services/NetPhos), was used to find the potential serine/threonine phosphorylation sites in EML3 and it revealed 46 serines and 12 threonines in EML3 that could be phosphorylated according to a selection of known kinase-binding motifs [122]. Among the potential 14-3-3 binding sites (shown in Figure 3.9), NetPhos2.0 found S157 to be the most likely phosphorylated (0.997 score), followed by S769 (0.994 score) and S888 (0.970 score). Additionally, PhosphoSitePlus, an online knowledgebase dedicated to mammalian post-translational modification in published Mass Spectrometry data (www.phosphosite.org), was

used to identify the residues in EML3 that have been previously tagged as being phosphorylated [123]. It predicts 11 serines and 1 threonine to be phosphorylated in mouse EML3 protein. Among the potential 14-3-3 binding sites, PhosphoSitePlus found S157 and S888 the be the most likely phosphorylated, with four MS data records each in support for that post-translational modification.

In conclusion, published studies along with presence of potential 14-3-3 phospho-binding sites in EML3 suggests that the ubiquitously expressed proteins, 14-3-3 gamma and 14-3-3 theta are potential interacting partners of EML3. To confirm the presence of an interaction between the proteins, further experiments such as co-immunoprecipitation assays will have to be performed.

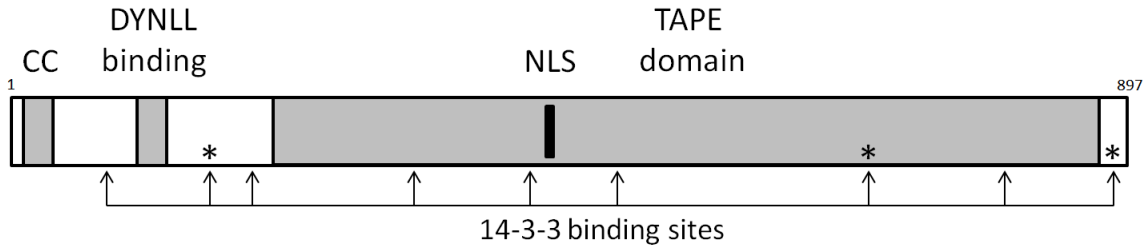

Figure 3.9: The map of EML3 protein domains with potential 14-3-3 phospho-serine/threonine-binding sites in EML3 represented with arrows. In silico prediction made with Phosphomotif Finder software (www.hprd.org/PhosphoMotif_finder) [121]. The three potential 14-3-3 binding sites with the strongest prediction for the presence of a phospho-serine residue are marked with an asterisk (S157, S769 and S888). The in silico predictions for phosphorylation were performed with NetPhos2.0 (www.cbs.dtu.dk/services/NetPhos) and PhosphoSitePlus (www.phosphosite.org).

3.2.7 Never in Mitosis A Related Kinase 6 & 7 (NEK6 & 7)

The Never in Mitosis A (NIMA) related family of serine/threonine protein kinases (NEKs) were first found in *Asperigillus nidulans* as key regulators of entry into cell cycle [120, 124]. The NEKS were then also found in most eukaryotes. In humans, there are 11 paralogs of NEKs (NEK1 to

NEK11). The current hypothesis is that the NEKs coordinate microtubule dependent processes in both dividing and non-dividing cells in addition to playing the role of key regulators of entry into cell cycle [125]. Amongst the paralogs, NEK1 and NEK8 function within the cilium, and NEK2, NEK6, NEK7 and NEK9 play a role in formation of the microtubule-based mitotic spindle. In human cells, NEK6 is required for mitotic progression of cells from metaphase to anaphase. SiRNA mediated depletion of endogenous NEK6 causes cell cycle arrest in metaphase followed by apoptosis [126]. In the same high-throughput study that identified 14-3-3 gamma and theta as potential EML3 interactors, the group of Daniel Figeys used NEK6 as bait in immunoprecipitation and high-throughput mass spectrometry (IP-HTMS) experiments. EML2, 3 and 4 were identified as prey proteins when NEK6 was used as a bait protein [120]. NEK6 and NEK7 share 87% sequence similarity within their N-terminal catalytic domains [127]. The two paralogs are both activated in mitosis and knock-down of either kinase leads to mitotic arrest followed by apoptosis in HeLa cells. While NEK6 localizes to the mitotic spindle during mitosis, NEK7 is found specifically in centrosomes [128]. In conclusion, based on the sequence similarity of NEK6 and NEK7, the localization of NEK6 and NEK7 to the microtubule based mitotic spindle and centrosomes, respectively, and evidence from high throughput studies where EML3 was identified as a prey protein when NEK6 was used as bait, NEK6 and NEK7 are both believed to be potential interacting partners of EML3.

3.2 Co-immunoprecipitation in transfected cells

Co-immunoprecipitation was used to assess the interaction of each of the candidate interacting proteins with EML3. Specifically, this technique allowed us to test whether a candidate

interacting partner of EML3 can be co-immunoprecipitated with EML3 when both proteins are over-expressed in cultured cells.

Mammalian HEK 293T cells were transfected with a full-length *Eml3* cDNA construct as well as the cDNA construct of the potential interacting partner protein. The cell extracts were collected under co-IP conditions and incubated with an antibody against the protein to be immunoprecipitated followed by magnetic beads containing anti-IgG antibodies (anti-rabbit IgG or anti-mouse IgG antibodies, depending on the source of the antibody used for immunoprecipitation). Aliquots of the input cell extracts and of the immunoprecipitated samples were subjected to SDS-PAGE and immunoblot using the antibodies indicated in Table 2.2 and in figure legends.

An interaction between EML3 and the potential interacting partner in the co-transfection system suggests that the interaction could potentially occur physiologically. Proteins that fail to interact in this cell culture system likely do not interact with EML3 in the context of endogenous proteins in mouse tissues. Interactions that manifest themselves in this system can be readily tested in the context of endogenous proteins in mouse tissues if there are specific antibodies available for the implicated proteins.

3.2.1 EML3 interacts with Dynein Light Chain 1 & 2 (DYNLL1 & 2)

One of the putative interactors of EML3 is a component of the Dynein motor protein complex that functions in retrograde transport along microtubules. EML3 is unique amongst all the EML paralogs as it is the only one that contains a DYNLL binding motif [95]. The LC8 family of dynein light chains comprises DYNLL1 and DYNLL2 which are highly conserved ubiquitous eukaryotic

homodimer proteins that are involved in diverse biological functions [86]. The two mammalian paralogs DYNLL1 and DYNLL2 share 93% sequence identity at the protein level [83, 85]. The two isoforms have identical *in vitro* binding characteristics to their interacting proteins studied so far [92, 96]. The high sequence similarity between the two paralogs indicates a possibility of interaction of EML3 with both DYNLL1 and DYNLL2. For this reason, I investigated whether EML3 interacts with DDK-tagged DYNLL1 and DYNLL2 in the co-transfection system (Figure 3.10).

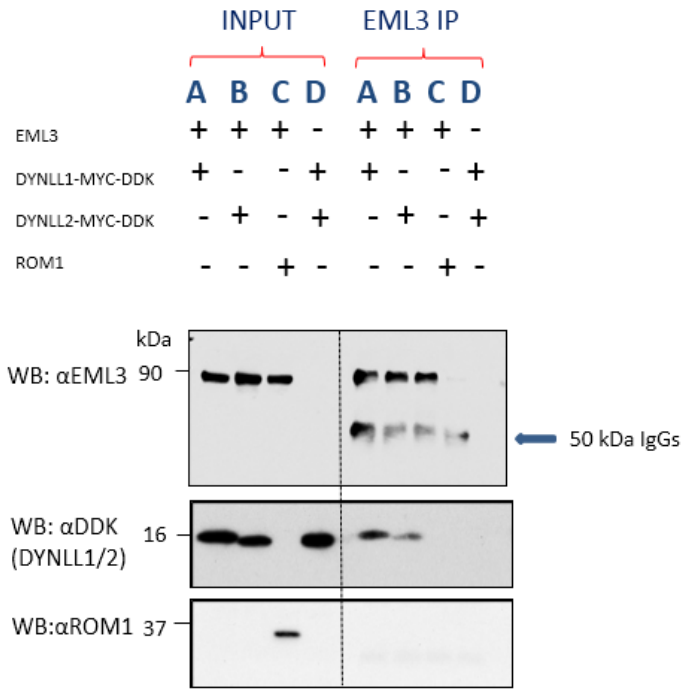

Figure 3.10: EML3 interacts with Dynein Light Chains DYNLL1 and DYNLL2. Immunoblots of immunoprecipitates from co-transfected HEK 293T cell lysates. The identities of the transfected cDNAs are shown in panel A. The western blots performed on the input and IP samples are shown in panel B. Anti-EML3C884A antibody was used for immunoprecipitation. Anti-EML3C884A, anti-DDK, and anti-ROM1 antibodies were used for immunoblotting. 1% of the input was loaded on the gel.

We found that the anti-EML3 antibody co-immunoprecipitated DYNLL1-DDK and DYNLL2-DDK from co-transfected HEK 293T cell lysates (Figure 3.10, IP lanes A & B, respectively). For this reason, the EML3-DYNLL2-DDK interaction was used as a positive control for the technique in subsequent co-IP experiments. The interaction of EML3 with DYNLL 1 & 2 was tested (and always observed) at least three times in the co-transfection system. Anti-EML3 antibody did not immunoprecipitate directly either DYNLL1, DYNLL2 (Figure 3.10, IP lane D) or ROM1 (data not shown) from HEK 293T cell lysates not transfected with *Eml3*.

3.2.2 EML3 does not interact with Retinal Outer Segment Membrane Protein 1 (ROM1)

The membrane protein ROM1 localizes to the disk rim of rod photoreceptor cells. Important functions of the ROM1 protein in the outer segment of rod photoreceptor cells include regulation of disk morphogenesis and viability of rod photoreceptors [45]. Analysis of the mouse genome sequence revealed that *Rom1* and *Eml3* share a common promoter region. Both *Rom1* and *Eml3* exhibit similar expression patterns in adult tissues. Similar expression patterns of both genes and the fact that both genes share a common promoter region suggests the possibility of an interaction between the two proteins. For this reason, we tested the interaction of EML3 with ROM1 in the co-transfection system (Figure 3.10). However, the anti-EML3 antibody was unable to co-immunoprecipitate ROM1 from co-transfected HEK 293T cell lysates (Figure 3.10, IP lane C). For this reason, the lack of interaction of EML3 with ROM1 was used as a negative control for the technique in subsequent co-IP experiments. The lack of interaction of EML3 with ROM1 was tested (and always observed) three times in the co-transfection system.

I therefore conclude from these experiments that EML3 interacts with DYNLL1 and DYNLL2 but that it does not interact with ROM1 in the co-transfection system.

3.2.3 Reciprocally, Dynein Light Chain 2 (DYNLL2) interacts with EML3

To confirm the interaction of EML3 with DYNLL2-DDK in the co-transfection system, I performed a converse co-immunoprecipitation experiment.

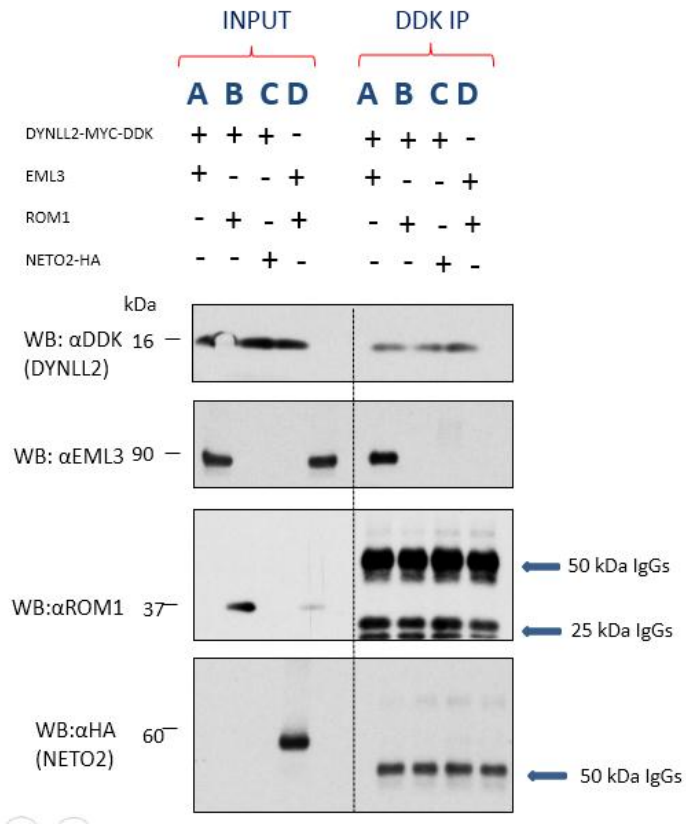

Figure 3.11: Dynein Light Chain 2 (DYNLL2) interacts with EML3. Immunoblots of immunoprecipitates from co-transfected HEK 293T cell lysates. The identities of the transfected cDNAs are shown in panel A. The western blots performed on the input and IP samples are shown in panel B. Anti-DDK antibody was used for immunoprecipitation. Anti-DDK, anti-EML3C884A, anti-ROM1 and anti-HA antibodies were used for immunoblotting. 1% of the input was loaded on the gel.

Anti-DDK tag antibodies that immunoprecipitated transfected DYNLL2-DDK co-immunoprecipitated EML3 from co-transfected HEK 293T cell lysates (Figure 3.11, IP lane A), thus confirming the interaction of DYNLL2-DDK with EML3 in the co-transfection system. The anti-DDK antibody was unable to co-immunoprecipitate either ROM1 (Figure 3.11, IP lane B) or NETO2-HA (Figure 3.11, IP lane C; used here as an additional negative control) from lysates of co-transfected HEK 293T cells. Anti-DDK antibody did not immunoprecipitate directly either EML3 or ROM1 from the HEK 293T cell lysates not transfected with DYNLL2-DDK (Figure 3.11, IP lane D).

We have not yet performed the equivalent co-IP experiment with the DYNLL1 protein. Although we strongly expect a DYNLL1-DDK immunoprecipitation to pull EML3 in a co-transfection system, the experiment should be performed for completeness.

In conclusion, DYNLL2-DDK interacts with EML3 but does not interact with either ROM1 or NETO2-HA in the co-transfection system.

3.2.4 Proteins of the EML family Hetero-oligomerize

Proteins of the EML family associate with MTs and are essential for the formation and function of both the interphase MT network and the mitotic spindle [60, 62, 63, 106]. The EML proteins affect MT dynamics and may act as scaffold proteins to localize mitotic kinases to MTs [60, 68, 107]. In contrast to the well-documented interactions of EML1-4 with MTs, the specific molecular functions of the EML family of proteins remain poorly studied.

The group of Richard Bayliss (Leicester, UK) recently determined the crystal structure of the N-terminal coiled-coil region of two human EML proteins and thus revealed a trimeric state of

oligomerization of EML2 and EML4. The trimerization was directed by a conserved region in the N-terminus of the protein, which corresponds to the coiled-coil and which they renamed the "trimerization domain". According to that study, the trimerization domain (TD), as the group re-named it, is strictly required for homo-oligomerization of the EML proteins. In addition, the Bayliss group determined that the TD and adjacent sequences in the N-terminal region of the protein are essential for MT binding of the EML proteins.

While the paralogs EML1-4 contain the TD in the N-terminal region, the more divergent paralogs EML5 and 6 do not possess the coiled-coil region but have three copies of the TAPE domain. Noteworthy, EML3 contains the most divergent TD [71]. To investigate the ability of EML3 to interact with the other EML proteins, the Bayliss group tested the interaction of YFP-EML3 with FLAG-EML1, FLAG-EML2 and FLAG-EML3. They found that YFP-EML3 interacts strongly with FLAG-EML3, weakly with FLAG-EML2 and failed to interact with FLAG-EML1. I performed co-immunoprecipitation experiments to investigate whether mouse EML3 interacts with mouse EML1, 2 or 4, and to confirm some of the previously published results in our system. The study we performed was novel in that we used an isoform of EML2 which was missing the coiled-coil region and we tested the interaction of EML3 with EML4 which was not done before (Figure 1.14).

3.2.4.1 Interaction of EML3 with paralogs EML1, EML2 and EML4

To elucidate whether EML3 interacts with the paralogs EML1, EML2, or EML4, I performed another co-immunoprecipitation experiment. The isoforms of EML1, EML2, EML3 and EML4 used in the co-immunoprecipitation experiments are presented in figure 1.14. As a positive

control, anti-EML3 antibody successfully co-immunoprecipitated DYNLL1-DDK (Figure 3.12, IP lane D). As a negative control, anti-EML3 antibody was unable to co-immunoprecipitate NETO2-HA (Figure 3.12, IP lane E) from lysates of co-transfected HEK293T cells.

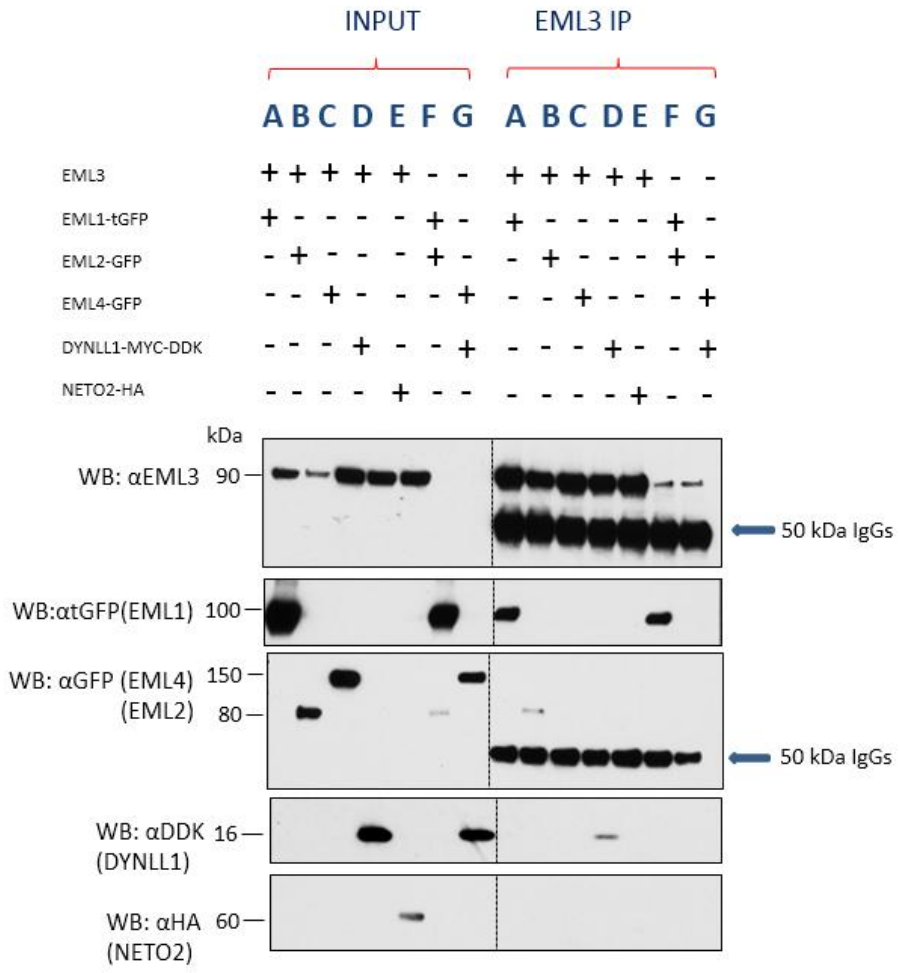

Figure 3.12: EML3 interacts with paralogs EML1 and EML2. Immunoblots of immunoprecipitates from co-transfected HEK 293T cell lysates. The identities of the transfected cDNAs are shown in panel A. Western blots performed on the input and IP samples are shown in panel B. Anti-EML3C884A antibody was used for immunoprecipitation. Anti-EML3C884A, anti-tGFP, anti-GFP, anti-DDK, and anti-HA antibodies were used for immunoblotting. 1% of the input was loaded on the gel. tGFP stands for “Turbo GFP”. It does not have the same sequence as standard GFP.

I found that the anti-EML3 antibody co-immunoprecipitated EML1-tGFP (Figure 3.12, IP lane A) and EML2-GFP (Figure 3.12, IP lane B, band at 80kDa) from lysates of co-transfected HEK 293T

cells. Interestingly, anti-EML3 antibodies failed to co-immunoprecipitate EML4-GFP from lysates of co-transfected HEK 293T cells (Figure 3.12, IP lane C, band at 150kDa).

Surprisingly, EML1-tGFP was also immunoprecipitated from lysates not transfected with *Eml3* (Figure 3.12, IP lane F). Note that anti-EML3 antibody seems to have immunoprecipitated endogenous EML3 from lysates of HEK 293T cells (Figure 3.12, IP lanes F and G), so it is tempting to interpret that endogenous EML3 may have been responsible for the co-immunoprecipitation of EML1-tGFP. In this case, though, endogenous EML3 should also have immunoprecipitated EML2-GFP and DYNLL-DDK but neither of them were detected in IP lanes F and G, respectively, on the immunoblots. A possible explanation for the absence of a band corresponding to EML2-GFP in IP lane F and DYNLL1-DDK in IP lane G is that a large amount of EML3 precipitates only a small amount of both EML2-GFP (compare input lane B and IP lane B on the anti-GFP immunoblot of Figure 3.12) and DYNLL-DDK (compare input lane C and G with IP lane C in the anti-DDK immunoblot of Figure 3.12), and the amount precipitated by endogenous EML3 is therefore below the detection limit of the two antibodies. The EML2-GFP expression was substantially lower in transfection F than in transfection B (compare input lane F and input lane B on α-GFP immunoblot of Figure 3.12). A similar observation where EML1 was immunoprecipitated by anti-EML3 antibody in lysates not co-transfected with *Eml3* was made in previous experiments although the band representing EML1 was much fainter and endogenous EML3 was not detected by WB (data not shown). Thus, a possible explanation for the presence of the band representing EML1-tGFP in Figure 3.12, IP lane F and previous experiments is that the anti-EML3 C884A antibody immunoprecipitates directly EML1-tGFP from lysates of (co-)transfected HEK 293T cells where *Eml3* was not transfected. However, in the

current experiment (Figure 3.12 Input lane F) and in the next experiment (Figure 3.13, INPUT and IP lanes B and C), the anti-EML3 antibody clearly fails to recognize EML1-tGFP by Western Blot (Figure 3.12 input lane F on the anti-EML3 immunoblot) Nonetheless, that does not rule out the possibility that the antibody can recognize EML1 under immunoprecipitation conditions, despite the apparent absence of the epitope within the EML1 sequence, and further investigation would be necessary to dismiss this hypothesis.

The anti-EML3 antibody did not co-immunoprecipitate directly EML4-GFP from lysates of co-transfected HEK 293T cells which were not transfected with *Eml3* (Figure 3.12, IP lane G).

Altogether, these results demonstrate that in the co-transfection system, EML3 interacts with the paralogs EML1-tGFP and EML2-GFP. However, EML3 does not interact with EML4-GFP. The interactions of EML3 with EML1-tGFP, EML2-GFP and EML4-GFP were tested a minimum of three times in the co-transfection system with the same results.

3.2.4.2 Reciprocally, EML1 interacts with EML3

To confirm the interaction of EML3 with EML1, I performed a converse co-immunoprecipitation experiment to verify the ability of EML1-tGFP to co-immunoprecipitate EML3 in the co-transfection system. This experiment was performed to find out whether anti-EML3 antibody can IP EML1- tGFP.

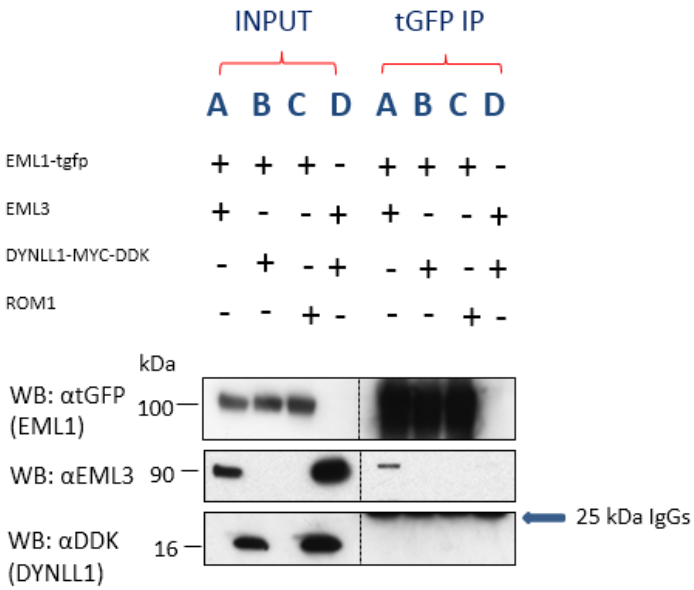

Figure 3.13: EML1 interacts with EML3. Immunoblots of immunoprecipitates from co-transfected HEK 293T cell lysates. The identities of the transfected cDNAs are shown in panel A. Western blots performed on the input and IP samples are shown in panel B. Anti-tGFP antibody was used for immunoprecipitation. Anti-EML3C884A, anti-tGFP, and anti-DDK antibodies were used for immunoblotting. 1% of the input was loaded on the gel.

The results show that the anti-tGFP antibody co-immunoprecipitated EML3 from co-transfected HEK 293T cell lysates (Figure 3.13, IP lane A), thus proving that EML1-tGFP interacts with EML3 in the co-transfection system. The anti-ROM1 immunoblots were not included because the anti-ROM1 antibody failed to immunolabel ROM1 in the input samples where it was transfected. Since EML1-tGFP failed to interact with DYNLL1-DDK (Figure 3.13, IP lane B), we used that result as a negative control in this experiment and did not re-probe with the new anti-ROM1 antibody

The anti-tGFP antibody did not immunoprecipitate directly either EML3 or DYNLL1-DDK from the HEK 293T cell lysates not transfected with *Eml3* (Figure 3.13, IP lane D). The results of the converse experiment confirm that EML1-tGFP interacts with EML3 in the co-transfection system.

3.2.4.3 Reciprocally, EML2 interacts with EML3

To confirm the interaction of EML3 with EML2, I performed a converse co-immunoprecipitation experiment. Anti-GFP antibodies co-immunoprecipitated EML3 from co-transfected HEK 293T cell lysates (Figure 3.14, IP lane A), thus validating that EML2-GFP is able to interact with EML3 in the co-transfection system. Anti-GFP antibodies were also able to co-immunoprecipitate EML1-tGFP from lysates of co-transfected HEK 293T cell lysates (Figure 3.14, IP lane B) establishing an Interaction between EML2-GFP and EML1-tGFP as previously published by the Bayliss group [71].

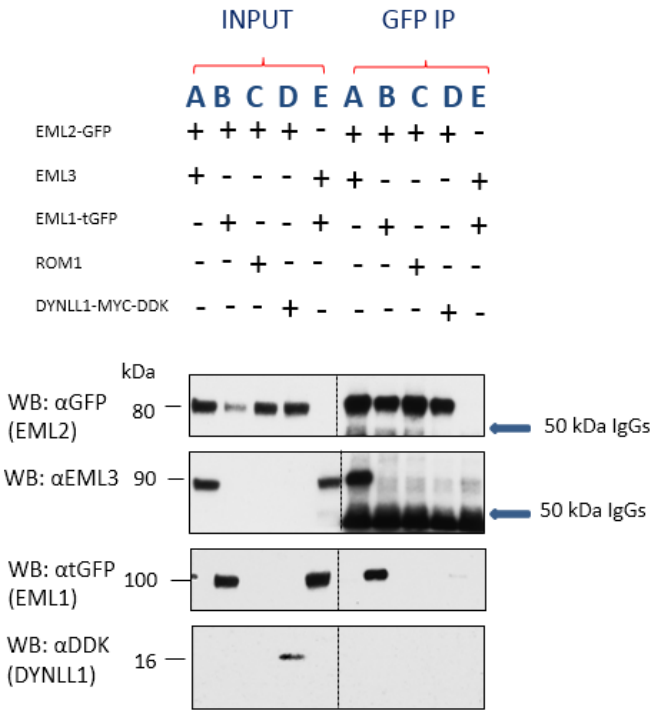

Figure 3.14: EML2 interacts with EML3. Immunoblots of immunoprecipitates from co-transfected HEK 293T cell lysates. The identities of the transfected cDNAs are shown in panel A. Western blots performed on the input and IP samples are shown in panel B. Anti-GFP antibody

was used for immunoprecipitation. Anti-EML3C884A, anti-tGFP, anti-GFP, and anti-DDK antibodies were used for immunoblotting. 1% of the input was loaded on the gel.

The anti-GFP antibody did not immunoprecipitate directly either ROM1 (Figure 3.14, IP lane C; data not shown) or DYNLL1-DDK (Figure 3.14, IP lane D) from lysates of co-transfected HEK 293T cells. The lack of interaction of EML2-GFP with DYNLL1-DDK serves as a negative control for this experiment. The anti-ROM1 immunoblot was again not presented as the anti-ROM1 antibody immune-labeled ROM1 only very weakly in the input sample where it was transfected. A fresh ROM1 antibody from the Molday lab was not deemed necessary due to the presence of another co-IP result that turned out to be negative (absence of interaction between EML2-GFP and DYNLL1-DDK).

Importantly, the anti-GFP antibody did not immunoprecipitate directly either EML3 or EML1-tGFP from the lysates of co-transfected HEK 293T cells not transfected with *Eml2-GFP* (Figure 3.14, IP lane E).

Altogether, the results confirm that EML2-GFP interacts with both EML3 and EML1-tGFP but that it does not interact with either ROM1 or DYNLL1-DDK in the co-transfection system.

3.2.4.4 EML4 does not interact with EML3

To confirm the absence of interaction between EML3 and EML4-GFP, I performed a co-immunoprecipitation experiment using mammalian HEK 293T cells. The results demonstrate that the anti-GFP antibody was unable to co-immunoprecipitate EML3 from co-transfected HEK 293T cell lysates (Figure 3.15, IP lane A). Therefore, EML4-GFP does not interact with EML3 in the co-transfection system.

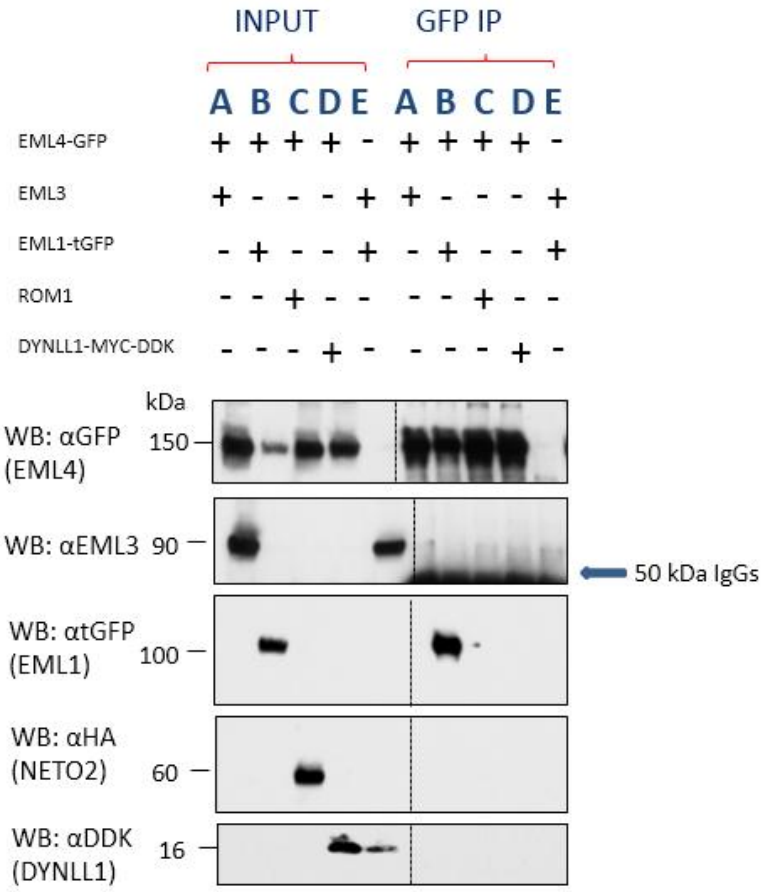

Figure 3.15: EML4 does not interact with EML3. Immunoblots of immunoprecipitates from co-transfected HEK 293T cell lysates. The identities of the transfected cDNAs are shown in panel A. Western blots performed on the input and IP samples are shown in panel B. Anti-GFP antibody was used for immunoprecipitation., Anti-GFP, anti-EML3C884A, anti-tGFP, anti-HA, and anti-DDK were used for immunoblotting. 1% of the input was loaded on the gel.

The anti-GFP antibody was able to co-immunoprecipitate EML1-tGFP from lysates of co-transfected HEK 293T cell lysates (Figure 3.15, IP lane B), thus demonstrating that EML4-GFP interacts with EML1-tGFP in the co-transfection system.

The anti-GFP antibody did not co-immunoprecipitate either NETO2-HA (Figure 3.15, IP lane C) or DYNLL1-DDK (Figure 3.15, IP lane D) from lysates of co-transfected HEK 293T cells. Therefore,

EML proteins that do not have a DYNLL-binding motif (EML1, EML2 and EML4) do not interact with EML3 in our co-transfection cell culture system

The anti-GFP antibody did not immunoprecipitate directly either EML3 or DYNLL1-DDK from lysates of co-transfected HEK293T cells not expressing EML4-GFP (Figure 3.15, IP lane E).

The results of the converse experiment, which was repeated three times with the same outcome, confirm that EML4-GFP interacts with EML1-tGFP but fails to interact with EML3 in the co-transfection system.

In conclusion, the results of the co-immunoprecipitation experiments demonstrate that in the *in vitro* mammalian co-transfection system EML3 interacts with DYNLL1-DDK, DYNLL2-DDK, EML1-tGFP and EML2-GFP. However, EML3 fails to interact with EML4-GFP, ROM1, and NETO2-HA (which was chosen as the negative control). Figure 3.16 presents a summary of all the EML3 interactions in the co-transfection system found in this study.

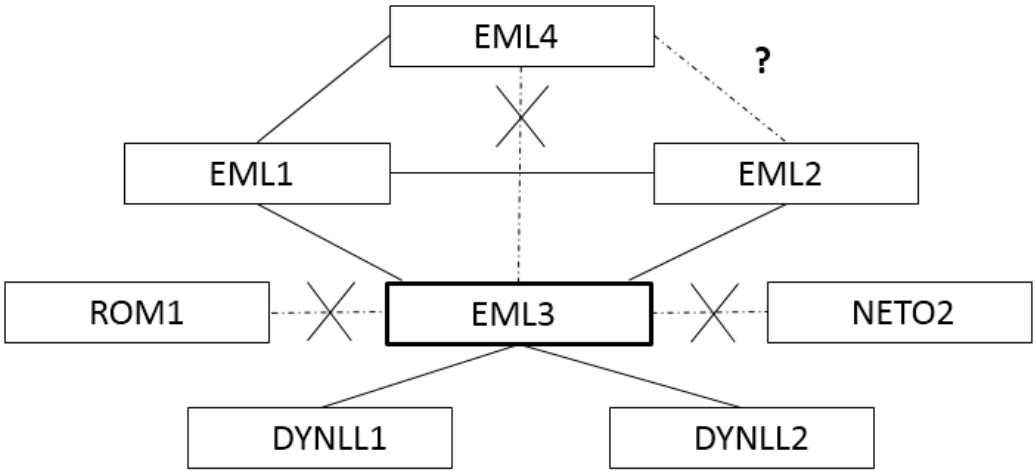

Figure 3.16: Summary of the positive and negative interactions of EML3 in the mammalian co-transfection system. Proteins are shown in rectangular boxes. Positive interaction between EML3 and the interacting proteins are shown by connecting the two proteins with a straight line. Negative interactions between two proteins are shown by connecting the two proteins with dotted lines and crosses. Unknown interactions are marked by dotted lines with a question mark.

3.3 Study of the co-localization of EML3 and DYNLL

Having established, using the co-immunoprecipitation assay, that EML3 interacts with DYNLL, I proceeded to investigate whether EML3 and DYNLL co-localize *in vivo*. Previously, confocal microscopy analysis of adult mouse retina stained against EML3 and ROM1, a marker of PR outer segments, demonstrated that EML3 is expressed in the inner segment (IS) of photoreceptors (PRs) and not in the outer segment (OS) (Isabelle Carrier; unpublished results). To test for co-localization of EML3 and DYNLL, immunofluorescence was again performed on post-natal day 24 (PN24) mouse retinal sections with antibodies against EML3, DYNLL and ROM1. Immunofluorescent staining for EML3 and ROM1 was performed using rabbit anti-EML3

antibody and mouse anti-ROM1 antibody respectively. Secondary antibodies (AF488-conjugated donkey anti-rabbit IgG and AF594-conjugated sheep anti-mouse IgG; Table 2.2) were used to stain EML3 and ROM1 indirectly, respectively. Since the antibody against DYNLL was also raised in rabbit, the anti-DYNLL antibody was conjugated with AF647 (Table 2.2) to directly label DYNLL and the staining was done sequentially. Hoechst was used to stain the nuclei.

3.3.1 EML3 Co-localizes with DYNLL in the IS of the retina

Consistent with previous immunofluorescence data from our lab, we observed intense EML3 immunostaining in the IS of PRs (green; Figure 3.17, A). Punctate immunostaining in the ONL of the wild-type (WT) retinal sections was also observed for EML3 (Figure 3.17, A). ROM1 is expressed in the OS of PRs (white; Figure 3.17, A, B and C). Immuno-labelling of WT and DKO retinal sections using anti-DYNLL-AF647 antibody revealed expression of DYNLL (red) in almost all the layers of the retina with predominant expression in the IS and outer plexiform layer (OPL) (Figure 3.17, A,C and D). Notably, the photoreceptor OSs are not stained (Figure 3.17, B, C and D) and the distribution does not appear affected by the absence of either EML3 or ROM1 (compare B and D of Figure 3.17). Merging signals from EML3 and DYNLL shows that both localize to the IS of PRs of the retina (yellow; Figure 3.17, C). Immunostaining for both EML3 and ROM1 was not detected in the retinal sections from the *Rom1/Eml3*-DKO mice indicating that the staining was specific for EML3 and ROM1 respectively (Figure 3.17, D).

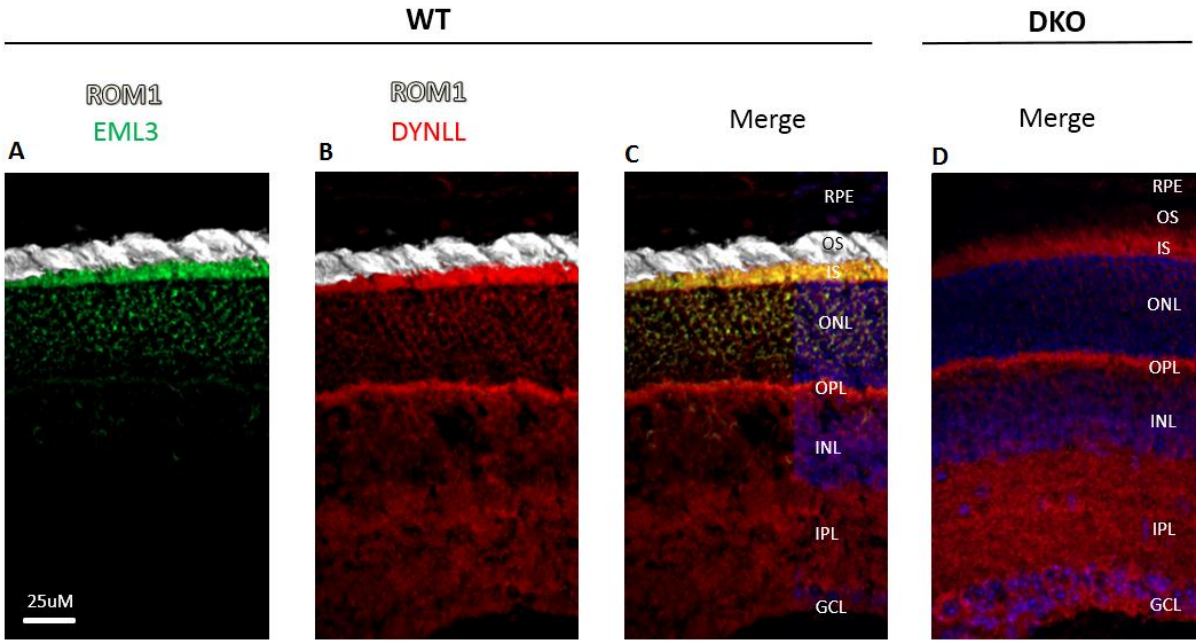

Figure 3.17: EML3 co-localizes with DYNLL in the inner segment of photoreceptors. Confocal microscopic images of immunostained WT and DKO PN24 mouse retinal sections labeled with anti-EML3N1 antibody (green), anti-ROM1 antibody (white), anti-DYNLL antibody conjugated to AF647 (red), and Hoechst (nuclear staining; blue). Secondary antibodies AF488-conjugated anti-rabbit IgG and AF594-conjugated anti-mouse IgG were used to label EML3 and ROM1 respectively (Table 2.2). Scale bar, 25 µm.

At higher magnification (63X objective), merging the green channel representing EML3 and red channel representing DYNLL further demonstrated co-localization in the IS of the PRs of the WT retina (yellow; Figure 3.18, A). Again, absence of both ROM1 and EML3 immunostaining in the PN24 DKO mouse retina (Figure 3.18, B) confirms the specificity of the anti-EML3 and anti-ROM1 antibodies for EML3 and ROM1 respectively.

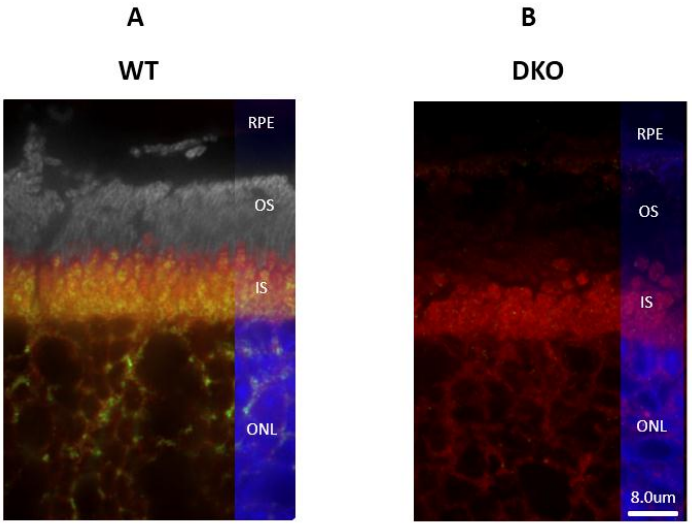

Figure 3.18: EML3 co-localizes with DYNLL in the inner segment of the PRs of the retina. Confocal microscopic images of immunostained WT (A) and DKO (B) PN24 mouse retinal sections labeled with anti-EML3N1 antibody (green), anti-ROM1 antibody (white), AF647-conjugated anti-DYNLL antibody (red), and Hoechst (nuclear staining; blue). Secondary antibodies AF488-conjugated anti-rabbit IgG and AF594-conjugated anti-mouse IgG were used to label EML3 and ROM1 respectively (Table 2.2). Merging signals from EML3 and DYNLL shows co-localization in yellow (A). Scale bar, 8 µm.

In conclusion, the immunofluorescence data demonstrates that EML3 and DYNLL are both expressed in the IS of PRs of the retina. Whether this represents a direct physical interaction *in vivo* is subject to further investigation.

3.4 Summary of results

This study revealed novel putative interactors of EML3 as identified by the co-immunoprecipitation technique, namely: EML1, EML2, DYNLL1 and DYNLL2. The interaction identified between EML3 and DYNLL in the *in vitro* assay was explored further using the immunofluorescence technique which showed the co-localization of EML3 and DYNLL in the IS of PRs of the retina.

Chapter 4: Discussion

The Echinoderm Microtubule Associated Protein (EMAP) was first discovered in sea urchins where it co-purified with microtubules [52]. In mammals, the homologs of the EMAP protein family make up the EML (EMAP-like) protein family. Six EML proteins (EML 1-6) have been identified [60-64]. EML3 merited further investigation after our initial studies indicated that EML3 is required for mouse development and post-natal viability. However, the *Eml3*-KO has not be made/tested previously in the literature. To validate this indication, our lab is currently generating an *Eml3*-KO mice. An understanding of the function of EML3 could not be fully acquired without knowledge about its interactome. Thus, the overall aim of my project was to characterize the molecular functions of EML3 by identifying the potential interacting partners of EML3. Initially, a thorough screening of the scientific literature and high-throughput interactome datasets was performed to generate a list of the potential interacting partners of EML3.

This study investigates the interaction of EML3 with putative interacting proteins in a mammalian cell co-transfection system. Immunofluorescence was then used to show co-localization of EML3 with a confirmed candidate interacting partner, DYNLL, in adult mouse retinal sections. The results of this study will be useful in further investigating the molecular functions of EML3.

4.1 Interaction of EML3 with DYNLL

DYNLL has two mammalian paralogs, DYNLL1 and DYNLL2, both of which share 93% sequence identity [83, 85]. For this reason, most antibodies and functional assays fail to distinguish the

two proteins. Hence, at present, there is no known difference in the molecular function of both proteins in my EML3 interaction data. Thus, the protein is often referred to simply as DYNLL. DYNLL, a 10kDa protein, is a component of the Cytoplasmic Dynein complex that transports cargo along cytoplasmic microtubules. In addition, some literature suggests that DYNLL acts as a cargo binding adaptor when in complex with dimeric proteins that contains a DYNLL-binding motif such as that found in EML3 [95, 129]. DYNLL is also considered to be a eukaryotic hub protein that functions as a dimerization engine (Figure-1.23) [85]. One of the ways in which DYNLL can regulate the function of its binding partners is by promoting dimerization of the binding protein and by stabilizing the dimeric structure [85, 93, 94]. Interestingly, DYNLL binding motifs are often in close proximity to potential dimerization domains such as coiled-coil domains [94, 98, 99].

EML3 has a DYNLL-binding motif which is indeed close to the N-terminal coiled-coil domain. This motif is unique to EML3 within the EML family. Human EML3 contains the exact match of the phage-selected consensus sequence motif - “VSRGTQTE”, required to bind DYNLL with nano-molar affinity [95]. The group of Gabor Pal applied a directed evolution approach by selecting DYNLL binders from a phage-displayed peptide library to define the *in vitro* evolved DYNLL-binding motif. In that study, Rapali and colleagues provided quantitative characterization of the binding preference of the DYNLL-binding site. Based on the *in vitro* evolved binding sequence pattern they predicted a large number of novel binding partners of DYNLL. One of the putative binding partners identified in that study was EML3. However, that conclusion was based on binding assays using a small fragment of the EML3 protein (residues 8-

94) [95, 96]. To test the interaction of EML3 with DYNLL1 and DYNLL2 we performed co-immunoprecipitation experiments with full-length proteins.

According to my *in vitro* co-immunoprecipitation assays, EML3 interacts with DYNLL1 and DYNLL2, at least in a co-transfection system, and that is in accordance with the results of the study mentioned above. However, provide the first experimental evidence of the interaction between full-length EML3 and DYNLL proteins (Figure 3.1, Figure 3.3).

The results of the co-immunoprecipitation assays confirmed that EML3 is the only member of the EML family that interacts with DYNLL. This is because EML3 has a DYNLL binding motif that is unique to EML3 within the EML family. EML1 (Figure-3.4, IP lane B), EML2 (Figure-3.5, IP lane D) and EML4 (Figure-3.6, IP lane D) could not co-immunoprecipitate DYNLL from lysates of co-transfected HEK 293T cells, thus, proving that EML3 is in fact the only member of the EML family to interact with DYNLL.

The co-immunoprecipitation and co-localization of EML3 and DYNLL do not necessarily prove that the two proteins directly interact *in vivo*. The *in vitro* results indicate that these proteins can interact physically when large quantities of the two proteins are present in a cell lysate, and may do so *in vivo*. Finding an interaction between EML3 and DYNLL in the mammalian co-transfection system was the first step towards finding out whether an EML3-DYNLL complex plays a role in some aspect of retrograde transport across photoreceptor PR microtubules.

Having found an interaction of EML3 with DYNLL1 and DYNLL2 in the co-transfection system, we focused on the characterizing the localization of EML3 with DYNLL in adult mouse retinal sections. We performed a co-localization study using the immunofluorescence technique. The

application of confocal microscopy following staining by antibodies directed against the two interacting proteins was used to show co-localization of EML3 and the interacting partner DYNLL. EML3 and DYNLL both co-localized to the inner segment (IS) of PRs of the retina.

Given that DYNLL is a protein that functions in retrograde transport across microtubules, one possibility is that, in the retina, EML3 interacts with DYNLL to bring cargo proteins produced in the IS to the connecting cilium (CC). Once the proteins reach the CC, different motor proteins (Kinesins) help transport cargo from the CC to the outer segment (OS), where the proteins function. Therefore, the interaction of EML3 with DYNLL in the mammalian co-transfection system provides the stepping stone to further understanding the microtubule function of EML3.

In this present work, we provide clear evidence that EML3 and DYNLL are components of the mouse retina. Both proteins localize to the IS of PRs of the retina. Those results, taken together with the qPCR analysis done previously in the lab which revealed that *Eml3* is predominantly expressed in the adult mouse retina suggest that EML3 plays an important role in the IS of PRs of the retina. However, the exact mode of interaction as well as the functional relevance of the EML3-DYNLL interaction is subject to further investigation.

EML3 and DYNLL could be part of a complex with other proteins and it is possible that they could accomplish some tasks together that neither could accomplish alone.

DYNLL2 has been shown to bind to Myosin Va (Myo Va), a motor protein involved in cargo transport along acting filaments. The DYNLL-recognition motif of Myosin Va motor protein, despite deviations from the consensus motif, accommodates the same binding groove of DYNLL2 as do all its other partners, such as EML3 [129]. DYNLL is therefore a subunit of two

intracellular transport protein complexes: Dynein and Myosin Va, which are respectively involved in the microtubule-based and actin-based movement of proteins, organelles and vesicles in cells such as neurons [129, 130]. I hypothesize that EML3, by interacting with DYNLL, may modulate cargo transport across both microtubules and actin filaments. Another report used yeast two-hybrid library screens to show that DYNLL1 interacts with the conserved C-terminus peptide of the PAX6 protein, a transcriptional regulator with a key role in ocular and neurological development. In that study, the authors proposed that the interaction of PAX6 with DYNLL1 is a mechanism by which synaptic activation could lead to changes in neuronal transcriptional activity. They proposed that PAX6 released from post synaptic densities (PSD) upon synaptic activation could then be delivered by DYNLL to its transcriptional targets in the nucleus. The PAX6/DYNLL complex would travel along the PSD-associated actin cytoskeleton via Myosin Va motors, followed by Dynein-mediated transport along the microtubule network, towards the nucleus [130]. It is interesting to speculate the interaction of EML3 with DYNLL (part of the PAX6/DYNLL complex) could be the basis of a mechanism by which synaptic signaling causes changes in gene expression in neurons.

4.2 Interaction of EML3 with Rod Outer Segment Membrane Protein 1 (ROM1)

Since *Eml3* and *Rom1* share a common promoter region, initially, we hypothesized that both genes are co-regulated. Consistent with that hypothesis, EML3 and ROM1 are both predominantly and abundantly expressed in the retina (Figure 1.17). Previously published studies provide evidence of genes belonging to the same functional group having similar expression patterns and sharing expression regulation mechanisms [131]. Therefore, a hypothesis of our lab was that co-regulation of *Eml3* and *Rom1* may indicate a functional

connection or even physical interaction between the gene products [132, 133]. Although the exact function of EML3 in the mammalian retina is being elucidated, we know that ROM1 is required in rod photoreceptors for the regulation of disk morphogenesis and viability of rod photoreceptors.

There is a possibility that after the production of ROM1 in the IS, EML3, in association with the microtubule components of the IS facilitate the transport of ROM1 from the IS to the CC of rod photoreceptor cells. From the CC, different motor proteins transport ROM1 to the OS where it functions.

Indeed, my co-localization studies using indirect IF revealed that ROM1 localized to the OS of the retina while EML3 was found to be expressed predominantly in the IS with punctate localization in the ONL. We found that ROM1 and EML3 do not interact in the co-transfection system (Figure 3.1). Anti-EML3C884A antibodies (Table 2.2) failed to co-imunoprecipitate ROM1 from lysates of co-transfected HEK 293T cells. Although the data presented in this study suggests that EML3 and ROM1 do not physically interact, it is still a possibility that EML3 is required for the transport of ROM1 into the CC of rod photoreceptors, via an indirect interaction. A formal test for this hypothesis requires analysis of the photoreceptors in the rod photoreceptor-specific EML3 null mice that we are currently generating in the lab. In these mice, if ROM1 is still properly localized in photoreceptors that do not express the EML3 protein, it will be proof that the hypothesis was wrong.

4.3 Hetero-oligomerization of the EML proteins

Recently, Richards and colleagues revealed the crystal structure of the N-terminal coiled-coil regions of EML proteins [71]. That group studied the structural basis of EML self-association and activation of the oncogenic EML-Kinase fusion proteins. The N-terminal region of the EML family of proteins is poorly conserved as opposed to the highly conserved TAPE domain. This region is subject to splice variation as well. However, within this disordered region is a conserved primary sequence that was predicted to form coiled-coils. It is that specific coiled-coil region of both EML2 and EML4 that was separately crystallized by Richards and colleagues. The crystal structures revealed that both proteins formed trimeric coiled-coils. In other words, the EML proteins were found in a trimeric state of oligomerization [71]. The TD is an amphipathic α-helix composed of nine conserved hydrophobic residues (predominantly leucine and valine) whose side chains form the core of the trimer. A conserved glutamine on the inner surface makes hydrogen bonds with main chain carbonyls in the core. This serves to maintain the shape of the coiled-coil. Side chains of conserved charged residues that are interspersed between the hydrophobic residues form salt bridges with that of adjacent protomers around the outside of the trimer. The pattern of conserved residues in the EML TD suggests that human EML1-4 are all trimeric. *In vitro* studies done by the same group revealed that the TD is also required for EML1 homo-oligomerization [71]. Presence of the TD in EML1-4 proteins suggests that the EML family of proteins can associate with each other to form homo- or hetero- trimers. Whether all such possible trimers exist remains to be determined carefully.

Noteworthy, the more divergent paralogs EML5 and EML6 do not possess coiled-coil regions but have three copies of the TAPE domain each. Formation of homo-trimers by EML1-4 could

result in the quaternary structure of all six EML proteins having three TAPE domains [71]. However, this hypothesis is subject to further verification.

The results of my co-immunoprecipitation assays show that EML3 interacts with DYNLL which is known to promote dimerization of its binding partner [83]. EML self-association through a trimerization domain and binding of DYNLL to EML3 homo-dimers appear to be two conflicting protein interactions. This raises many questions and new hypotheses about the protein interactions for the EML3 protein specifically, most of which deal with apparent competition between self-association and binding to DYNLL. One hypothesis that does not rely on competition is the possibility that DYNLL promotes dimerization of EML3 trimers. If EML3 can bind EML1 under the same conditions (as in the co-IPs), it is possible that EML1 and DYNLL end up in the same multiprotein complex. It is a possibility that perhaps EML hetero-oligomerizations compete with EML3 homodimer binding to DYNLL. However, this will require further experiments. For now, we have not performed a three way transfection with the three proteins EML1, EML3 and DYNLL to know if DYNLL will pull EML1, vice versa. Most of the experiments required to test such hypotheses will require collaborative efforts with structural biology experts.

The key residues within the TD that are involved in self-association are imperfectly conserved. According to the recent study on the TD of EML proteins, EML3 has the most divergent TD. For this reason, Richards and colleagues tested the ability of YFP-EML3 to co-immunoprecipitate FLAG-EML1, FLAG-EML2 and FLAG-EML3 from lysates of co-transfected HEK 293 cells. According to their results, YFP-EML3 co-immunoprecipitated with FLAG-EML3 and more weakly with

FLAG-EML2. The authors claim that YFP-EML3 failed to co-immunoprecipitate with FLAG-EML1 [71].

However, my results showed that EML3 successfully co-immunoprecipitated EML1-tGFP from lysates of co-transfected HEK 293T cells (Figure-3.4). This is not necessarily surprising because the *Eml1-tGFP* cDNA clone (catalog number MG217188), ordered from Origene, encodes the full-length EML1 protein containing the N-terminal coiled-coil region that was thought to be necessary for association of the EML proteins.

Our results established/detected that EML3 interacts with EML2-GFP in the co-transfection system. However, the *Eml2-GFP* cDNA clone that we obtained from Susanne Bechstedt (Brouhard lab, McGill University) does not encode for the full-length EML2 protein. The entire TD is missing in the *Eml2-GFP* cDNA clone that was used in our study.

How is it possible that we obtain EML2-EML3 and EML2-EML1 interactions in our studies without the EML2 TD? First, it is important to note that the Bayliss group determined that the TD is sufficient for EML2 self-trimerization and both sufficient and necessary for EML1 self-association [71]. Therefore, the Bayliss group did not test the ability of ΔTD EML2 proteins to interact with either EML3 or EML1 proteins like we did. It is also relevant to point out that the Bayliss group used human EML2 proteins instead of mouse EML2 proteins – although the two proteins display 95.6% sequence similarity. Therefore there is a second interaction region in EML2 that facilitates the interaction of EML2 with EML3 in the mammalian co-transfection system.

There are two splice variants of EML2 (Figure 1.14). Northern blot analysis performed by the Suprenant group indicates that EML2 transcripts may be differentially spliced in neuronal tissues [104]. According to the work published by the Suprenant and the Bayliss groups, the more widely expressed isoform-1 of EML2 lacks the coiled-coil region [71, 104]. That is the isoform used in our co-IP work (Figure 1.14). The N-terminal coiled-coil region is present in the brain/spinal cord-specific variant isoform-2 that the Bayliss group used in their recently published study. Therefore, it is not surprising that the results from their study showed that YFP-EML3 interacts with FLAG-EML2 isoform-2 in the co-transfection system [71]. We could make our experiment more complete if we clone the full-length mouse *Eml2* cDNA and compare side-by-side the interaction of EML3 with full-length mouse EML2 and ΔTD mouse EML2 in the co-transfection system.

Our identification of the interaction of EML3 with EML2-GFP raises the possibility that perhaps, in absence of the coiled-coil region, the TAPE domain of EML2 allows it to form hetero-oligomers with other members of the EML family. The TAPE domain is composed of two β-propellers formed from the WD40 repeat region and the HELP motif [67]. The β-propeller structure, formed by folding of the WD40 repeats is known to form a platform without any catalytic activity that provides multiple protein-protein binding surfaces for reversible protein complex formation [65]. Even though, work performed by Richards and colleagues confirm that the TD is necessary for self-association of EML1 [71], the findings from my own experiments indicate that the TAPE domain could in fact be playing a crucial role in mediating interaction of the EML proteins with each other in absence of the coiled-coil region. However, additional experimental evidence would be required to independently confirm the ability of the TAPE-

domain to mediate association of the EML proteins in absence of the N-terminal coiled-coil region. An over-expression study of various EML3 constructs could show the ability of the TAPE domain to mediate interaction of EML3 with EML2 in the mammalian co-transfection system in presence and absence of the coiled-coil domain.

The Bayliss group in their recently published study presented an alignment of the TDs of EML1-4. This study correlated the interaction between YFP-EML3 and FLAG-EML1, FLAG-EML2 and FLAG-EML3 with the degree of conservation within the 17 key residues involved in self-association (Figure 1.25, Panel B). Between EML1 and EML3 there are 6 identical residues and 5 residues are conservatively substituted. Between EML2 and EML3 there are 9 identical residues and 3 residues are conservatively substituted (Figure 1.25, Panel B). This study suggested that the association of EML3 with itself and the paralogs EML1 and EML2 is in accordance with the similarity of residues within the 17 key residues involved in self-association [71]. Essentially, the Bayliss group suggests that the EML3-EML2 interaction is stronger than the EML3-EML1 interaction because EML2 is more closely related to EML3 within its coiled-coil. Our results cast some doubt on that hypothesis as we obtained strong EML3-ΔTD - EML2 interactions. Interestingly, the Bayliss group did not show any data about the interaction of EML3 with EML4.

We found that EML3 was unable to co-immunoprecipitate EML4-GFP from lysates of co-transfected HEK 293T cells (Figure 3.3, IP lane C). Despite the fact that the *Eml4* cDNA clone from Susanne Bechstedt (Brouhard lab, McGill University) encodes the full-length mouse EML4, the differences between the interaction of EML3 with EML1, EML2 and EML4 suggest that different mechanisms might be involved in regulating the association of the EML proteins. It is

also possible that the interaction between EML3 and EML4 is suppressed in the context of the full-length proteins.

According to annotations in the UCSC genome browser, the *Eml4* isoform that was used in our study corresponds to "*Eml4* transcript variant 4". Alignment of all four isoforms of EML4 protein sequences using Clustal Omega 1.2.1 [134] revealed that they are 87.3% identical over all (Figure 4.1). The C-terminal region residues are identical amongst the four isoforms of EML4 according to the multiple sequence alignment. The four splice variants of EML4 vary in the N-terminal disordered region preceding the TAPE domain. The four EML4 isoforms are annotated as Q3UMY5-1 to -4 in the Uniprot database [135], The EML4 isoform used in our study is 941 amino acids long (Uniprot ID: Q3UMY5-3). Isoform-1 has an extra 58 amino acid sequence between the TD and TAPE domains that is not found in any of the other three isoforms. In isoform-2 and isoform-4, a major part of the N-terminal disordered region between the TD and TAPE domain is missing.

Figure 4.1: Alignment of the N-terminus end of the four splice isoforms of EML4. Q3UMY5-3 represents the isoform of EML4 used in this study. Residues that are identical in all four isoforms are marked with an asterisk and highlighted in dark grey. The C-terminal coiled-coil domain in the EML4 isoforms are shown in a black box. The beginning of the TAPE domain in the EML4 isoforms is shown in a red box [135].

In comparison to the other mouse *Eml4* isoforms (Q3UMY-1, Q3UMY-2, and Q3UMY-4), we identified an alternative exon 1 and an extra exon (exon 2) that is exclusive to the isoform of *Eml4* that was used in our study (Uniprot ID: Q3UMY5-3). One publication reports the cloning of a full-length cDNA sequence of *Eml4* from adult mouse brain [106]. Interestingly, Houtman and colleagues cloned the isoform that we have used in our studies but already acknowledged that there is tissue-specific alternative splicing of *Eml4.* Although the isoform that they first cloned is the one with extra exon 2, Houtman and colleagues tried to find where the exon 2-containing isoform of *Eml4* was expressed and they did not see this specific *Eml4* isoform as strongly expressed as the other *Eml4* isoforms without exon 2. Houtman and colleagues suggested that

the *Eml4* transcripts containing exon 2 were therefore expressed either at very low levels or expressed in areas not examined in their study [106]. Indeed there are many EST clones that represent *Eml4* in databases but only one that represents our exon 2-containing isoform.

At the protein level, the splice variants do not affect the EML4 domain structure. However, according to Houtman and colleagues, transcripts that include exon 2 disrupt the N-terminal coiled-coil domain [106, 136, 137]. This suggests that the N-terminal coiled-coil region of the EML4 isoform used in our study was disrupted, which lead to failure of EML3 to interact with EML4-GFP in the co-transfection system. Unfortunately, although that statement by Houtman and colleagues appears to explain our data, it is not supported by experimental evidence in their report. If the statement is based on coiled-coil prediction software failing to detect the secondary structure on the exon 2-containing isoform back in 2004; current online prediction software COILS (www.ch.embnet.org/software/COILS_form), that predicts coiled-coil regions in proteins, has no problem detecting an intact coiled-coil (Figure 4.2). COILS compares a protein sequence to a database of known parallel two-stranded coiled-coils and derives a similarity score. By comparing this score to the distribution of scores in globular and coiled-coil proteins, the program then calculates the probability that the sequence will adopt a coiled-coil conformation [136]. According to COILS, the *Eml4* isoform used in our study (Q3UMY5-3) and the longer *Eml4* isoform (Q3UMY5-1) are predicted to contain an N-terminal coiled-coil region.

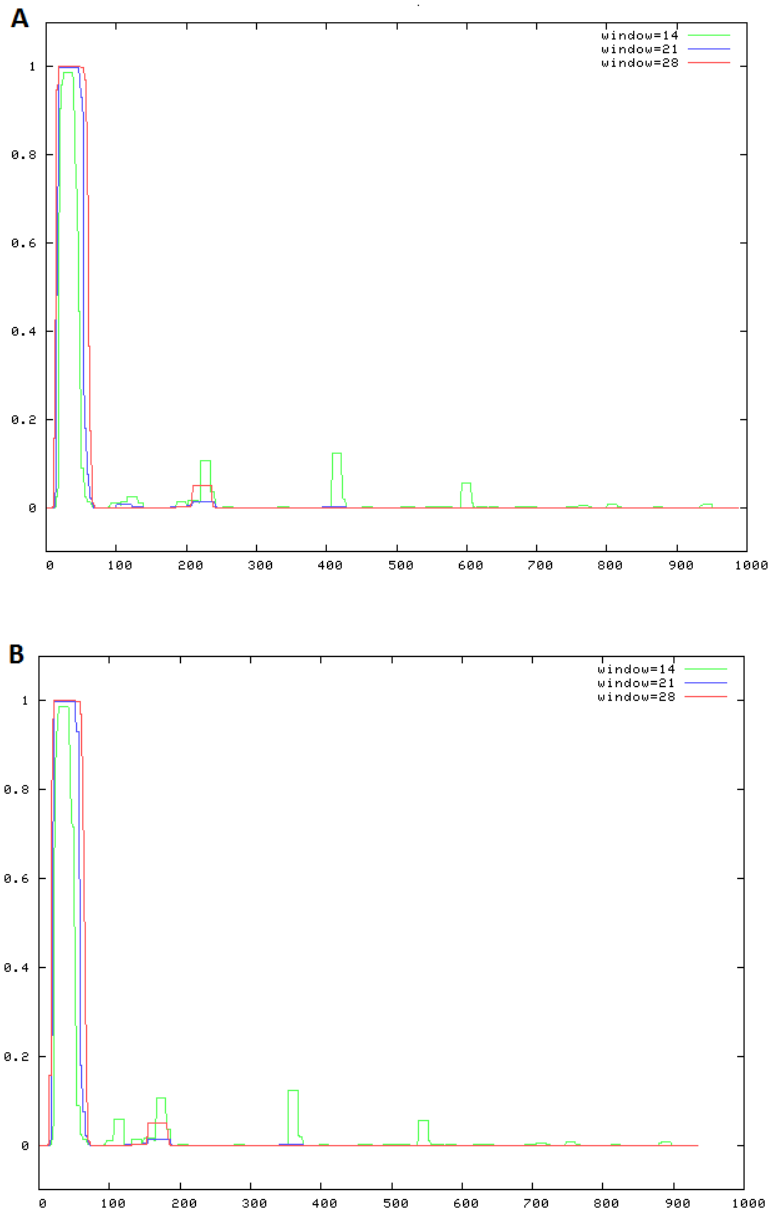

Figure 4.2: Prediction of coiled-coil region in the long EML4 isoform (Q3UMY5-1)(A) and the EML4 isoform (Q3UMY5-3)(B) used in our study. The Y-axis shows the probability score for presence of coiled-coil region along the amino acid resides shown on the X-axis. The region identified as the coiled-coil lies between residues 30-60 in both EML4 isoforms [136].

Multiple sequence alignment of the EML1-4 protein sequences used in our study was performed using Clustal Omega 1.2.1 (Figure-4.3) [134]. As mentioned above, the EML2 isoform used in our study did not contain the N-terminal coiled-coil region. The alignment shows a good

degree of conservation and sequence identity in the C-terminal regions of EML1-4, which forms the TAPE domain. The sequence identity as well as the sequence conservation is poor in the N-terminal region of EML1, 3 and 4 particularly between the TD and TAPE domain. The lack of conservation of the protein sequence of the N-terminal region of EML 1, 3 and 4 could be responsible for the difference in interaction of EML3 with EML1 and EML4.

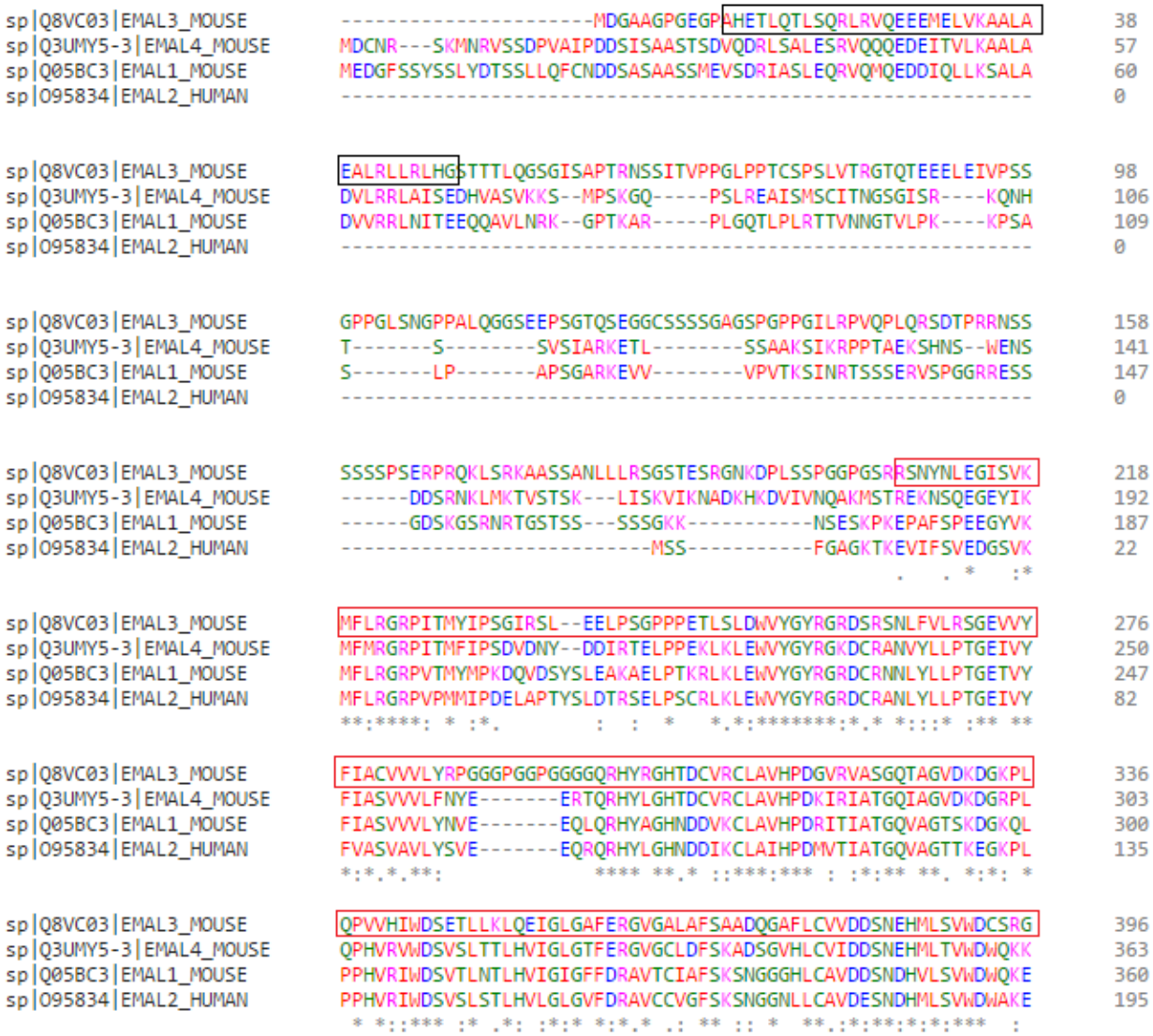

Figure 4.3: Multiple sequence alignment of the N-terminal regions of EML1, EML2, EML3 and EML4 used in my co-IP experiments. Residues are color-coded according to the nature of the side chains. Hydrophobic residues are represented in red. Acidic residues are represented in

blue. Basic residues are represented in magenta, other residues are represented in green. Identical residues are marked with an asterisk below. Conserved residues are marked with a colon below. Residues that form the coiled-coil region in EML3 are enclosed in a black rectangle. The residues that indicate a segment of the TAPE domain in EML3 are enclosed in a red rectangle [134].

However, the fact that an EML2 protein which is missing most of the N-terminal region can still interact with EML3 and EML1 in our experiments suggests that the N-terminal region might not directly mediate the hetero-oligomerizations but rather modulate them. Under that hypothesis, the N-terminus encoded by the EML4 isoform used in our experiments would have the ability to interfere with the hetero-oligomerization with EML3 but not with EML1 (EML4-EML2 oligomerization not tested yet). And, under that same hypothesis, a complete truncation of the N-terminal region (as in the EML2 clone used in our experiments) would not interfere with any of the EML hetero-oligomerizations. Since the N-terminal region of EML1, EML2 and EML4 proteins was shown by Richards and colleagues to mediate homo-oligomerization, our hypothesis can be fine-tuned to state that perhaps homo-oligomerization of EML proteins through the TD interferes with their ability to hetero-oligomerize through their TAPE domain. A proper challenge for that hypothesis requires the identification of the minimal EML4 protein domain necessary for hetero-oligomerization with EML3 followed by selective addition of EML4 sequences that will eventually result in a loss of interaction as was found in my current studies.

4.4 Future work

The first step we took towards understanding the molecular function of EML3 in the retina, was to investigate whether EML3 interacts with the motor protein DYNLL in the mammalian co-transfection system. Co-IP experiments confirmed that EML3 interacts with both DYNLL1 and DYNLL2 in the mammalian co-transfection system. Co-localization studies confirmed that both

EML3 and DYNLL (please note that anti-DYNLL antibodies recognize both isoforms of DYNLL) are co-expressed in the IS of PRs of the adult mouse retina. The functional relevance of the interaction of EML3 with DYNLL still remains elusive.

The next step would be to confirm the presence of an interaction between EML3 and DYNLL in the context of endogenous proteins in mouse tissues in order to further characterize the function of EML3 in the retina. To test whether EML3 and DYNLL interact physically in mouse tissues, co-immunoprecipitation of EML3 and DYNLL could be performed using adult mouse retinal lysates. Since both proteins are expressed in the IS of PRs of the retina, a physical interaction between EML3 and DYNLL in the context of endogenous proteins in mouse retinal lysates could hint at a possible functional relationship between the two proteins in the retina. If physical interaction of both proteins is established in mouse retinal tissues, then we will be able to frame questions about the molecular mechanisms responsible for the distinctive ciliopathy-related phenotypes in the *Eml3*-knockout mice and the role of EML3 in the mature retina.

In vitro experiments performed in this study provided evidence of interaction between EML3 and a subset of the EML protein family. Interestingly, EML3 interacted with the paralogs EML1 and EML2, but not with EML4. As mentioned above, we hypothesize that perhaps homo-oligomerization of the EML proteins through the TD interferes/competes with their ability to hetero-oligomerize through their TAPE domain. A proper challenge for that hypothesis requires the identification of the minimal protein domain necessary for EML hetero-oligomerization followed by selective addition of EML4 sequences that will eventually result in a loss of interaction as was found in my current studies.

The isoform of EML4 that was used in our study (Uniprot ID: Q3UMY5-3) had an extra exon compared to the other EML4 isoforms. According to the literature, presence of exon 2 leads to disruption of the N-terminal coiled-coil region [106]. One possibility is that in the EML4 isoform used in our study (Q3UMY5-3), presence of exon 2 led to EML3 being unable to co-immunoprecipitate EML4 from lysates of co-transfected HEK 293T cells.

To test whether the other isoforms of EML4 can interact with EML3, co-immunoprecipitation experiments should be performed using the other isoforms of EML4 (Uniprot IDs: Q3UMY5-1, Q3UMY5-2, Q3UMY5-4) in the mammalian co-transfection system. Presence of interaction between EML3 and the EML4 isoforms (Uniprot IDs: Q3UMY5-1, Q3UMY5-2, Q3UMY5-4) would add credence to the hypothesis that it was the extra exon that lead to a disruption of the protein sequence of the N-terminal coiled-coil region in EML4 (Uniprot ID: Q3UMY5-3). Testing for the interaction of EML3 with the various splice isoforms of EML4 could help us investigate whether the variation of residues in the putatively disordered N-terminal region is responsible for variable interaction of EML3 with the different isoforms of EML4.

Although the biological relevance of the differential binding preference of EML3 with EML1, 2 and 4 is not clear, we hypothesize that EML3 forms dimers and/or trimers with itself and/or with the other members of the EML protein family to finally interact with DYNLL and facilitate transport of cargo proteins from the IS to the CC of photoreceptor cells provided that the proteins are co-expressed in the PR.

I presented a list of potential interactors for the EML3 protein but I have only tested some of them in the co-transfection system. There are therefore other EML3 interactions that still need

to be tested with similar methodology. Out of the initial list of interactors, NPHP4 (Nephrocystin-4) is a candidate protein that needs to be tested with high priority because it is a ciliary protein. A published high-throughput study identified EML3 as one of the prey proteins that was pulled by NPHP4, a member of the NPHP1-4-8 complex that functions at the transition-zone of the cilium (Figure-1.29) [110]. The transition zone at the base of the cilium marks the boundary between the cilium and the rest of the cell.

To identify EML3 interactions that are relevant during mouse development, co-immunoprecipitation experiments could be performed using embryonic lysates. Noteworthy, EML3 protein expression time-course revealed highest relative expression of EML3 at E14.5-E15.5 during embryonic development of mice. For this reason, E15.5 mouse embryonic lysates may be prioritized to do the co-Ips in the context of endogenous proteins in mouse tissues. We are performing unbiased screenings for EML3 interactors by following the co-IPs with MS analysis in the context of endogenous proteins in mouse tissues.

4.5 Conclusion

The current thesis presents data on the interacting partners of EML3 by providing evidence of the association of EML3 with a subset of proteins of the EML protein family as well as with DYNLL. Hopefully this study will have an impact on our understanding of human health and disease.

EML3 is an evolutionarily conserved microtubule-associated protein (MAP) whose homolog was first identified in dividing echinoderm eggs and embryos, where it modulates microtubule dynamics [52, 68]. EML3 is expressed abundantly in the adult mouse retina, as well as in the

developing mouse. *Eml3* loss of function mutants produce a striking constellation of phenotypes, including perinatal lethality, suggesting that EML3 is critical for mouse development and post-natal viability.

Pursuit of the following research questions will provide further insight into the importance of EML3 in the retina and in mouse development. To reveal the molecular functions of EML3, the first question we asked was, what are the putative interacting partners of EML3? We began to answer this question by screening through published studies (high-throughput protein interaction studies for the most part) to generate a list of the potential interacting partners of EML3.

A candidate interacting protein of particular importance is DYNLL, a component of the Cytoplasmic Dynein Complex that functions in retrograde transport across microtubules. The reason we became interested in DYNLL is because EML3 contains a DYNLL-binding motif which is unique to EML3 within the EML protein family [95]. We demonstrated that EML3 is expressed in the IS of PRs of the adult mouse retina. Persistence of EML3 expression in the adult mouse retina suggests that EML3 plays an important role in the retina. Noteworthy, the CC of PR cells is a modified cilium in which motor proteins such as Kinesin and Dynein participate in retrograde and anterograde transport of cargo proteins across microtubules, respectively. We hypothesized that EML3 in association with DYNLL could be playing a role in the transport of cargo proteins from the IS to the CC of photoreceptors.

Interestingly, the majority of the phenotypes observed in our rare weaned *Eml3*-knockout mice (*Rom1* present) are identical to many of the phenotypes observed in the *Mdnah5*-knockout

mouse which is the mouse model of Kartagener's syndrome, a ciliopathy. Because of the similarity in phenotypes between the *Eml3*-knockout mouse and the *Mdnah5*-knockout mouse [37], we hypothesized that the absence of EML3 could be responsible for the formation and/or maintenance of the photoreceptor modified cilium, thus also suggesting that EML3 is a protein that is part of the ciliome. It will be interesting to determine if EML3 could potentially be playing a role in the onset of diseases such as Primary Ciliary Dyskinesia (Kartagener's syndrome), Retinitis Pigmentosa, Senior-Loken, Joubert, Usher or Bardet-Biedel syndromes; all examples of photoreceptor ciliopathies in humans.

As it progresses, our work could help unravel the functional network of the EML protein family. The studies in my thesis have touched upon a few aspects of trying to elucidate the molecular functions of EML3 and the role it plays during development by identifying some of the interacting partners of EML3. Continued investigation of the interaction of each of the putative interacting partners with EML3 will surely provide significant insight into the role played by EML3 in photoreceptors and in mouse development.

References

1. Masland, R.H., *The fundamental plan of the retina.* Nat Neurosci, 2001. **4**(9): p. 877-86.
2. Marmorstein, A.D., *The polarity of the retinal pigment epithelium.* Traffic, 2001. **2**(12): p. 867-72.
3. Mustafi, D., A.H. Engel, and K. Palczewski, *Structure of cone photoreceptors.* Prog Retin Eye Res, 2009. **28**(4): p. 289-302.
4. Purves, D., *Neuroscience*. 2008, Sunderland, Mass.: Sinauer.
5. Dowling, J.E., *The retina : an approachable part of the brain*. 1987, Cambridge, Mass.: Belknap Press of Harvard University Press.
6. Rodieck, R.W., *The vertebrate retina; principles of structure and function*. 1973, San Francisco: Freeman.
7. Matsuda, T. and C.L. Cepko, *Analysis of gene function in the retina.* Methods Mol Biol, 2008. **423**: p. 259-78.
8. Adler, R. and D. Farber, *The Retina : a model for cell biology studies*. 1986, Orlando: Academic Press.
9. Agathocleous, M. and W.A. Harris, *From progenitors to differentiated cells in the vertebrate retina.* Annu Rev Cell Dev Biol, 2009. **25**: p. 45-69.
10. Chang, B., *Mouse models for studies of retinal degeneration and diseases.* Methods Mol Biol, 2013. **935**: p. 27-39.
11. Marquardt, T., *Transcriptional control of neuronal diversification in the retina.* Prog Retin Eye Res, 2003. **22**(5): p. 567-77.
12. Muller, F. and R. O'Rahilly, *The first appearance of the neural tube and optic primordium in the human embryo at stage 10.* Anat Embryol (Berl), 1985. **172**(2): p. 157-69.
13. *The atlas of mouse development, by M.H. Kaufman, Academic Press, San Diego, CA, 1992, 512 pp, $80.* MRD Molecular Reproduction and Development, 1994. **37**(1): p. 120.
14. Hu, M. and S.S. Easter, *Retinal neurogenesis: the formation of the initial central patch of postmitotic cells.* Dev Biol, 1999. **207**(2): p. 309-21.
15. Chow, R.L. and R.A. Lang, *Early eye development in vertebrates.* Annu Rev Cell Dev Biol, 2001. **17**: p. 255-96.
16. Young, R.W., *Cell proliferation during postnatal development of the retina in the mouse.* Brain Res, 1985. **353**(2): p. 229-39.
17. Young, R.W., *Cell differentiation in the retina of the mouse.* Anat Rec, 1985. **212**(2): p. 199-205.
18. Kozminski, K.G., et al., *A motility in the eukaryotic flagellum unrelated to flagellar beating.* Proc Natl Acad Sci U S A, 1993. **90**(12): p. 5519-23.
19. D'Angelo, A. and B. Franco, *The dynamic cilium in human diseases.* Pathogenetics, 2009. **2**: p. 3.
20. Fliegauf, M., T. Benzing, and H. Omran, *When cilia go bad: cilia defects and ciliopathies.* Nat Rev Mol Cell Biol, 2007. **8**(11): p. 880-93.
21. Satir, P. and T. Christensen Sø, *Structure and function of mammalian cilia.* Histochem Cell Biol, 2008. **129**(6): p. 687-93.
22. Pan, J., Q. Wang, and W.J. Snell, *Cilium-generated signaling and cilia-related disorders.* Lab Invest, 2005. **85**(4): p. 452-63.
23. Yang, J., et al., *The ciliary rootlet maintains long-term stability of sensory cilia.* Mol Cell Biol, 2005. **25**(10): p. 4129-37.
24. Liu, Q., et al., *The proteome of the mouse photoreceptor sensory cilium complex.* Mol Cell Proteomics, 2007. **6**(8): p. 1299-317.
25. Ou, G., et al., *Functional coordination of intraflagellar transport motors.* Nature, 2005. **436**(7050): p. 583-7.

26. Arikawa, K., et al., *Localization of peripherin/rds in the disk membranes of cone and rod photoreceptors: relationship to disk membrane morphogenesis and retinal degeneration.* J Cell Biol, 1992. **116**(3): p. 659-67.
27. Brown, P.K., I.R. Gibbons, and G. Wald, *THE VISUAL CELLS AND VISUAL PIGMENT OF THE MUDPUPPY, NECTURUS.* J Cell Biol, 1963. **19**: p. 79-106.
28. Kaplan, M.W., R.T. Iwata, and R.C. Sears, *Lengths of immunolabeled ciliary microtubules in frog photoreceptor outer segments.* Exp Eye Res, 1987. **44**(5): p. 623-32.
29. Sale, W.S., J.C. Besharse, and G. Piperno, *Distribution of acetylated alpha-tubulin in retina and in vitro-assembled microtubules.* Cell Motil Cytoskeleton, 1988. **9**(3): p. 243-53.
30. Eckmiller, M.S., *Renewal of the ciliary axoneme in cone outer segments of the retina of Xenopus laevis.* Cell Tissue Res, 1996. **285**(1): p. 165-9.
31. Insinna, C. and J.C. Besharse, *Intraflagellar transport and the sensory outer segment of vertebrate photoreceptors.* Dev Dyn, 2008. **237**(8): p. 1982-92.
32. Worley, L.G., E. Fischbein, and J.E. Shapiro, *The structure of ciliated epithelial cells as revealed by the electron microscope and in phase-contrast.* Journal of Morphology, 1953. **92**(3): p. 545-577.
33. Sjostrand, F.S., *The ultrastructure of the innersegments of the retinal rods of the guinea pig eye as revealed by electron microscopy.* J Cell Physiol, 1953. **42**(1): p. 45-70.
34. Spira, A.W. and G.E. Milman, *The structure and distribution of the cross-striated fibril and associated membranes in guinea pig photoreceptors.* Am J Anat, 1979. **155**(3): p. 319-37.
35. Yang, J. and T. Li, *The ciliary rootlet interacts with kinesin light chains and may provide a scaffold for kinesin-1 vesicular cargos.* Exp Cell Res, 2005. **309**(2): p. 379-89.
36. Guenette, S., et al., *Essential roles for the FE65 amyloid precursor protein-interacting proteins in brain development.* EMBO J, 2006. **25**(2): p. 420-31.
37. Ibanez-Tallon, I., S. Gorokhova, and N. Heintz, *Loss of function of axonemal dynein Mdnah5 causes primary ciliary dyskinesia and hydrocephalus.* Hum Mol Genet, 2002. **11**(6): p. 715-21.
38. Satir, P., L.B. Pedersen, and S.T. Christensen, *The primary cilium at a glance.* J Cell Sci, 2010. **123**(Pt 4): p. 499-503.
39. Krock, B.L., I. Mills-Henry, and B.D. Perkins, *Retrograde intraflagellar transport by cytoplasmic dynein-2 is required for outer segment extension in vertebrate photoreceptors but not arrestin translocation.* Invest Ophthalmol Vis Sci, 2009. **50**(11): p. 5463-71.
40. Qin, H., et al., *Intraflagellar transport (IFT) cargo: IFT transports flagellar precursors to the tip and turnover products to the cell body.* J Cell Biol, 2004. **164**(2): p. 255-66.
41. Pazour, G.J., B.L. Dickert, and G.B. Witman, *The DHC1b (DHC2) isoform of cytoplasmic dynein is required for flagellar assembly.* J Cell Biol, 1999. **144**(3): p. 473-81.
42. Yoder, B.K., *Role of primary cilia in the pathogenesis of polycystic kidney disease.* J Am Soc Nephrol, 2007. **18**(5): p. 1381-8.
43. Bascom, R.A., et al., *Cloning of the cDNA for a novel photoreceptor membrane protein (rom-1) identifies a disk rim protein family implicated in human retinopathies.* Neuron, 1992. **8**(6): p. 1171-84.
44. Molday, R.S., D. Hicks, and L. Molday, *Peripherin. A rim-specific membrane protein of rod outer segment discs.* Investigative ophthalmology & visual science, 1987. **28**(1): p. 50-61.
45. Clarke, G., et al., *Rom-1 is required for rod photoreceptor viability and the regulation of disk morphogenesis.* Nat Genet, 2000. **25**(1): p. 67-73.
46. Ferrari, S., et al., *Retinitis Pigmentosa: Genes and Disease Mechanisms.* Curr Genomics, 2011. **12**(4): p. 238-49.
47. Dryja, T.P., et al., *Dominant and digenic mutations in the peripherin/RDS and ROM1 genes in retinitis pigmentosa.* Invest Ophthalmol Vis Sci, 1997. **38**(10): p. 1972-82.

48. Sato, H., et al., *A monogenic dominant mutation in Rom1 generated by N-ethyl-N-nitrosourea mutagenesis causes retinal degeneration in mice.* Mol Vis, 2010. **16**: p. 378-91.
49. Mitchell, K.J., et al., *Functional analysis of secreted and transmembrane proteins critical to mouse development.* Nat Genet, 2001. **28**(3): p. 241-9.
50. Skarnes, W.C., B.A. Auerbach, and A.L. Joyner, *A gene trap approach in mouse embryonic stem cells: the lacZ reported is activated by splicing, reflects endogenous gene expression, and is mutagenic in mice.* Genes Dev, 1992. **6**(6): p. 903-18.
51. Skarnes, W.C., et al., *A conditional knockout resource for the genome-wide study of mouse gene function.* Nature, 2011. **474**(7351): p. 337-42.
52. Suprenant, K.A., et al., *EMAP, an echinoderm microtubule-associated protein found in microtubule-ribosome complexes.* J Cell Sci, 1993. **104**(2): p. 445-50.
53. Olmsted, J.B., *Microtubule-associated proteins.* Annu Rev Cell Biol, 1986. **2**: p. 421-57.
54. Wiche, G., C. Oberkanins, and A. Himmler, *Molecular structure and function of microtubule-associated proteins.* Int Rev Cytol, 1991. **124**: p. 217-73.
55. Lewis, S.A., et al., *Organization of microtubules in dendrites and axons is determined by a short hydrophobic zipper in microtubule-associated proteins MAP2 and tau.* Nature, 1989. **342**(6249): p. 498-505.
56. Kanai, Y., et al., *Expression of multiple tau isoforms and microtubule bundle formation in fibroblasts transfected with a single tau cDNA.* J Cell Biol, 1989. **109**(3): p. 1173-84.
57. Dinsmore, J.H. and F. Solomon, *Inhibition of MAP2 expression affects both morphological and cell division phenotypes of neuronal differentiation.* Cell, 1991. **64**(4): p. 817-26.
58. Baas, P.W., T.P. Pienkowski, and K.S. Kosik, *Processes induced by tau expression in Sf9 cells have an axon-like microtubule organization.* J Cell Biol, 1991. **115**(5): p. 1333-44.
59. Li, Q. and K.A. Suprenant, *Molecular characterization of the 77-kDa echinoderm microtubule-associated protein. Homology to the beta-transducin family.* J Biol Chem, 1994. **269**(50): p. 31777-84.
60. Eichenmuller, B., et al., *The human EMAP-like protein-70 (ELP70) is a microtubule destabilizer that localizes to the mitotic apparatus.* J Biol Chem, 2002. **277**(2): p. 1301-9.
61. O'Connor, V., et al., *Eml5, a novel WD40 domain protein expressed in rat brain.* Gene, 2004. **336**(1): p. 127-37.
62. Pollmann, M., et al., *Human EML4, a novel member of the EMAP family, is essential for microtubule formation.* Exp Cell Res, 2006. **312**(17): p. 3241-51.
63. Tegha-Dunghu, J., et al., *EML3 is a nuclear microtubule-binding protein required for the correct alignment of chromosomes in metaphase.* J Cell Sci, 2008. **121**(Pt 10): p. 1718-26.
64. Hueston, J.L., et al., *The C. elegans EMAP-like protein, ELP-1 is required for touch sensation and associates with microtubules and adhesion complexes.* BMC Dev Biol, 2008. **8**: p. 110.
65. Smith, T.F., et al., *The WD repeat: a common architecture for diverse functions.* Trends Biochem Sci, 1999. **24**(5): p. 181-5.
66. Xu, C. and J. Min, *Structure and function of WD40 domain proteins.* Protein Cell, 2011. **2**(3): p. 202-14.
67. Richards, M.W., et al., *Crystal structure of EML1 reveals the basis for Hsp90 dependence of oncogenic EML4-ALK by disruption of an atypical beta-propeller domain.* Proc Natl Acad Sci U S A, 2014. **111**(14): p. 5195-200.
68. Hamill, D.R., et al., *Purification of a WD repeat protein, EMAP, that promotes microtubule dynamics through an inhibition of rescue.* J Biol Chem, 1998. **273**(15): p. 9285-91.
69. Chen, D., et al., *EML4 promotes the loading of NUDC to the spindle for mitotic progression.* Cell Cycle, 2015. **14**(10): p. 1529-39.

70. De Keersmaecker, K., et al., *Fusion of EML1 to ABL1 in T-cell acute lymphoblastic leukemia with cryptic t(9;14)(q34;q32).* Blood, 2005. **105**(12): p. 4849-52.
71. Richards, M.W., et al., *Microtubule association of EML proteins and the EML4-ALK variant 3 oncoprotein require an N-terminal trimerization domain.* Biochem J, 2015. **467**(3): p. 529-36.
72. Tsai, L.H. and J.G. Gleeson, *Nucleokinesis in neuronal migration.* Neuron, 2005. **46**(3): p. 383-8.
73. Abdel Razek, A.A., et al., *Disorders of cortical formation: MR imaging features.* AJNR Am J Neuroradiol, 2009. **30**(1): p. 4-11.
74. Kielar, M., et al., *Mutations in Eml1 lead to ectopic progenitors and neuronal heterotopia in mouse and human.* Nat Neurosci, 2014. **17**(7): p. 923-33.
75. Croquelois, A., et al., *Characterization of the HeCo mutant mouse: a new model of subcortical band heterotopia associated with seizures and behavioral deficits.* Cereb Cortex, 2009. **19**(3): p. 563-75.
76. Rosenbaum, J.L. and G.B. Witman, *Intraflagellar transport.* Nat Rev Mol Cell Biol, 2002. **3**(11): p. 813-25.
77. Pazour, G.J. and J.L. Rosenbaum, *Intraflagellar transport and cilia-dependent diseases.* Trends Cell Biol, 2002. **12**(12): p. 551-5.
78. Waters, A.M. and P.L. Beales, *Ciliopathies: an expanding disease spectrum.* Pediatr Nephrol, 2011. **26**(7): p. 1039-56.
79. Pazour, G.J., et al., *The intraflagellar transport protein, IFT88, is essential for vertebrate photoreceptor assembly and maintenance.* Journal of Cell Biology, 2002. **157**(1): p. 103-113.
80. Broekhuis, J.R., W.Y. Leong, and G. Jansen, *Chapter Three - Regulation of Cilium Length and Intraflagellar Transport*, in *International Review of Cell and Molecular Biology*, W.J. Kwang, Editor. 2013, Academic Press. p. 101-138.
81. Tang, M., et al., *Neto2 interacts with the scaffolding protein GRIP and regulates synaptic abundance of kainate receptors.* PLoS One, 2012. **7**(12): p. e51433.
82. Phizicky, E.M. and S. Fields, *Protein-protein interactions: methods for detection and analysis.* Microbiol Rev, 1995. **59**(1): p. 94-123.
83. Pfister, K.K., R.B. Fay, and G.B. Witman, *Purification and polypeptide composition of dynein ATPases from Chlamydomonas flagella.* Cell Motil, 1982. **2**(6): p. 525-47.
84. Woehlke, G. and M. Schliwa, *Walking on two heads: the many talents of kinesin.* Nat Rev Mol Cell Biol, 2000. **1**(1): p. 50-58.
85. Pfister, K.K., et al., *Genetic analysis of the cytoplasmic dynein subunit families.* PLoS Genet, 2006. **2**(1): p. e1.
86. Rapali, P., et al., *DYNLL/LC8: a light chain subunit of the dynein motor complex and beyond.* FEBS J, 2011. **278**(17): p. 2980-96.
87. Puthalakath, H., et al., *The proapoptotic activity of the Bcl-2 family member Bim is regulated by interaction with the dynein motor complex.* Mol Cell, 1999. **3**(3): p. 287-96.
88. Puthalakath, H., et al., *Bmf: a proapoptotic BH3-only protein regulated by interaction with the myosin V actin motor complex, activated by anoikis.* Science, 2001. **293**(5536): p. 1829-32.
89. Lo, K.W., et al., *The 8-kDa dynein light chain binds to p53-binding protein 1 and mediates DNA damage-induced p53 nuclear accumulation.* J Biol Chem, 2005. **280**(9): p. 8172-9.
90. Herzig, R.P., U. Andersson, and R.C. Scarpulla, *Dynein light chain interacts with NRF-1 and EWG, structurally and functionally related transcription factors from humans and drosophila.* J Cell Sci, 2000. **113 Pt 23**: p. 4263-73.
91. Stelter, P., et al., *Molecular basis for the functional interaction of dynein light chain with the nuclear-pore complex.* Nat Cell Biol, 2007. **9**(7): p. 788-796.
92. Day, C.L., et al., *Localization of dynein light chains 1 and 2 and their pro-apoptotic ligands.* Biochem J, 2004. **377**(Pt 3): p. 597-605.

93. Barbar, E., *Dynein light chain LC8 is a dimerization hub essential in diverse protein networks.* Biochemistry, 2008. **47**(2): p. 503-8.
94. Wagner, W., et al., *The binding of DYNLL2 to myosin Va requires alternatively spliced exon B and stabilizes a portion of the myosin's coiled-coil domain.* Biochemistry, 2006. **45**(38): p. 11564-77.
95. Rapali, P., et al., *Directed evolution reveals the binding motif preference of the LC8/DYNLL hub protein and predicts large numbers of novel binders in the human proteome.* PLoS One, 2011. **6**(4): p. e18818.
96. Radnai, L., et al., *Affinity, avidity, and kinetics of target sequence binding to LC8 dynein light chain isoforms.* J Biol Chem, 2010. **285**(49): p. 38649-57.
97. Espindola, F.S., et al., *The light chain composition of chicken brain myosin-Va: calmodulin, myosin-II essential light chains, and 8-kDa dynein light chain/PIN.* Cell Motil Cytoskeleton, 2000. **47**(4): p. 269-81.
98. Hodi, Z., et al., *Alternatively spliced exon B of myosin Va is essential for binding the tail-associated light chain shared by dynein.* Biochemistry, 2006. **45**(41): p. 12582-95.
99. Nyarko, A., et al., *The intermediate chain of cytoplasmic dynein is partially disordered and gains structure upon binding to light-chain LC8.* Biochemistry, 2004. **43**(49): p. 15595-603.
100. Rapali, P., et al., *DYNLL/LC8: a light chain subunit of the dynein motor complex and beyond.* FEBS FEBS Journal, 2011. **278**(17): p. 2980-2996.
101. Hall, J., et al., *Differences in dynamic structure of LC8 monomer, dimer, and dimer-peptide complexes.* Biochemistry, 2008. **47**(46): p. 11940-52.
102. Song, C., et al., *Serine 88 phosphorylation of the 8-kDa dynein light chain 1 is a molecular switch for its dimerization status and functions.* J Biol Chem, 2008. **283**(7): p. 4004-13.
103. Crooks, G.E., et al., *WebLogo: a sequence logo generator.* Genome Res, 2004. **14**(6): p. 1188-90.
104. Lepley, D.M., J.M. Palange, and K.A. Suprenant, *Sequence and expression patterns of a human EMAP-related protein-2 (HuEMAP-2).* Gene, 1999. **237**(2): p. 343-9.
105. Workman, P. and R. van Montfort, *EML4–ALK Fusions: Propelling Cancer but Creating Exploitable Chaperone Dependence.* Cancer Discovery, 2014. **4**(6): p. 642-645.
106. Houtman, S.H., et al., *Echinoderm microtubule-associated protein like protein 4, a member of the echinoderm microtubule-associated protein family, stabilizes microtubules.* Neuroscience, 2007. **144**(4): p. 1373-82.
107. Brisch, E., M.A. Daggett, and K.A. Suprenant, *Cell cycle-dependent phosphorylation of the 77 kDa echinoderm microtubule-associated protein (EMAP) in vivo and association with the p34cdc2 kinase.* J Cell Sci, 1996. **109 (Pt 12)**: p. 2885-93.
108. Hildebrandt, F., M. Attanasio, and E. Otto, *Nephronophthisis: disease mechanisms of a ciliopathy.* J Am Soc Nephrol, 2009. **20**(1): p. 23-35.
109. Zaghloul, N.A. and N. Katsanis, *Mechanistic insights into Bardet-Biedl syndrome, a model ciliopathy.* J Clin Invest, 2009. **119**(3): p. 428-37.
110. Sang, L., et al., *Mapping the NPHP-JBTS-MKS protein network reveals ciliopathy disease genes and pathways.* Cell, 2011. **145**(4): p. 513-28.
111. Benzing, T. and B. Schermer, *Transition zone proteins and cilia dynamics.* Nat Genet, 2011. **43**(8): p. 723-4.
112. Torres, J.Z., J.J. Miller, and P.K. Jackson, *High-throughput generation of tagged stable cell lines for proteomic analysis.* Proteomics, 2009. **9**(10): p. 2888-91.
113. Tzivion, G. and J. Avruch, *14-3-3 proteins: active cofactors in cellular regulation by serine/threonine phosphorylation.* J Biol Chem, 2002. **277**(5): p. 3061-4.
114. Symposium on, P., et al. *Physiological and biochemical aspects of nervous integration*. Englewood Cliffs, N.J.: Prentice-Hall.

115. Muslin, A.J., et al., *Interaction of 14-3-3 with signaling proteins is mediated by the recognition of phosphoserine.* Cell, 1996. **84**(6): p. 889-97.
116. Yaffe, M.B. and L.C. Cantley, *Signal transduction. Grabbing phosphoproteins.* Nature, 1999. **402**(6757): p. 30-1.
117. Yaffe, M.B. and A.E. Elia, *Phosphoserine/threonine-binding domains.* Curr Opin Cell Biol, 2001. **13**(2): p. 131-8.
118. Qi, W., et al., *Isoform-specific expression of 14-3-3 proteins in human lung cancer tissues.* Int J Cancer, 2005. **113**(3): p. 359-63.
119. Pozuelo Rubio, M., et al., *14-3-3-affinity purification of over 200 human phosphoproteins reveals new links to regulation of cellular metabolism, proliferation and trafficking.* Biochem J, 2004. **379**(Pt 2): p. 395-408.
120. Ewing, R.M., et al., *Large-scale mapping of human protein-protein interactions by mass spectrometry.* Mol Syst Biol, 2007. **3**: p. 89.
121. Amanchy, R., et al., *A curated compendium of phosphorylation motifs.* Nat Biotechnol, 2007. **25**(3): p. 285-6.
122. Blom, N., S. Gammeltoft, and S. Brunak, *Sequence and structure-based prediction of eukaryotic protein phosphorylation sites.* J Mol Biol, 1999. **294**(5): p. 1351-62.
123. Hornbeck, P.V., et al., *PhosphoSitePlus, 2014: mutations, PTMs and recalibrations.* Nucleic Acids Res, 2015. **43**(Database issue): p. D512-20.
124. Oakley, B.R. and N.R. Morris, *A mutation in Aspergillus nidulans that blocks the transition from interphase to prophase.* J Cell Biol, 1983. **96**(4): p. 1155-8.
125. Fry, A.M., et al., *Cell cycle regulation by the NEK family of protein kinases.* J Cell Sci, 2012. **125**(Pt 19): p. 4423-33.
126. Yin, M.J., et al., *The serine/threonine kinase Nek6 is required for cell cycle progression through mitosis.* J Biol Chem, 2003. **278**(52): p. 52454-60.
127. Feige, E. and B. Motro, *The related murine kinases, Nek6 and Nek7, display distinct patterns of expression.* Mech Dev, 2002. **110**(1-2): p. 219-23.
128. O'Regan, L. and A.M. Fry, *The Nek6 and Nek7 protein kinases are required for robust mitotic spindle formation and cytokinesis.* Mol Cell Biol, 2009. **29**(14): p. 3975-90.
129. Bodor, A., et al., *DYNLL2 dynein light chain binds to an extended linear motif of myosin 5a tail that has structural plasticity.* Biochemistry, 2014. **53**(45): p. 7107-22.
130. Cooper, S. and I. Hanson, *A screen for proteins that interact with PAX6: C-terminal mutations disrupt interaction with HOMER3, DNCL1 and TRIM11.* BMC Genetics, 2005. **6**(1): p. 43.
131. Yang, W., et al., *Promoter-sharing by different genes in human genome – CPNE1 and RBM12 gene pair as an example.* BMC Genomics, 2008. **9**: p. 456.
132. Eisen, M.B., et al., *Cluster analysis and display of genome-wide expression patterns.* Proc Natl Acad Sci U S A, 1998. **95**(25): p. 14863-8.
133. Clements, M., et al., *Integration of known transcription factor binding site information and gene expression data to advance from co-expression to co-regulation.* Genomics Proteomics Bioinformatics, 2007. **5**(2): p. 86-101.
134. Sievers, F., et al., *Fast, scalable generation of high-quality protein multiple sequence alignments using Clustal Omega.* Molecular Systems Biology, 2011. **7**(1).
135. Magrane, M. and U. Consortium, *UniProt Knowledgebase: a hub of integrated protein data.* Database, 2011. **2011**.
136. Lupas, A., M. Van Dyke, and J. Stock, *Predicting coiled coils from protein sequences.* Science, 1991. **252**(5009): p. 1162-4.
137. Mason, J.M. and K.M. Arndt, *Coiled Coil Domains: Stability, Specificity, and Biological Implications.* ChemBioChem, 2004. **5**(2): p. 170-176.